Disrupting dynamic f-actin enhances skeletal muscle contraction due to mechanical softening

by

Vivek Sivathanu

B.Tech. Mechanical Engineering (2010), Indian Institute of Technology, Madras
S.M. Mechanical Engineering (2013), M.I.T.

Submitted to the Department of Mechanical Engineering
in Partial Fulfillment of the Requirements for the Degree of

Doctor of Philosophy in Mechanical Engineering

at the

MASSACHUSETTS INSTITUTE OF TECHNOLOGY

February 2018

Signature of Author: Signature redacted

Department of Mechanical Engineering
January 08, 2018

Certified by: Signature redacted

Roger D. Kamm
Professor of Mechanical Engineering
Professor of Biological Engineering
Thesis Supervisor

Accepted by: Signature redacted

Rohan Abeyaratne
Chairman, Committee on Graduate Students
Professor of Mechanical Engineering

Disrupting dynamic f-actin enhances skeletal muscle contraction due to mechanical softening

By
Vivek Sivathanu

Submitted to the Department of Mechanical Engineering
on January 08, 2018 in Partial Fulfillment of the Requirements for the Degree of
Doctor of Philosophy in Mechanical Engineering

ABSTRACT

Skeletal muscle wasting disorders such as sarcopenia affect the daily mobility of millions of aging people globally due to decreased muscle mass and decreased muscle efficiency. In this study we discover a novel target to improve the efficiency of skeletal muscle by targeting the dynamic f-actin cytoskeleton.

Using two model systems, an ex-vivo mouse muscle model and a novel *in vitro* optogenetic skeletal muscle micro-tissue model, we show that disruption of the dynamic f-actin cytoskeleton using small molecule actin dynamics inhibitors leads to a persistent 2-fold improvement in muscle active contractility. We explored possible drawbacks of f-actin disruption, including loss of mechanical integrity, cell death, and intracellular organelle damage. None of these downsides actually present themselves with f-actin disruption. Muscle fatigue resistance however does seem to be slightly affected.

We performed a detailed characterization of the cytoskeletal modifications that occur during f-actin disruption using dose-response-recovery studies, live f-actin imaging, fluorescence recovery after photobleaching and more targeted f-actin disruption. Using these studies we conclude that treatments which shorten f-actin filaments seem to improve contraction. We also uncovered previously unidentified roles of branched and tropomyosin stabilized f-actin in force transmission.

Biomechanical testing at the cell level using AFM and at the tissue level using a micro-tensile test shows a drop in mechanical stiffness that correlates well with a corresponding improvement in muscle force. We ruled out a range of alternate hypotheses involving changes to sarcomeric proteins and energetic activity, that could explain the force improvement, concluding that the force improvement due to f-actin disruption is due to mechanical softening of the cells which pose to a lower resistance to their own contraction. As a potential application, we show that a weak 3D printed muscle powered biological robot starts walking with f-actin disruption. This target has significant therapeutic potential in muscle disorders due to its disease non-specificity. We conclude by discussing possible future experiments that could reveal the best therapeutic applications.

Key words: Muscle strength, f-actin, cytoskeleton, Skeletal Muscle Tissue Engineering, Muscle Disorders

Thesis Advisor:
Roger D. Kamm, Professor of Biological and Mechanical Engineering, MIT

Thesis Committee Members:
Alan Grodzinsky, Professor of Biological, Electrical and Mechanical Engineering, MIT
Michael Levin, Professor of Biology, Tufts University
Rohit Karnik, Professor of Mechanical Engineering, MIT

Acknowledgements

First and foremost, I would first like to thank Professor Roger Kamm, my thesis advisor for inviting me to join his lab and mentoring me as a scientist, while giving me ample room to develop my independence and explore the wealth of opportunities MIT has to offer. Working with Roger has been one of the great honors of my life. His critical nature when it comes to the science, coupled with his pleasant personality and great leadership have all significantly molded my own style. It has given me the confidence to take on the next challenges in life.

I would also like to thank my thesis committee members, Professor Alan Grodzinsky, Professor Michael Levin and Professor Rohit Karnik. Each time I have a meeting with them, I would be left with many more ideas to progress our scientific work. Their inputs were critical in shaping the thesis to its current form.

I owe special thanks to my collaborator Dr. Hesham Azizgolshani, one of the most skilled scientists and engineers I've known, for his critical insights in shaping this work and in help with the mechanical designs used throughout this work. In aggregate, I'd estimate his inputs to have saved me years of time. I would also like to thank Dr. Emad Mooendarbary for his mentorship and collaboration. His inputs have been pivotal to defining the scope of this work. I would like to acknowledge Dr. Brianne Connizzo for her help with the mouse explant studies discussed herein. Dr. Sebastien Uzel and Dr. Devin Neal deserve special thanks for introducing me to the world of skeletal muscle biology and leaving me with the initial skillset required to get started with this work. Dr. Tatsuya Osaki and Dr. Ran Li have provided immense help both with experiments and with ideas throughout this thesis. My collaborator Dr. Stefano Ugolini, present during the initial phase on this work, was a great partner to provide the initial momentum for this work. I would also like to thank my collaborators Dr. Ritu Raman, Dr. Caroline Cvetkovic, Professor Rashid Bashir and Jorge Escribano for their great inputs to this work. The talented undergraduates who I've had a chance to work and mentor over the years include Zhuoning Zou, Blake Zhou, Divya Ravinder, Noopur Ranganathan, Licelotte Fernandez and Sarah Clarkson. It is tough to overestimate how much the youthful energy of each of these undergraduate students contributed to the momentum of the work.

Working in the Kamm lab has been an immense pleasure due in large part to the camaraderie. Roger has a fantastic ability to fill his lab with people who are not only great scientists, but also have wonderful personalities. Special gratitude goes to Dr. Jordan Whisler, Dr. Michelle Chen and Dr. Ran Li who have been an immense source of mental support over the years and have significantly shaped my personality and my future directions. Over the years, the Kamm lab members including Dr. Ioannis Zervantonakis, Dr. Michael Mak, Dr. Andrea Malandrino, Jean Carlos Serrano, Dr. Giovanni Offeddu and Anya Roberts have always been wonderful to be around.

I would like to thank the brilliant and inspiring folks I've met over the years in the MIT community. Special thanks to my MIT Global Startup Workshop family, especially to Dr. Anurag Bajpayee, Dr. Nevan Hanumara, Dr. Melinda Hale, Joshua Schuler, Professor Ambika Goel Bajpayee, Abhishek Bajpayee and Dr. Rohit Singh. I should thank them for initiating my interest in business. I would also like to thank the range of business mentors I've had over the years through the MIT Legatum Center for Entrepreneurship and Development, the MIT IDEAS Global Challenge, the MIT Public Service Center, the MIT $100K Competition, the MIT Sloan School of Management and Flagship Ventures. Special thanks also goes to all my friends in Boston, in the US and elsewhere.

I would not have had any of these opportunities if my teachers didn't believe in me. Special thanks go to my undergraduate mentor Professor Sarit K. Das who has been a great mentor, persuaded me to shift fields in to the life sciences at just the right time and has been a tremendous source of inspiration from near and far.

Finally, I would like to thank my family. My parents Sivathanu Pillai and Dr. Shobhana Sivathanu have been remarkable. The sacrifices they've made over the years to provide for every opportunity I've desired has been inspiring and left me with a debt I can only pay forward. Both of them, my sisters Shreaya and Priya, as well as my extended family have always believed me, even during my formative years when I've doubted myself. I thank all of them for their unconditional support.

This thesis work is supported by funding from National Science Foundation Emergent Behavior on Integrated Cellular Systems (NSF EBICS STC) as well as BioSym.

Dedication

Dedicated to my late grandmother Sarojini

Table of Contents

List of Figures

Fig. 9: About half of the CytoD treated tissues (n=5) decline in contraction just like DMSO treated controls (n=5). The natural decline of all tissues was measured once every 10 minutes for 1 hour. After 1 hour, either DMSO or CytoD 3μM was applied to the tissues. The two colored envelopes of each kind grey, blue and red each represent the 68% and 95% confidence intervals (1 and 2 sigma) of the corresponding data

Fig. 10: About half of the CytoD treated tissues (n=4) exhibit a transient improvement in contraction just like DMSO treated controls (n=5). The natural decline of all tissues was measured once every 10 minutes for 1 hour. After 1 hour, either DMSO or CytoD 3μM was applied to the tissues. The two colored envelopes of each kind grey, blue and red each represent the 68% and 95% confidence intervals (1 and 2 sigma) of the corresponding data

Fig. 11: C2C12-ChR2[H134R] plasmid schematic

Fig. 12: Effect of CytoD 3μM (30 mins) on change in morphology of C2C12 myotubes grown on IBIDI-treat dishes. Scalebar is 100um. Also shown is the change in index of movement with CytoD application, which is a measure of change in local pixel grayscale values with time. Closer to red is indicative of larger pixel changes, which happens when there are larger displacements. Closer to blue indicates almost no displacement, indicating areas without any contraction.

Fig. 13: Effect of CytoD 3μM (30mins) and DMSO on change in active displacements of C2C12 myotubes grown on IBIDI-treat dishes. CytoD treatment dramatically increases the active displacements of the myotubes, while DMSO treated controls result in only a very mild increase. The five point star points to the mean values of the displacements, which are also shown in green below the swarm plot. * $p = 0.0045$ One-tailed Mann Whitney U-test. ** $p < 0.0001$ One-tailed Mann Whitney U-test

Fig. 14: Acrylic/kapton base mount for 3D muscle formation and force sensing. The distance between the faces of the 2 cantilevers is 3mm. Also the entire acrylic base was inserted to fit snugly in a regular 35mm petri dish.

Fig. 15: Sequential process for the fabrication of a 3D muscle bundle attached to a compliant and a rigid cantilever, for measurement of optically stimulated contractile force. Process adapted from the sacrificial molding process described elsewhere[1]

Fig. 16: Phase contrast images of the development of the muscle fiber bundle. The myoblast/ECM gel compacts soon after cell seeding and compacts successively over the course of the differentiation. In this case, the culture was switched to differentiation medium 2 days after cell seeding and the final assay (force, stiffness etc.) was conducted on day 12 after switching.

Fig. 17: Image processing pipeline to detect (A) cantilever active movement. (B) A typical pipeline is shown with the final output of the algorithm being the position of the edge of the cantilever as shown in red overlaid on top of the raw image. The green lines are many lines output by the Hough transform algorithm which detects many lines along the cantilever edge. A linear regression is then performed to estimate a single edge based on all these edged (shown in red). The position of this cantilever is tracked over time to estimate the displacement (both the x-location and slope of the line are considered).

Fig. 17: Image processing pipeline to detect cantilever active movement. A typical pipeline is shown with the final output of the algorithm being the position of the edge of the cantilever as shown in red overlaid on top of the raw image. The green lines are many lines output by the Hough transform algorithm which detects many lines along the cantilever edge. A linear regression is then performed to estimate a single edge based on all these edged (shown in red). The position of this cantilever is tracked over time to estimate the displacement (both the x-location and slope of the line are considered).

Fig. 18: Timecourse of active contraction of C2C12 based 3D muscle tissues. The contractility seems to saturate (or change slower) after day 8 and peak contraction is reached between day 8-12. The two colored envelopes represent the 68% and 95% confidence intervals. n = 10 independent muscle fibers were used for this experiment. The contractility of each muscle fiber was normalized with respect to its respective maximum during the timecourse of differentiation.

Fig. 19: Timecourse of active contraction changes of C2C12 based 3D muscle tissues, within 3 hours. Statistically significant differences ($p < 0.05$) between the CytoD (n=5) and the DMSO (n=5) are observed as early as 15 minutes

Fig. 20 Dose response test of 3D muscle active contractility with Cytochalasin D. The contractions are measure prior to treatment (Pre-Treatment) as well as 2 hours after CytoD or DMSO treatment. Normalization is with respect to the contraction prior to treatment. In the case of Blebbistatin, treatment with 50μM of this myosin inhibitor completely nullified the active force within 5 minutes of treatment. ** One-tailed Mann-Whitney test $p = 0.00539$. NS, $p > 0.05$ One-tailed Mann-Whitney test. * $p = 0.0105$ One-tailed Mann-Whitney U-test

Fig. 21 Dose response test of 3D muscle active contractility with Latrunculin A. The contractions are measure prior to treatment (Pre-Treatment) as well as 2 hours after LatA or DMSO treatment. Normalization is with respect to the contraction prior to treatment.

Fig. 22 Caspase-3 mRNA quantification (n=3) after 2 hours of CytoD 0.3μM or DMSO treatment. $p = 0.37$. A one-tailed 2-sample t-test was used for statistical significance testing.

Fig. 23 Cell viability changes (n=6) after 52 hours of CytoD 0.3μM or DMSO treatment. $p = 0.46$ A one-tailed 2-sample t-test was used for statistical significance testing.

Fig. 24 CytoD treatment likely leaves the plasma membrane intact. It does not significantly change the activity of Creatine Kinase in the supernatant of the optically stimulated C2C12 myotubes relative to DMSO treated and optically stimulated controls. However, as expected for positive controls, Triton 0.1% treated samples as expected, show a significant 4-fold increase in CK activity relative to DMSO controls, indicating the presence of CK in the cells. A one-tailed 2-sample t-test was used for statistical significance testing. $p = 0.16$ NS for CytoD (n=6) vs DMSO(n=6). $p = 7.5*10^{-7}$ for Triton (n=3) vs DMSO(n=6)

Fig. 25 Effect of a fatigue loading optical stimulus on muscle active contractility with (or without) f-actin disruption using CytoD (or DMSO). DMSO controls show a self-strengthening behavior after 15minutes of fatigue load, while CytoD treated tissues do not. A one-tailed Mann

Whitney U-test was used for statistical significance testing. NS ($p>0.05$). *($p=0.032$). N=3 samples were used for each condition.

Fig. 26 F-actin disruption with CytoD does not affect autophagy as indicated by the CytoID fluorescent based assay. N=3 samples were used for each condition. A 2-sample one-tailed t-test was used for statistical significance testing.

Fig. 27 The DMSO control tissues don't show any significant change in active muscle contractility. Shown are the effects of DMSO application to C2C12 skeletal muscle active contractility 2 hours after treatment, 1 day after treatment, as well as 1 day after washout (which is 2 days after the treatment was initiated). The active force measured at different times for each device are normalized to the corresponding pre-treatment force (n=5). Statistical significance tests were conducted using a paired one-tailed t-test to check if any potential increases are significant.

Fig. 28 Mild f-actin disruption with CytoD 0.3μM shows a significant increase in active muscle contractility within 2 hours (1.6X) and a smaller (but not statistically significant) increase a day after treatment. The plot shown is the effect of CytoD 0.3μM application to C2C12 skeletal muscle active contractility 2 hours after treatment, 1 day after treatment, as well as 1 day after washout (which is 2 days after the treatment was initiated). The active force measured at different times for each device are normalized to the corresponding pre-treatment force (n=7). Statistical significance tests were conducted using a paired one-tailed t-test to check if any potential increases are significant. There is a statistically significant drop in active contraction 1 day after washout of CytoD 0.3μM indicating at least partial reversibility of CytoD's effect, partial because the force is still 50% greater than force prior to treatment (statistically significant).

Fig. 29 Strong f-actin disruption with Cyto 3μM shows a significant increase in active muscle contractility within 2 hours (2.6X), a deleterious decrease relative to the peak of nearly 50% down to 1.4X and a recovery to nearly the level of the 2 hour peak (2.3X) within a day of CytoD washout. The plot shown is the effect of Cyto 3μM application to C2C12 skeletal muscle active contractility 2 hours after treatment, 1 day after treatment, as well as 1 day after washout (which is 2 days after the treatment was initiated). The active force measured at different times for each device are normalized to the corresponding pre-treatment force (n=10). Statistical significance tests were conducted using a paired one-tailed t-test to check if any potential increases are significant. There is a statistically significant drop in active contraction 1 day after washout of Cytod 0.3μM indicating at least partial reversibility of CytoD's effect, partial because the force is still 50% greater than force prior to treatment (statistically significant).

Fig. 30 Comparison of the effect of CytoD for longer term (2hrs to 2 days) on muscle contractility relative to the forces during muscle differentiation. In the case of CytoD 3μM and DMSO, a 2 hour pulse was applied and then washed out to test the recovery and reversibility long term. This was compared with a continuous mild f-actin disruption with CytoD 0.3μM for

days. Clearly, both the high dose (3μM) pulse of CytoD and the low dose continuoud treatment both led to sustainable improvement in active contraction beyond the DMSO pulse control and relative to the maximum force during differentiation (all fibers were normalized with respect to their respective peaks during days 2-12 of differentiation. The colored envelopes around each means curve (black, blue, green and red) represent 68% and 95% confidence intervals.

Fig. 31 Fluorescence intensity of CytoD EverFluor-TMR measured 2 hours after treatment and after washout. (A) a phase contrast image showing a typical 3D muscle fiber. (B) The first row of images contains the raw images used for quantification purposes in **Fig.** 32. The second row contains histogram normalized versions of images in the first row. The normalization with respect to the 2 day washout image in order to make the visibility of the muscle fiber clear, while still maintaining the relative intensity. Clearly there is a significant drop in intensity, almost imperceptible by 1 or 2 days after washout. Scalebar 300μm

Fig. 32 Fluorescence intensity of CytoD EverFluor-TMR measured 2 hours after treatment and after washout. All the intensities were normalized between 0 and 1 with respect to the maximum average intensity measured as well as the minimum (throughout the experiment). The background intensity could vary from day to day, due to changes in environmental conditions as well as variations in the laser. So the intensity values corresponding to zero CytoD concentration are ~ $6*10^{-4}$ for both the pre-treatment and 2 hour cases. In the 2 hour image, the background is high because it contain CytoD-EverFluor. However, the intensity of the muscle fiber is even higher than that as it seems that CytoD reacts with f-actin and accumulates inside the muscle. 2 hours after treatment, the average intensity on the muscle fiber is ~1000-fold larger than the pre-treatment background. One day 1 after washout, the muscle intensity drops to being 5-fold larger than background (~200-fold reduction) and on day 2, it drops to being 1.4-fold larger than background (i.e. a ~700-fold reduction compared to the 2 hour peak)

Fig. 33: Diffusion of Cytochalasin D – Everfluor conjugate through a muscle fiber. (A) Confocal fluorescence timelapse images of the Cytochalasin D – Everfluor conjugate penetrating the 3D muscle tissue. Scale bar in images is 100μm. (B) Quantification of the fluorescence intensity variation, with time. All intensities are normalized with respect to the same maximum 16-bit greyscale spectrum. Every line at any given time point represents the average intensity across the muscle fiber averaged over 30 cross sections along the length of the muscle.. 3 of the cross sections are shown in the first image in (A).

Fig. 34: Visualization of f-actin in mature and immature myotubes using Sir-Actin and confocal timelapse microscopy reveals that sarcomeric f-actin in mature myotubes is not depolymerized by CytoD 0.3μM. However, a small fraction of the non-sarcomeric f-actin is depolymerized with CytoD. For instance, in window 2: the arrows mark areas with f-actin clustering at T=30 and 150mins(dark rounded spots), which is typical when filamentous actin breakdown appears (also see **Fig.** 36B for more obvious clustering). Also shown using arrows in window2 (between T=60 and 90mins) as well as in window 3 (T= 90mins) is the sudden appearance of a lighter background, indicating the disappearance of the dark f-actin. Scalebar is 10μm.

Fig. 35: Visualization of f-actin (Sir-Actin) in mature sarcomeric myotubes with CytoD 0.3μM application using confocal timelapse microscopy reveals that while sarcomeric f-actin in mature myotubes are not depolymerized by CytoD 0.3μM, the non-sarcomeric non-specific f-actin (darker) around the periodic f-actin structures do get depolymerized. This is also illustrated in the intensity line plot showing that the periodic structures remain after 12 hours, while the overall intensity level comes down, due to depolymerization of some of the non-specific, non-periodic background f-actin. The scalebar is 10μm.

Fig. 36: Visualization of f-actin (Sir-Actin) in immature sarcomeric myotubes as well as immature non-sarcomeric myotubes with CytoD 0.3μM application using confocal timelapse microscopy reveals that (A) Even the period sarcomeric f-actin gets disrupted if the myotube organization is immature as seen in A with the imperfectly aligned developing sarcomeric structure. (B) Several f-actin filaments in the non-sarcomeric immature myotubes are severed. There is also a lot of f-actin clustering (all within 2 hours). Scalebar is 10μm.

Fig. 37: (A) Quantification of the non-sarcomeric stress-fiber like f-actin breakdown in pre-sarcomeric immature myotubes shows that the distribution of linear f-actin filaments gets skewed towards shorter filaments with CytoD treatment (B) There seem to be many more stress-fiber like f-actin filaments with CytoD treatment. i.e. CytoD treatment converts a few long f-actin filaments into many more shorter filaments. (C) Quantification is performed by manually counting stress-fiber like f-actin structures and measuring their length using the length tool of ImageJ software. An example of an stress-fiber like actin filament in shown with a red curly brace showing the extent of the filamentous. The beginning and ends were chosen (subjectively) based on the location where there appears to be a branching of the bundled stress-fiber like f-actin or a clear stop.

Fig. 38: Schematic of fluorescence recovery after photobleaching of GFP-tagged actin monomers. Monomer recovery occurs first and is the most rapid (GFP-tagged monomers indicated by the green blobs and the background green used to doubly emphasize the location of unbleached GFP-tagged monomers). F-actin turnover driven recovery is slower than the diffusion of monomers (10X slower), and so can be considered to occur after monomer recovery is complete. This is schematically indicated by the grey (bleached) f-actin filaments acquiring some green blobs (unbleached monomers) from the barbed/polymerizing end of f-actin. Some of the bleached f-actin filaments recover much more slowly (10s of minutes) due to protective capping proteins. These are schematically shown to never recover (always grey after bleaching) in the timescale of the experiments conducted (2-3 minutes).

Fig. 39: A typical FRAP recovery curve and pictures from actual experiments. C2C12 myotubes with GFP-actin monomers are bleached with a rectangular window covering the entire width of the cell throughout the entire depth. Scalebar is 10μm. By plotting the intensity recover within the bleach window over time and by using the remaining image to compute the rate of photobleaching we obtain a corrected recovery curve, which has a rapid diffusion limited recovery in the ~1s timescale followed by a slower turnover limited recovery.

Fig. 40: The first few seconds of the FRAP recovery curve, plotted based on 19 individual FRAP experiments conducted at different regions along 3 different myotubes. The rapid initial rise is

driven purely by diffusion of monomers. We use this recovery profile to compute the timescale of diffusion and estimate the diffusion coefficient (shown in the inset).

Fig. 41: Relative change ratio of the fractions of the various actin compartments (actin monomer, dynamic f-actin and stable f-actin). The Y-axis represents the ratio of (Dynamic F-actin fraction after treatment)/(Dynamic F-actin fraction before treatment) etc for the various compartments (Dynamic, stable F-actin as well as Monomeric actin). The various treatment conditions (DMSO, CytoD) are shown in shades of green. The red dots represent the mean values. * $p = 0.029$ with a one-tailed unpaired 2-sample t-test with respect to the DMSO controls. N=5 was used for DMSO and CytoD 3μM conditions. N = 9 was used for the CytoD 0.3μM condition.

Fig. 42: Relative change ratio of the timescales of dynamic f-actin turnover with the various treatments. Significance tests were 1-tailed t-tests. The turnover time change with CytoD 0.3μM is barely statistically significant, while the change due to CytoD 3μM is highly statistically significant relative to the DMSO treated controls. A one-tailed unpaired 2-sample t-test with respect to the DMSO controls. N=5 was used for DMSO and CytoD 3μM conditions. N = 9 was used for the CytoD 0.3μM condition.

Fig.43: Treatment with 100μM SMIFH2, a small molecule inhibitor of formin homology domain 2 improves active skeletal muscle contractility within 2 hours of treatment. This is likely due to inhibition of the FH2 domain of formins which leads to disruption of formin associated f-actin filaments and/or inhibition of formation of such filaments as formin is an f-actin nucleator. At SMIFH2 doses of 20μM or lower, no improvement in contraction was observed. Statistical significance testing was performed with a one-tailed unpaired 2-sample t-test with respect to the DMSO controls.

Fig.44: Treatment with CK666 100μM, an inhibitor of the Arp2/3 complex leads to a gradual decline of contractility. The data for the change in contraction 2 hours (not-significant) and 1 day (statistically significant) after treatment with CK666 100μM are shown. This makes it plausible that the branched Arp2/3 mediated f-actin filaments do help in sarcomeric force transmission. At SMIFH2 doses of 20μM or lower, no statistically significant change in contraction was observed after 2 hours (shown) of contraction or after 1 day (not shown). Statistical significance testing was performed with a one-tailed unpaired 2-sample t-test with respect to the DMSO controls.

Fig. 45: Treatment with TR100, an anti-tropomyosin compound targeting the non-sarcomeric tropomyosin isoform Tpm3.1 leads to a decline in muscle contractility 2 hours after treatment. Statistical significance testing was performed with a one-tailed unpaired 2-sample t-test with respect to the DMSO controls.

Fig. 46: Treatment with ATM3507, another anti-tropomyosin compound targeting the non-sarcomeric tropomyosin isoform Tpm3.1 leads to a decline in muscle contractility 2 hours after treatment. Statistical significance testing was performed with a one-tailed unpaired 2-sample t-test with respect to the DMSO controls.

Fig. 47: Gene expression analysis using RT-PCR for 21 genes including housekeeping gene 18s rRNA, with CytoD 0.3μM application for 2 hours. The relative expression levels are colored with a $\log_2$ scale (10^{-3} to 10^{3}). No significant changes in gene expression were found. There

were 3 samples used for both CytoD and the control (DMSO), labeled 1-3. A 2 sample t-test was used to obtain significance levels of the relative expression, with samples made in triplicate.

Fig. 48: AFM indentation of C2C12-based myotubes reveals a drop in mechanical stiffness. (A) AFM approach retraction curve (red) with a curve-fit (green) to the approach curve. A Hertz model was fit to the data to compute the apparent elastic modulus. (B) CytoD treatment clearly lowers the apparent elastic modulus relative to DMSO treated controls (AFM) by 50%. N=30 cell indentations were used for this test.

Fig. 49: Micro-tensile testing of a muscle tissue. (A) The setup used for testing of the axial stiffness of a muscle tissue. The typical muscle tissue used in this study is ~100μm in diameter, 3mm in length anchored between two clamped kapton cantilevers (orange in color), one relatively compliant and the other relatively rigid (as described earlier in Chapter 2). The setup allows simultaneous measurement of the active contraction by observing the movement of the compliant cantilever (see the text in Sec. 4.2.2). Furthermore, the slidable rigid cantilever allows the muscle to be stretched and relaxed by 50 μm steps, which also allows estimation of the axial stiffness. For a sense of scale, the circular tissue mount fixture is ~6cm in diameter. The distance between the cantilevers in the fixture is 3mm. (B) The image processing pipeline used for stiffness computation. The first image represents the raw image of the initial position of the compliant cantilever edge. The second image represents difference image between the initial and final positions of the compliant cantilever as the rigid cantilever is moved to stretch the muscle tissue. The thickness of the bright rectangular zone is the displacement. An edge detection algorithm similar to the one described in Chapter 2 (see appendix 2) is used to detect the two edges of the bright strip. (C) Shows the cantilever position displacement (black), the cantilever displacement (red) and the normalized stiffness (blue).

Fig. 50: CytoD treatment leads to a simultaneous decrease in axial tissue stiffness and improvement in active contraction as measured by the micro-tensile testing assay. The timescale of the 2 changes match each other well. (n=5) was used for this experiment.

Fig. 51: CytoD (0.3μM) treatment does not significantly change the baseline glucose consumption rate of the differentiated C2C12 cells. A 1-tailed 2 sample t-test was used for statistical significance testing.

Fig. 52: CytoD treatment (0.3μM or 3μM) for 2 hours does not significantly change the phosphorylation of AKT at the 2 phosphorylation sites (Ser473 and Thr308). A) Western blots showing pAKT expression levels for both sites Ser473 and Thr308 along with AKT as a function of CytoD concentration. β-tubulin and β-actin are also shown as loading controls B) Averaged results showing the ratio of phosphorylated AKT to total AKT. A 2-sample 1-tailed t-test was used for statistical significance testing ($p > 0.05$). N=3 for all experiments.

Fig. 53: CytoD treatment (0.3μM or 3μM) does not significantly change cellular metabolic activity as assessed by an MTT assay. See text for details about the time of exposure. A 2-sample 1-tailed t-test was used for statistical significance testing ($p > 0.05$). N=4 was used for these experiments.

Fig. 54: CytoD treatment does not significantly change mitochondrial activity as assessed by no significant changes in accumulation of TMRE a fluorescent dye that accumulates only in active mitochondria. A 2-sample 1-tailed t-test was used for statistical significance testing NS ($p > 0.05$). N=3 was used for these experiments.

Fig. 55: Mechanical basis of active force improvement due to f-actin disruption in skeletal muscle.

Fig. 56: Jasplakinolide 5μM treatment decreases active contractility of C2C12 based 3D engineered muscle by 25% within 2 hours of exposure and 33% within 24 hours of exposure. Statistical significance testing is based on the 1-tailed 2 sample t-test

Fig. 57: Phalloidin 100μM treatment decreases active contractility of C2C12 based 3D engineered muscle by 25% within 24 hours of exposure. 2 hours after treatment, there was no significant change in contractility relative to DMSO treated controls. Statistical significance testing is based on the 1-tailed 2 sample t-test

Fig. 58: Biobot fabrication process involving 3D printed hydrogel molds, molding optogenetic skeletal muscle and assembly of the bio-hybrid structure.

Fig. 59: CytoD treatment increases the twitch length of a weak biobot and this improvement also results in translation of the biobot (which was so weak prior to treatment that it didn't exhibit net translation upon optogenetic stimulation). The yellow lines are fixed and were overlaid on the timelapse for easier visualization of the translation.

Chapter 1: Introduction

1.1 Motivation

We live in historic times due to advances in modern medicine. The discovery of antibiotics and vaccines has eradicated many fatal infectious diseases and widespread access to the modern healthcare infrastructure is transforming our lives. A byproduct of this transformation is that we live longer today than ever before; we live in an aging world. The population of people aged 60+ is increasing each year, with an expected 100M+ Americans aged 60+ expected by 2050 (**Fig.** 0). The unfortunate side effect of this aging demographic is the increase in age-associated diseases and disorders. Such disorders include age-related neurological diseases such Alzheimer's and Parkinson's disease, age-related visual disorders such as macular degeneration and glaucoma and age-related muscle disorders such as Sarcopenia.

Fig. 0: US population demographics aged 60+ (U.S. Bureau of the Census)

Sarcopenia is a skeletal muscular disorder characterized by decline in skeletal muscle mass and strength of muscle function. It is part of the so-called frailty syndrome, which is characterized by excessive decline in one's health worse than what is expected due to normal aging. Decline in muscle mass and strength leads to increased weakness and decreasing mobility for performing the same daily tasks. This leads the typical patient to exert themselves

less and less. Such lack of activity further worsens muscle function which worsens mobility even more. This vicious cycle of loss of muscle function in Sarcopenia is surprisingly common, thought to affect 1 in 4 people aged 65+.

1.2 Strategies to combat declining muscle function

Efforts combating declining muscle function could be characterized in to two types: pharmacological or non-pharmacological. Non-pharmacologically, exercise and resistance training have been shown to demonstrably improve muscle function [2-27]. However, this doesn't stop the vicious cycle of muscle loss without significant self-motivation. Pharmacologically, there have been several targeted attempts at improving muscle function. Muscle function is driven by muscle mass and muscle contractility per unit mass.

The vast majority of pharmacological strategies today target improvement of muscle mass (eg. see **Fig.** 1) . Examples include anabolic steroids that have been shown to increase muscle hypertrophy as well as formation of new muscle fibers partially through the activation of satellite cells. Landmark discoveries [28,29] about the role of the AKT/mTOR pathway in increasing muscle hypertrophy has opened up a whole decade of research [28-47] dedicated to understanding this mechanism.

Likewise, inhibiting myostatin [48-71] decreases protein breakdown and increases muscle mass as a result (**Fig.** 1).. All the above modalities have received significant attention both from academia and commercial entities pursuing therapeutic programs based on them. However, there is a lack of pharmacological interventions directly targeting the improvement of muscle contractility. Intr

Muscle contractility per unit area is driven by the intrinsic strength of the muscle fibers as well as the effectiveness of neuro muscular coupling which may change the fraction of activated muscle fibers at any given time. Both of these targets have received relatively little attention from a pharmacological standpoint. In this study, we focus on the intrinsic strength of muscle fibers and explore strategies to improve this metric.

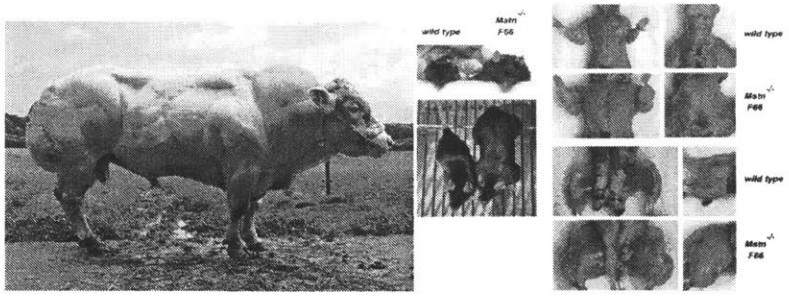

Fig.1. Cow with defective myostatin gene, as well as myostatin knockout mice displaying increased muscle mass [72]

1.3 Thesis direction and outline

Even decades after Huxley's Nobel prize winning discovery of acto-myosin sliding contraction[73,74] in striated muscle, we still don't completely understand how the acto-myosin force transmits from the sarcomeres to perform external work. We hypothesize that the non-sarcomeric cytoskeleton (f-actin structures that are not part of the sarcomeric f-actin, intermediate filaments and microtubules) plays a significant role in muscle force transmission. This is plausible because these 3 cytoskeletal structures are the usual load bearing networks within cells.

Among these 3 structures, it is likely that the non-sarcomeric f-actin is especially important as a mechanical link that helps in force transmission because of the known f-actin binding sites on the Z-disk of the sarcomeres, on dystrophin and in the integrin complex[75](**Fig.** 2A). Furthermore, the sarcomeric acto-myosin cytoskeleton follows an exquisite periodic structure that is intact even in the mechanically active environment of skeletal muscle. This leads to the hypothesis that there may be cytoskeletal structures (beyond the titin molecule that runs along each sarcomeric unit), that scaffold the sarcomeres holding them in place. If the non-sarcomeric f-actin is involved in either of these 2 roles (force transmission or sarcomeric scaffolding), it is likely that disrupting f-actin would be deleterious to muscle force transmission.

On the other hand, it is known that f-actin adds rigidity to cells. So the very presence of non-sarcomeric f-actin may impede contraction according to the Hill model of muscle contraction (**Fig.** 2B), due to the additional parallel resistance. Based on this purely biomechanical model, disrupting f-actin could improve contraction.

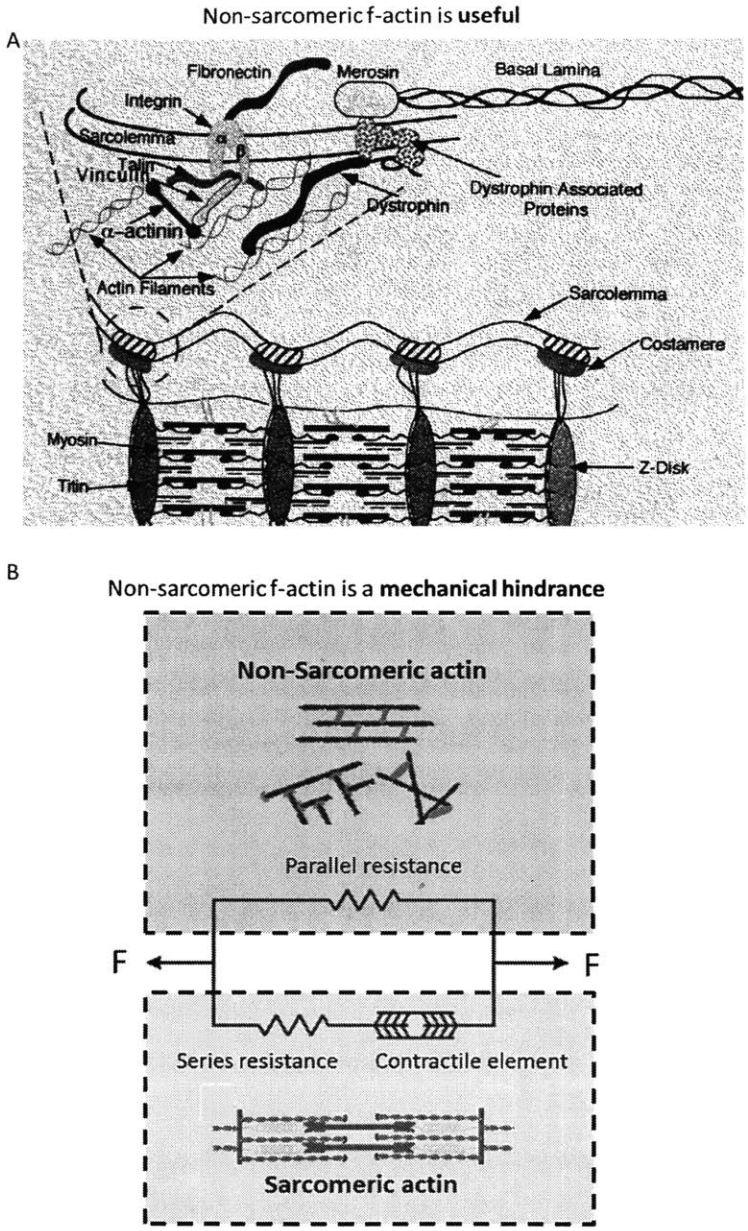

Fig.2: The unclear role of the non-sarcomeric f-actin in skeletal muscle force transmission. (A) Figure from [75]. Protein binding studies have led to the hypothesis that f-actin links the sarcomeres to the costameres (which are the sites of connection of myotubes to extracellular sites). If this f-actin link is critical, disrupting non-sarcomeric f-actin may negatively affect force transmission. (B) Alternatively the non-sarcomeric f-actin may make the cell more rigid mechanically impeding contraction. In the Hill muscle model shown, the non-sarcomeric f-actin may contribute additional mechanical resistance to the parallel element, thereby mechanically posing an additional barrier to muscle contraction. In this case, disrupting the non-sarcomeric f-actin may enhance muscle contraction.

So there are ***2 alternate hypotheses*** for the role of the non-sarcomeric f-actin:

1. Disrupting non-sarcomeric f-actin is deleterious to muscle force transmission due to interference with the ability of the sarcomere-generated force to be transmitted to external structures.
2. Disrupting non-sarcomeric f-actin enhances muscle force transmission since in normal muscle it acts to constrain contraction, acting against the muscle.

Surprisingly, to-date there is very little evidence that would conclusively support one hypothesis over another. The goal of this thesis is to elucidate the role of the non-sarcomeric f-actin to answer the question: Is the non-sarcomeric f-actin beneficial to contraction, or does it biomechanically impede contraction?

The thesis is organized as follows:

In **Chapter 2**, we develop an *ex vivo* murine skeletal muscle model and measure the contractile response of the tissue to actin disruption with Cytochalasin D. If the presence of f-actin helps force transmission, we expect the disruption of f-actin to have a significant deleterious effect on the muscle function. On the contrary, CytoD treatment of the explant reveals two distinct phenotypes, one of which shows a 2-fold improvement in muscle contractility, until the muscle stops contracting due to rigor mortis hours later. In order to verify if this phenotype of functional improvement due to actin disruption is a real biological phenomenon or merely artifactual, we need a more stable muscle model that doesn't undergo rigor mortis.

To overcome the shortcomings of the *ex vivo* model, we use an *in vitro* muscle model using optogenetically engineered skeletal myoblasts. This model doesn't undergo rigor mortis and is stable for days after peak differentiation, during which time we may perform detailed actin disruption experiments. Furthermore the optogenetic activation of muscle contraction helps decouple neuro-muscular coupling from the intrinsic muscle strength. With a 2D differentiated myotube model, we show that the active displacements of the myotubes improve almost 15-fold after actin disruption with CytoD. However, this apparent functional improvement could be due to weaker cell substrate adhesions that occur during actin disruption.

In order to rule out this possibility and to test if increased active displacements translate to increased active forces, we developed a 3D engineered mouse muscle *in vitro* model. This model has a muscle tissue cast on flexible supports and differentiated *in situ*. The displacement of the supports provides a measure of the active contractile force. Even the 3D engineered model shows a dramatic 2-fold improvement in contractile force with actin disruption with CytoD. Furthermore, we show that Latrunculin A treatment also leads to a similar level of improvement in contractility showing that f-actin disruption underlies the force improvement, not other non-specific pleiotropic effects of CytoD.

This counterintuitive functional improvement due to actin disruption led us to consider potential downsides of actin disruption. We tested if there are changes in apoptosis, cell death, mechanical integrity of the cell under an exercising stimulus, intracellular protein/organelle damage and fatigue resistance. The assays show almost no downside, with no detectable changes in apoptosis, cell death, autophagy or mechanical integrity with mild f-actin disruption. The only potential functional downside we have uncovered so far is a small decrease in fatigue resistance. This is indeed promising and very surprising that f-actin disruption, which is typically thought to have negative functional consequences, shows such a positive functional improvement in active force in skeletal muscle, with seemingly very few measured tradeoffs.

In **Chapter 3**, we perform experiments that pinpoint the dynamics of the cytoskeletal changes underlying the observed functional improvement. Using a dose response of the force to Cytochalasin D and the force recovery after washout, we hypothesize that both dynamic f-actin components as well as some of the stable actin must be disrupted. Longer term exposure to CytoD still seems beneficial at low doses, leading to the hypothesis that the sarcomeric f-actin must not be affected by CytoD.

To test these hypotheses, we performed live 3D confocal timelapse microscopy to visualize changes in f-actin structure using low doses (100nM) of a fluorogenic small molecule that binds to f-actin. These experiments reveal that Cytochalasin D disrupts the non-specific f-actin structures and long f-actin cables, while leaving the sarcomeric f-actin structures remain intact, agreeing with our earlier hypothesis. Presumably some of these well-defined f-actin cables do not recover soon after washout and this explains the irreversible improvement in contraction even after complete CytoD washout.

Furthermore, we also performed a fluorescence recovery after photobleaching (FRAP) assay to study f-actin dynamics in further detail. GFP-tagged actin monomers were transfected in to differentiated myotubes and a FRAP assay conducted. The FRAP assay revealed that the speed of f-actin turnover slows down with increasing doses of CytoD, implying that dynamic f-actin filaments that have fast turnover increasingly get disrupted with increasing doses of CytoD. This confirms our hypothesis that dynamic f-actin is getting disrupted.

To further narrow down the specific sub-compartments of f-actin that lead to functional improvement, we tested the changed in contractility with more specific actin inhibitors. As a result we found that disruption of formin mediated actin assembly also improves muscle contraction. The commonality between the CytoD treatment and formin inhibition is the disruption of several f-actin filaments leading to shorter filaments.. On the other hand, disrupting Arp2/3 mediated branched actin or f-actin filaments stabilized by tropomyosin seems to have a deleterious effect on muscle contraction, implying an essential functional role of these specific f-actin subtypes in sarcomeric force transmission.

In **Chapter 4**, we analyze the mechanistic underpinning of the force improvement. We test a mechanical hypothesis that the force improvement is due to a drop in internal mechanical resistance of the cell. To test the hypothesis, we performed experiments that capture changes in internal mechanical resistance (AFM, micro-tensile testing) as well as changes in the energetic activity of the cell. This is because, for the output contractility of a "motor" such as the muscle tissue to increase, either the input (energetic consumption) increases, energetic metabolism changes, or the efficiency of force transmission changes due to a lower internal resistance. We find that there is no significant change in energetic consumption (glucose), mitochondrial TCA cycle enzymatic activity (MTT) or mitochondrial activity (TMRE). There are no significant changes in a range of genes involved in energy metabolism as well as sarcomeric protein activity, pointing towards mechanical resistance changes as a likely candidate. Both the AFM and micro-tensile testing reveal a 50% drop in mechanical stiffness. This was to be expected as f-actin is known to have a structural role in most cells. It's just that in skeletal muscle, it seems to be over-expressed impeding its contraction. We also tested if f-actin stabilization which would potentially lead to increased internal resistances decreases force, and indeed it does. All of the above data point towards a mechanical effect that leads to functional improvement in skeletal muscle.

In **Chapter 5**, we explore practical applications of f-actin disruption and propose several future studies. The preceding sections show that the twitch force improves with f-actin disruption. Here we discuss the practical significance of this. We explore a model of walking using a 3D printed biohybrid skeletal muscle powered robot and demonstrated significant improvement in the functional performance of the bio-bot due to f-actin disruption. Future studies could be directed towards 1) testing f-actin disruption in muscle disease models 2) developing drug delivery systems and 3) discovering better targets for f-actin disruption.

Chapter 2: Effect of f-actin disruption on skeletal muscle function

2.1 Actin disruption in an ex vivo mouse muscle

2.1.2 Does f-actin disruption enhance muscle contraction ex vivo?

In this thesis, we primarily explore the role of the actin cytoskeleton on the functional output of skeletal muscle, namely active force transmission. As a model system, we start with an *ex vivo* mouse muscle to study this. To re-iterate the two alternative theories discussed in the previous chapter (Sec. 1.3), it is unclear if disrupting f-actin might improve skeletal muscle contraction (if f-actin mechanically impedes contraction) or worsen it (if f-actin has an essential function in skeletal muscle cells, perhaps in linking the sarcomeres to the ECM)? In this section, we experimentally measure the change in contraction due to f-actin disruption to test these two theories.

2.1.3 Experimental model

2.1.3.1 Tissue dissection

We measure the change in muscle function in a mouse hindlimb extensor digitorum longus (EDL) muscle explant model due to f-actin disruption using Cytochalasin D (CytoD). Our rationale for choosing the EDL explant model is as follows:

The mouse EDL muscle explant model is an appropriate model for 3 reasons: 1) mouse hindlimb muscles have been used for several studies of human muscle disorders [76-83] 2) mature muscle tissues such as this are more appropriate to test our hypothesis that dynamic f-actin may not be essential for mature skeletal muscle tissue function than using in vitro engineered muscle models which are still developing tissues 3) EDL muscles are structurally convenient to test this hypothesis. Being thinner than other muscle tissues (the tibialis anterior or soleus muscle tissues), we hypothesize that EDL tissues may be more viable after dissection than much thicker muscle tissues such as the tibialis anterior or soleus muscles. Furthermore, small molecule actin disrupters such as CytoD may diffuse through the EDL muscle tissue more completely in shorter timescales than thicker alternatives. Furthermore, it

has well-defined and intact tendons at both of the ends, permitting easier handling and anchoring without damaging the muscle fiber belly.

All muscles in this study were harvested from 2-3 month old male C57BL/6 mice which were sacrificed for an unrelated study and obtained with approval from the MIT Committee on Animal Care. First, skin was removed from both hind limbs to expose the hind limb muscles and fascia was removed from over the tibialis anterior (TA) muscle (**Fig.** 3). The distal TA tendon was cut and then pulled to peel the TA muscle from the limb. The TA muscle was carefully dissected at its proximal attachment and discarded. Sterile gauze was used to absorb excess bleeding caused by the rupture of vessels in the TA muscle. The distal EDL tendon was then cut with microscissors and then pulled gently to peel the EDL muscle from the limb. An incision was made in the distal portion of the biceps femoris muscle to expose the proximal extensor digitorum longus (EDL) tendon and subsequently the proximal EDL tendon was cut with microscissors. The EDL muscle with associated tendons was then removed from the hind limb (**Fig.** 4) and submerged in an isotonic medium (DMEM + 10% FBS + 1%PS) cooled on ice until functional assays were performed. These muscle explants are viable up to 12 hours after dissection if kept in ice. If at room temperature or 37C, the explant rapidly undergoes rigor mortis within 3-4 hours and does not contract any further.

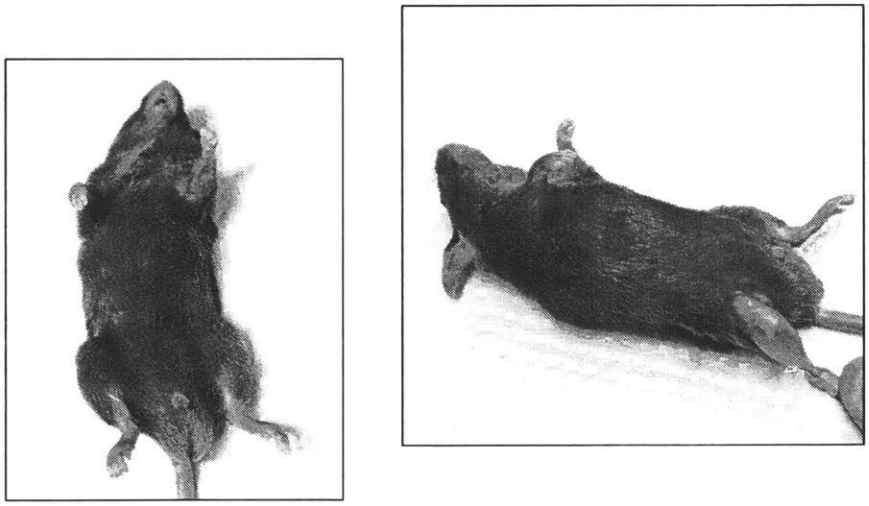

Fig. 3: Euthanized 2-3 month old wild type male mouse with skin removed ready for muscle dissection. Dissection was complete within an hour of sacrificing the animal.

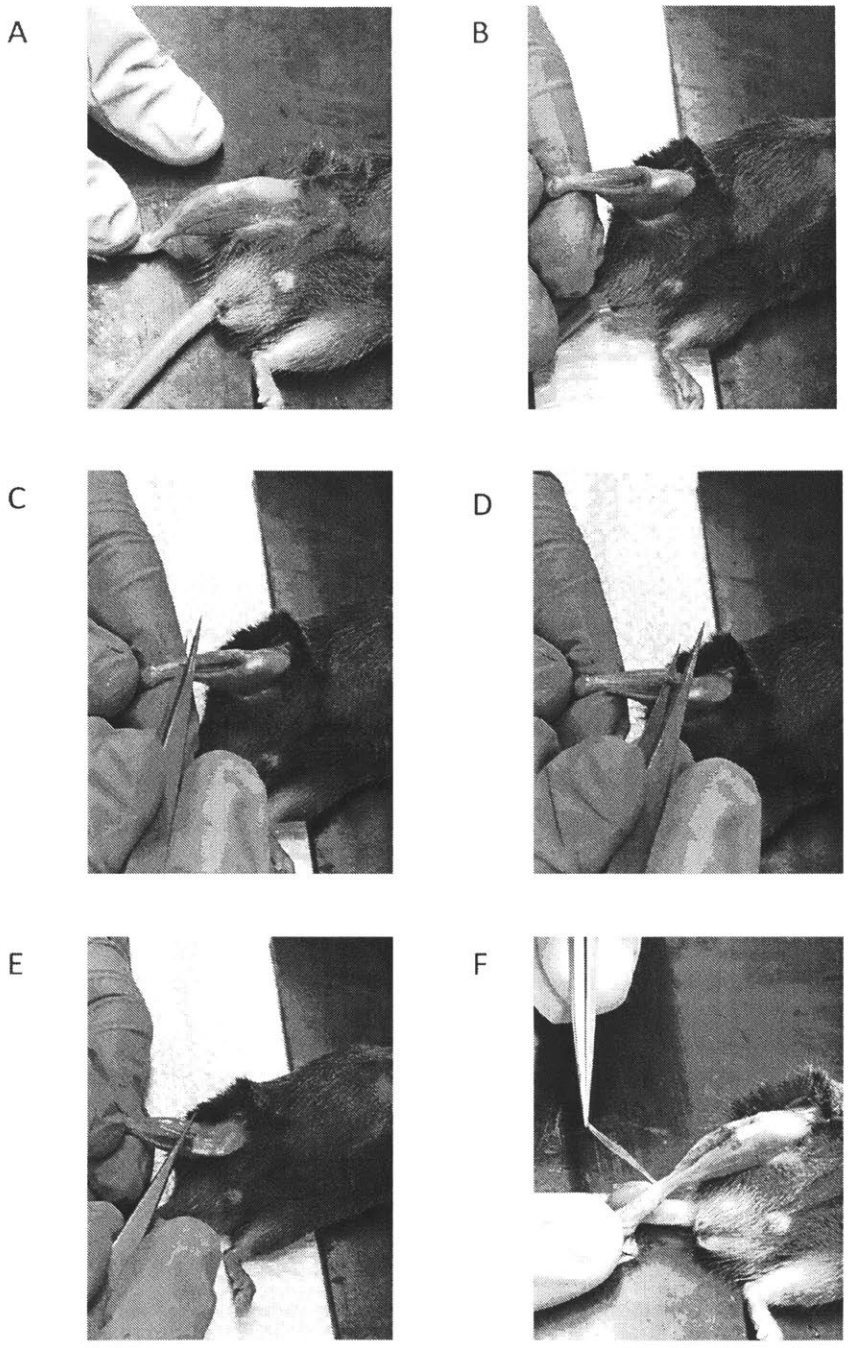

Fig. 4: EDL Muscle dissection from the hindlimb. (A-E): Sequential steps of dissection involving removing the tibialis anterior muscle as well as isolating the EDL muscle from the rest of the muscle belly. (F): dissection of the proximal tendon of the EDL muscle.

2.1.3.2 Contractility measurement

We designed a setup to mount the EDL muscle explants on flexible cantilevers with kapton cantilevers (8N/m stiffness) as supports. The features of the setup being the ability to mount an EDL muscle on the cantilever, with in built electrodes for electrical stimulation of the muscle and the ability to adjust the resting length of the muscle using an anchor slidable with a micromanipulator.

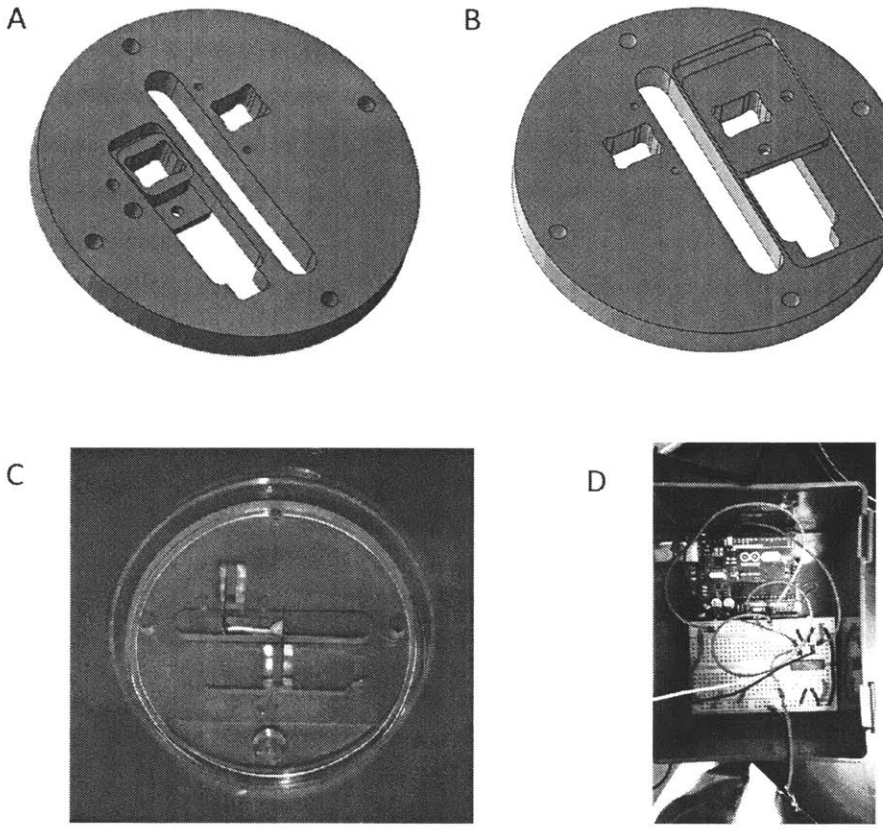

Fig. 5: Tissue mount for the EDL muscle explant with adjustable length and built-in electrodes for electrical stimulation. (A and B) The CAD models show the top (A) and bottom (B) of the assembly respectively, with the slidable anchor that is used to adjust the resting length of the muscle. (C) Kapton based cantilevers are held together with an acrylic-silicone-acrylic sandwich and inserted in to the rectangular through-holes of the anchor. Furthermore, an EDL muscle tissue is bonded to the cantilever anchors as shown (D) An Arduino and motor driver setup is used for electrical stimulation of the muscle tissue.

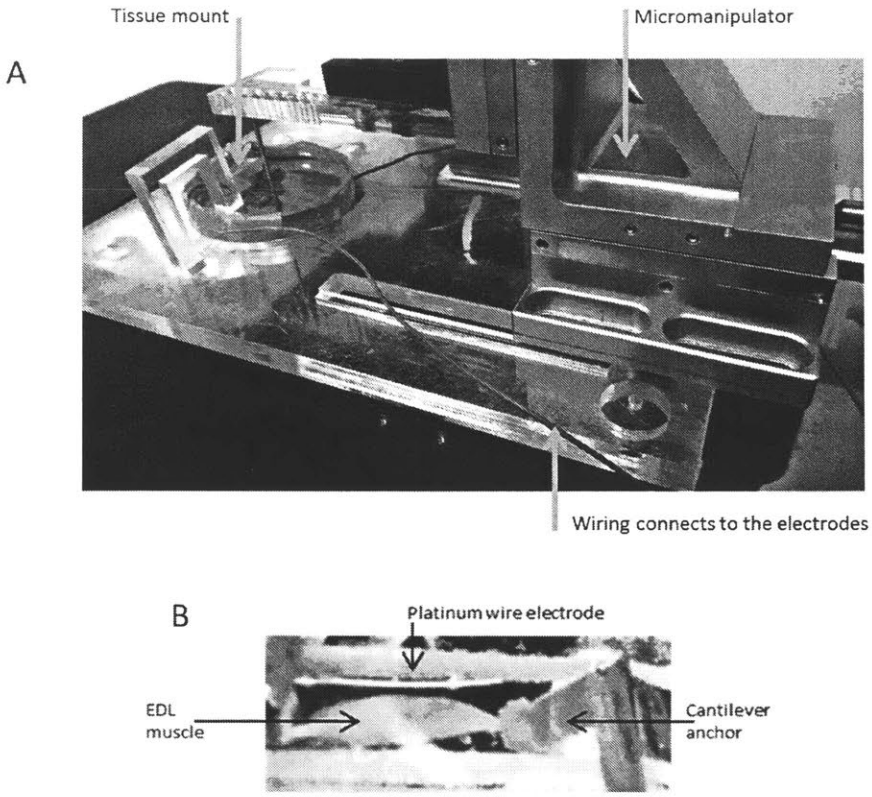

Fig. 6: Overall EDL muscle explant assembly connected to a circuit for electrical stimulation. (A) Zoomed-out view of the tissue mount with the EDL muscle connected to the micromanipulator for length adjustment. (B) Zoomed-in view showing the mounted EDL muscle with platinum wire electrodes on either side of the muscle

A drop of cyanoacrylate (quick dry super glue) was applied to the tip of the kapton supports and was allowed to partially set for 30s. At this point, the EDL muscle explant that was stored in ice cooled medium, was held with a pair of precision tweezers, primarily held by the tendons so that damage to the muscle belly was minimized. Then we carefully attached the tendons to the supports and held it in place for 30 more seconds to fully set. At this point, warm medium 37C was added to the explants quickly so that they do not dry out. The explant was incubated in this medium for 10 minutes without any electrical stimulation to wait for the tissue to warm up. The electrical stimulation setup was ready, connected to a 15V power supply that can provide an electric field of 15V/cm across the muscle tissue. The electrical stimulation parameters were 30Hz pulses with pulse width of 5ms, which led to a twitch of the muscle. A tetanic stimulus (>=100Hz) was not applied in order to delay fatigue and rigor

mortis of the muscle tissue for as long as possible. This was necessary as the explant is expected to undergo rigor mortis, not being perfused like when *in vivo* in the animal. Furthermore, a direct *in vivo* testing of CytoD would not be ethical as it is known to have significant cardiotoxic effects.

2.1.4 Results and Discussion

2.1.4.1 F-actin disruption in ex vivo mouse muscle improves contractility in a responsive subset of specimens

First, we verified that CytoD treatment does disrupt f-actin in explant tissues. We treated explant tissues with CytoD 3μM or DMSO for 1 hour and fixed the tissues. These tissues were stained with phalloidin to visualize the presence of f-actin. As shown in **Fig.** 7, it appears that CytoD does disrupt f-actin in these tissues.

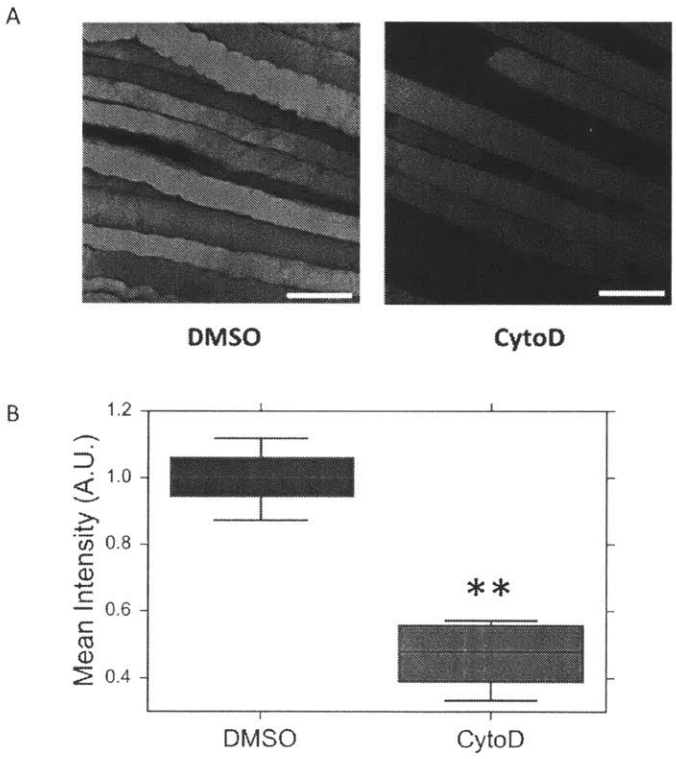

Fig. 7: CytoD disrupts f-actin in mouse explant muscle tissues. (A) Phalloidin (Alexfluor 647) stained tissues of muscle EDL explants with CytoD 3μM or DMSO for 1 hour reveal that CytoD does disrupt the f-actin structures as reflected by lower phalloidin intensity under identical fluorescence microscopy settings. Scalebar is 60μm. (B) The intensity changes were

quantified with respected to the mean DMSO intensity (n=6). The changes are statistically significant, as analyzed by a one-tailed 2-sample t-test $p = 7.59*10^{-6}$

At this point, the length of the tissue was adjusted in increments of 100μm using the micromanipulator, with electrical stimulation applied at each length to find the peak contraction, measured optically via deflection of the kapton supports. The length was fixed at this point and the electrically stimulated contraction measured every 10 minutes for 60 minutes. As shown in **Fig.** 8, the explants become less functional with time, perhaps due to the natural incidence of rigor mortis in non-perfused excised tissues.

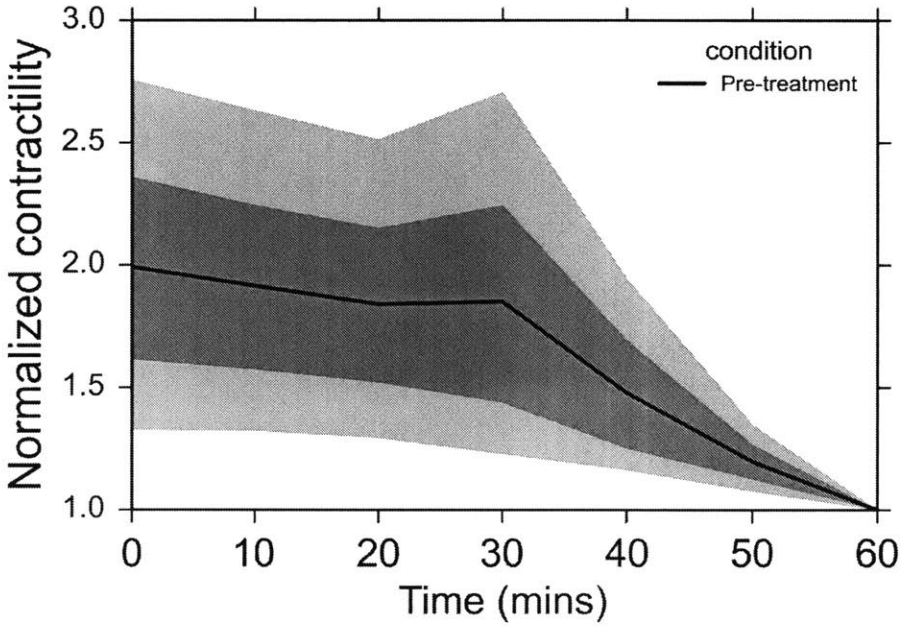

Fig. 8: Decline of EDL muscle explant contractility with time, normalized with respect to the contractility at 60 mins. The two colored envelopes represent the 68% and 95% confidence intervals (1 and 2 sigma) of the data. The data represents the average and variation of 14 explant samples.`

At 60 mins, we introduce our intervention, fresh medium containing either 3μM CytoD or the carrier DMSO, and continue to monitor changes in the muscle function for 2 more hours or until rigor mortis sets in. While, all the DMSO treated control tissues display a monotonic decline in muscle function until complete rigor mortis sets in, we noticed 2 qualitatively

different response phenotypes in the CytoD treated tissues. Roughly 50% of the CytoD tissues decline in function in a matter similar to that of the DMSO treated tissues (**Fig.** 9). This makes it seem like CytoD has no effect on explant tissue contraction. Also, it doesn't seem to accelerate the decline any further than DMSO treated controls. This implies that either CytoD does not disrupt any of the actin (this is not true, as shown in **Fig.** 7), or disrupting f-actin has no effect on muscle contraction. The later supports neither of the two hypotheses discussed in the beginning of this chapter (and Sec. 1.3).

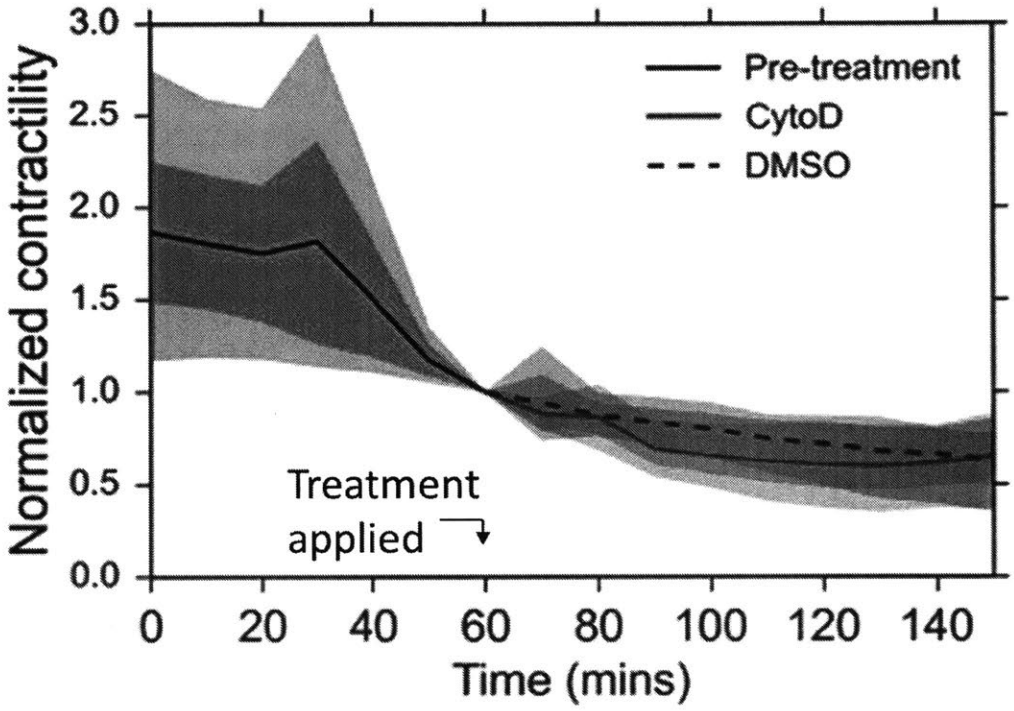

Fig. 9: About half of the CytoD treated tissues (n=5) decline in contraction just like DMSO treated controls (n=5). The natural decline of all tissues was measured once every 10 minutes for 1 hour. After 1 hour, either DMSO or CytoD 3μM was applied to the tissues. The two colored envelopes of each kind grey, blue and red each represent the 68% and 95% confidence intervals (1 and 2 sigma) of the corresponding data

However, in the other half of the CytoD treated tissues (**Fig.**10), we notice a transient *improvement* in overall function to ~2X the contractility just before treatment followed by a decline. The average tissue contractility in this set of CytoD treated tissues was statistically

significantly improved relative to the DMSO treated controls (the mean CytoD curve lies outside of the 95% envelope of the DMSO treated controls). The response of this set of tissues supports the hypothesis that f-actin disruption enhances contraction (perhaps due to lowering of the mechanical hindrance posed by f-actin).

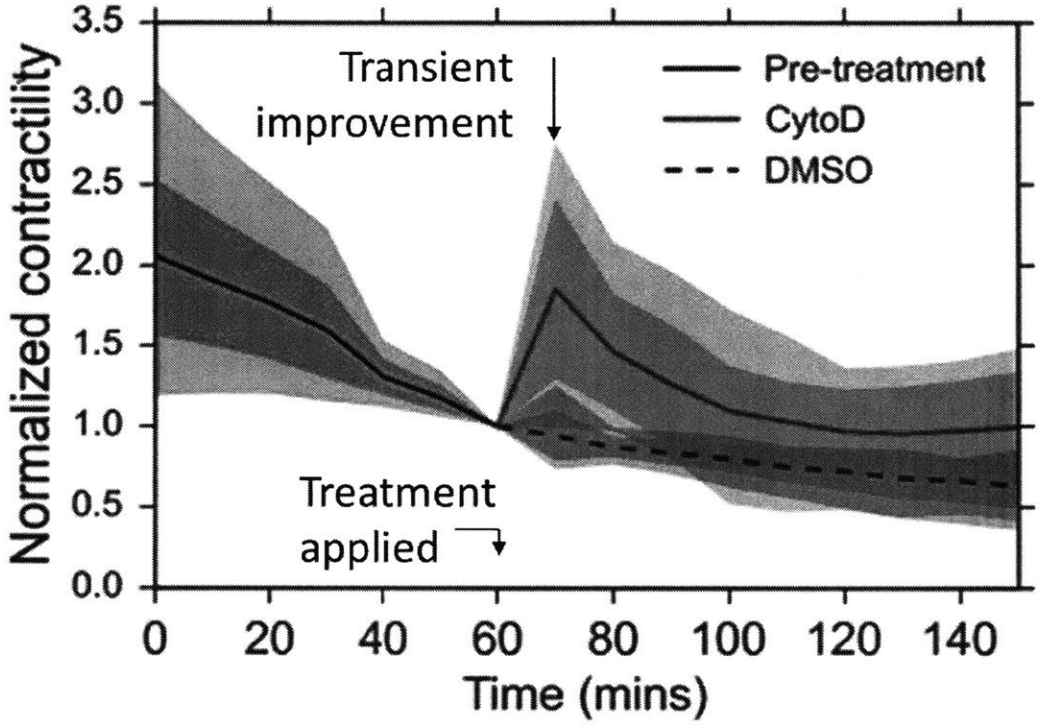

Fig. 10: About half of the CytoD treated tissues (n=4) exhibit a transient improvement in contraction just like DMSO treated controls (n=5). The natural decline of all tissues was measured once every 10 minutes for 1 hour. After 1 hour, either DMSO or CytoD 3μM was applied to the tissues. The two colored envelopes of each kind grey, blue and red each represent the 68% and 95% confidence intervals (1 and 2 sigma) of the corresponding data

2.1.4.2 Conclusion and limitations of the explant model

Overall, this experiment shows that f-actin disruption *may* have a beneficial effect on skeletal muscle tissue contraction. However, admittedly the explant experiment is not conclusive due to the variability in response observed, and if all the data are combined, the increase is still apparent but lacks statistical significance. There could be several sources for the observed variability: 1) inherent animal to animal, and tissue to tissue variability (we tried to minimize any potential bias due to this by using both EDL muscles from a given animal for

CytoD and DMSO respectively). 2) variability in tissue dissection. Tissue dissection has its inherent variability due to the difficulty of handling and cutting the small EDL muscle from the mouse hindlimb. Moreover, the epimysium covering the EDL muscle may be damaged to differing extents which could alter the transport properties of CytoD and the tissue response 3) variability in tissue mounting. This too is variable and may sometimes lead to drying out of the tissue while mounting.

On top of the variability, the rigor mortis of the tissue is by far the biggest limitation of the explant experiment. The fact that the tissue is not perfused outside of the animal causes the rigor mortis shown in **Fig.** 8. This makes it impossible to study the long term response to f-actin disruption. A key unanswered question is the following: *if rigor mortis was not a concern, is the functional improvement due to f-actin disruption transient or persistent*? Due to the limited lifetime of explants, we need other methods to test this. To overcome these limitations of explant-function measurements, we develop an in vitro engineered muscle tissue model by differentiating mouse myoblasts either in 2D or 3D.

2.2 F-actin disruption in a 2D in vitro model

2.2.1 Hypothesis: F-actin disruption improves 2D myotube contraction

Drawing upon the preliminary findings of the explant experiment, we hypothesize that F-actin disruption with CytoD improves 2D myotube contraction. We want to create a model that is stable for the time course of the experiment, does not undergo rigor mortis and test its response to f-actin disruption.

2.2.2 Experimental model

2.2.2.1 Optogenetic C2C12 2D myotube differentiation

We used the murine myoblast cell line C2C12 (ATCC) and transfected them with a pLenti2-EF1a-ChR2[H134R]-tdTomato-WPRE plasmid to express a mutated variant of the light-sensitive ion channel, Channelrhodopsin-2(ChR2[H134R]) as shown in **Fig.** 11. Detailed protocols are described elsewhere[84]. Briefly, cells were transfected with 10 mg of EF1a-ChR2[H134R]-tdTomato, 15mg of psPAX2, 10 mg of pMD2.G, 100 ml of Lipofectamine 2000 (ThermoFisher), and 200 ml of PLUS Reagent (ThermoFisher). Lentiviral packaging plasmids (psPAX2 and pMD2.G) were a gift from D. Trono (Addgene, plasmid #12260 and #12259).

C2C12 cells were grown until 70% confluence in a T150 flask and re-suspended in a Matrigel coated (100ug/ml, 1hr at 37C) IBIDI-treat 35mm dish at a density of 500K cells per dish. Cells were cultured in growth medium (Dulbecco's Modified Eagle Medium (DMEM) supplemented with 10% fetal bovine serum (FBS), 1% penicillin and streptomycin (PS) until they reached confluence. At this point, they were switched to myogenic differentiation medium DM, composed of DMEM supplemented with 4% horse serum (HS), 50 ng/ml mouse insulin-like growth factor-1 (mIGF-1), 1 mg/ml ε-aminocaproic acid (AA) and 1% PS. All cells were cultured at 37°C with 5% CO2 in a humidified incubator.

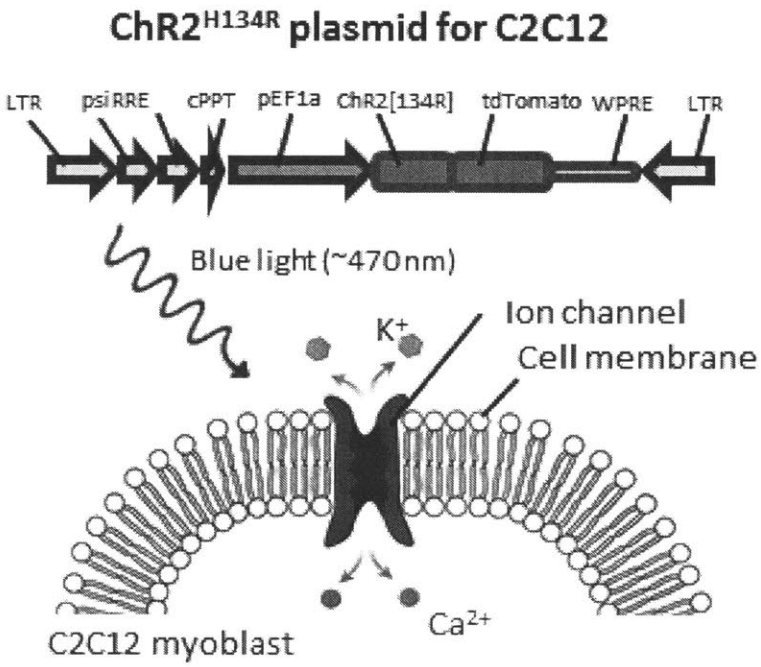

Fig. 11: C2C12-ChR2[H134R] plasmid schematic

2.2.2.2 Optogenetic stimulation

At day 12 after introducing differentiation medium, the differentiation of the cells was checked by exposing the cells to blue light. Optical stimulation was performed using a SOLA light engine (Lumencor) excitation unit. The blue light emission peak is at 470nm. Blue light was supplied through Zeiss filter set #38 (BP 470/40). The optical stimulations of the differentiated myofibers was conducted through a 4× objective, yielding an irradiance of 1.2

mW mm^{-2}, both the highest intensity of the Lumencor engine as well as an intensity higher than the intensity at which the contraction started to plateau (~0.6mW/mm^2). The shutter was controlled via the TTL port of the Lumencor engine through an Arduino Uno board.

2.2.3 Results and Discussion

2.2.3.1 CytoD increases 2D myotube active contractions 14-fold

Cells were stimulated with blue light pulses (5ms ON, 30Hz) to record the active displacement prior to CytoD treatment. They were then treated with CytoD 3μM or DMSO for 30 minutes. **Fig.** 12 shows the change in morphology. The change in active displacements was significant with CytoD as also illustrated in **Fig.** 12 using an index of movement metric, (I(0.5s)-I(0)), normalized within each condition, and color mapped between 0 (blue) and 255 (red). The active displacements were quantified using the ImageJ Mosaic 2D particle tracking plugin by tracking 200 random points on myotubes in both the DMSO and CytoD treated samples, before and after treatment. DMSO treated cells showed only a small change in average active displacements before and after treatment (0.89 to 1.02μm), while CytoD treated tissues showed a very significant increase in the contraction, an increase in the average active displacements of approximately 14-fold from 1.4μm to 20μm ($p < 0.0001$, one-tailed Mann-Whitney U-test) as shown in **Fig.** 13.

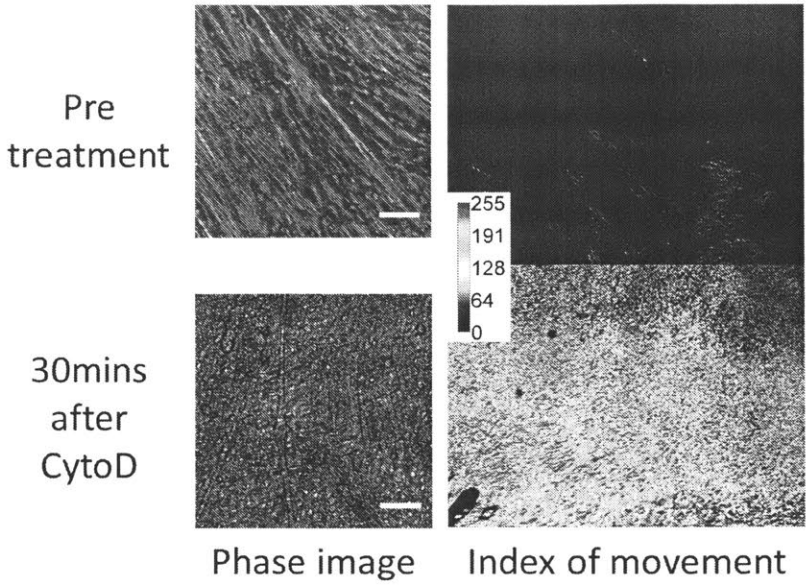

Fig. 12: Effect of CytoD 3μM (30 mins) on change in morphology of C2C12 myotubes grown on IBIDI-treat dishes. Scalebar is 100um. Also shown is the change in index of movement with CytoD application, which is a measure of change in local pixel grayscale values with time. Closer to red is indicative of larger pixel changes, which happens when there are larger displacements. Closer to blue indicates almost no displacement, indicating areas without any contraction.

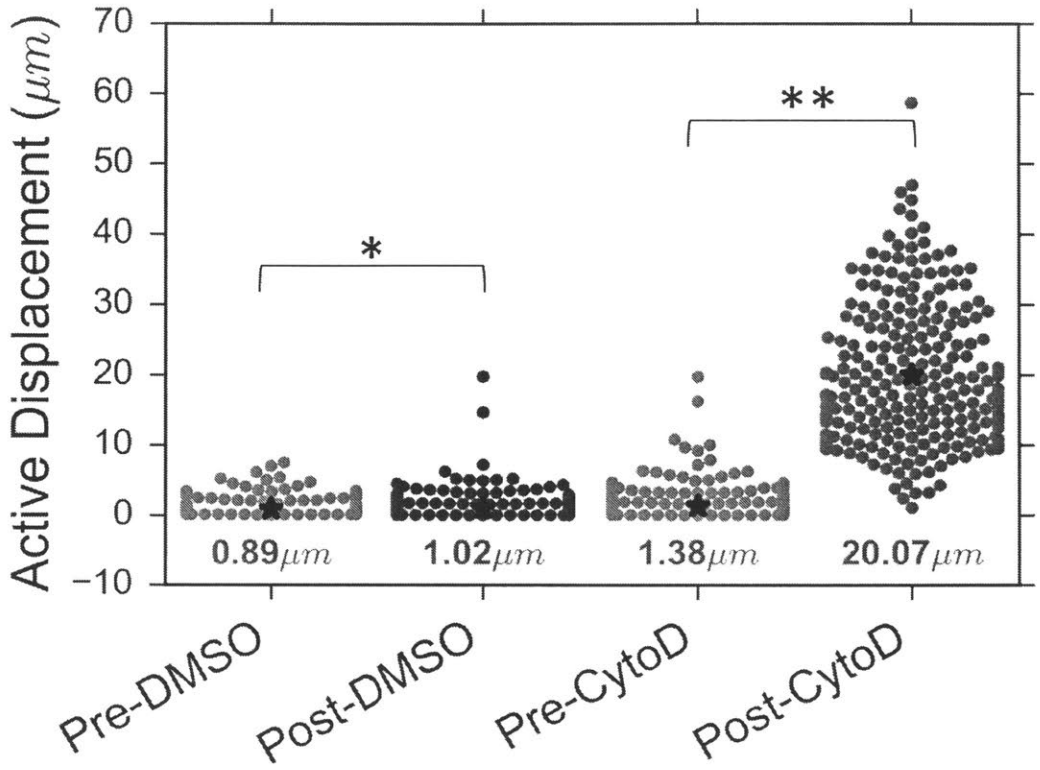

Fig. 13: Effect of CytoD 3μM (30mins) and DMSO on change in active displacements of C2C12 myotubes grown on IBIDI-treat dishes. CytoD treatment dramatically increases the active displacements of the myotubes, while DMSO treated controls result in only a very mild increase. The five point star points to the mean values of the displacements, which are also shown in green below the swarm plot. * p = 0.0045 One-tailed Mann Whitney U-test. ** p < 0.0001 One-tailed Mann Whitney U-test

2.2.3.2 Conclusion and limitations of the 2D myotube model

In conclusion, clearly f-actin disruption using CytoD treatment amplifies the active displacement significantly. This is yet another surprising result in the context of our general understanding of the importance of f-actin to cellular function. However, it does partly support the improved active contractility observed in the *ex vivo* model.

One of the limitations of this model is that increased active displacements do not necessarily translate to increased active forces. This is because with CytoD treatment the 2D cell monolayer detaches from the surface and eventually collapses (by 1-2hours). This change in

cell substrate adhesion could explain the increased contractions as the monolayer probably faces very little resistance from the substrate. In order to control for this factor, and to measure actual forces, we developed a 3D muscle tissue model.

2.3 F-actin disruption in a 3D in vitro model

2.3.1 Hypothesis: F-actin disruption improves 3D muscle force

The 2D model is unstable when treated with 3μM CytoD in that the monolayer collapses after an hour. This weaker cell-substrate adhesion could result in increased active displacements. So in order to quantify change in forces with skeletal muscle contraction, we developed a stable 3D muscle tissue model.

2.3.2 Experimental model

2.3.2.1 Fabrication of the force sensing support and mount

A 1/16 in optically clear acrylic sheet (McMaster) was cut with rectangular through holes using an Epilog 120W CO_2 based laser cutter. Also two cantilevers were cut out of 0.125mm thick kapton sheets (McMaster) using a UV laser cutter with a tiny 0.65mm hole at their tips for the muscle tissue to pass through. One of the cantilevers was compliant with an estimated stiffness of 0.34 N/m, while the other cantilever was much stiffer with an estimated stiffness of ~8N/m. Estimations were based on COMSOL 3D elastic FEM simulations of clamped cantilevers. The concept is to cast a thin cylindrical shaped muscle tissue anchored in 3D between the two cantilevers and optogenetic stimulation would only lead to minute displacements of the compliant cantilever which could be recorded using an optical microscope. The two cantilevers were assembled on the acrylic backbone with further acrylic cutouts and a silicone gasket as shown in **Fig.** 14, such that the faces of the cantilevers were parallel to each other, with a 3mm gap between the two and such that the holes at the tip of the cantilever were aligned coinciding with each other.

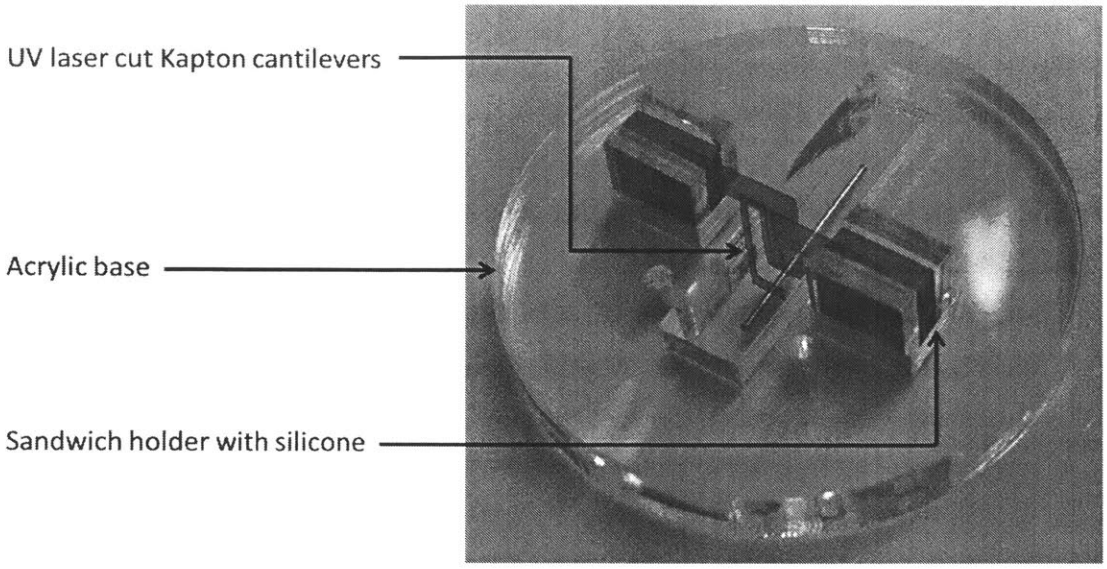

Fig. 14: Acrylic/kapton base mount for 3D muscle formation and force sensing. The distance between the faces of the 2 cantilevers is 3mm. Also the entire acrylic base was inserted to fit snugly in a regular 35mm petri dish.

2.3.2.2 Fabrication of the 3D differentiated muscle bundle

The skeletal muscle tissue was cast using a sacrificial molding technique described in detail elsewhere[1]. Briefly, the acrylic mount shown in **Fig.** 14 was autoclaved at 121C for 45 minutes, dried for 30 minutes and then placed in a 35mm petri dish using a pair of sterile tweezers. A sterile stainless steel rod 0.02in in diameter was aligned and inserted through the holes of the cantilever. 50mg/ml porcine skin based gelatin, dissolved in GM+, which is growth medium (DMEM + 10% FBS + PS) supplemented with 1 mg/ml ε-aminocaproic acid (AA) and warmed up to 37C was pipetted in to the rectangular cavity containing the steel rod and the cantilevers as shown in Figures 14 and 15. This was then rapidly cooled in a -20C freezer for 5 minutes to partially solidify the gelatin liquid. At this point, the gelatin away from the cantilevers was aspirated using a Pasteur pipette, leaving the gelatin in between the cantilevers intact. This was cooled down to -20C again for 10 minutes to allow the gelatin to fully solidify. The steel rod was then removed carefully from the assembly using a pair of sterile tweezers, leaving a cylindrical cavity in the gelatin for the muscle tissue. C2C12-ChR2 cells were trypsinized and resuspended in a mixture of 10% Matrigel (Corning, growth factor reduced), 2UI/ml thrombin, 2.5mg/ml Fibrinogen at a cell density of 15M/ml. 10μL of this solution was inserted into

gelatin cavity with a 10μL pipette tip held carefully close to the edge of the cylindrical cavity. Capillary action would typically lead to the gel filling the entire cylindrical cavity. Lastly, 5μL of this cell gel solution were pipetted specifically on each end of the cantilever to form cell-based anchors.

After the gel fully polymerized (20 minutes at room temperature), 2ml of GM+ was added to the dish and the assembly incubated at 37C overnight. During this time, the cells compact, generate tension and form an aligned dense tissue of myoblasts. The gelatin melts at 37C and is slowly diluted away with medium changes.

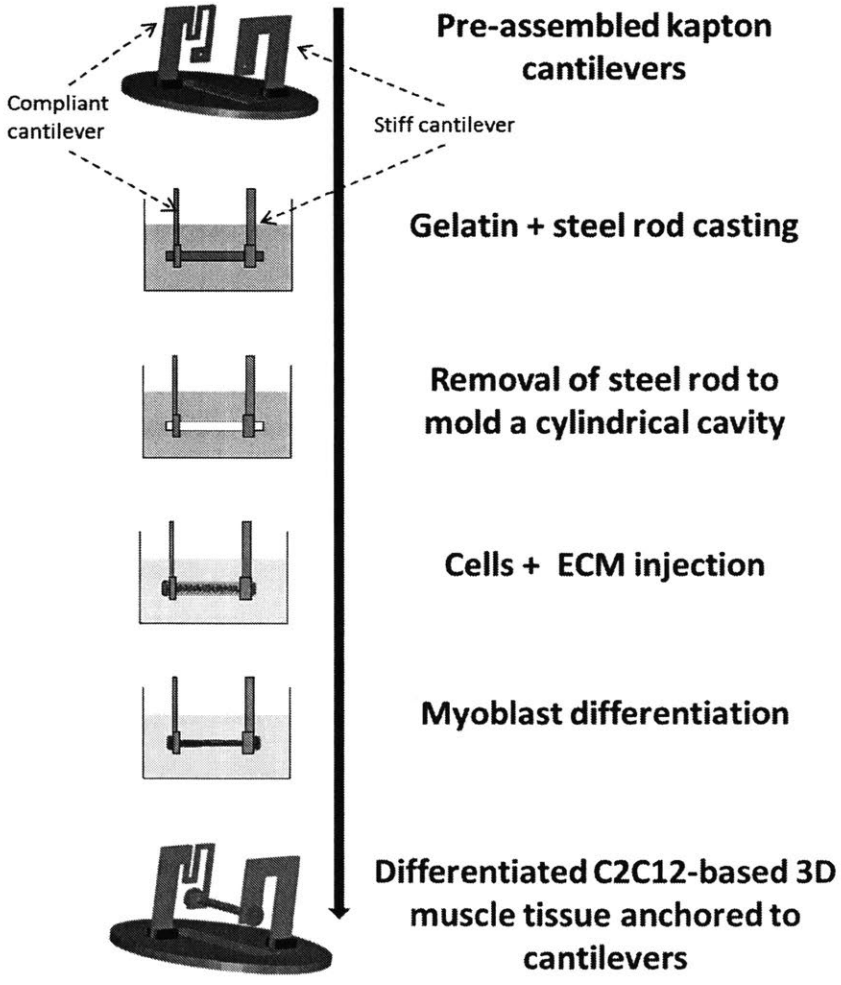

Fig. 15: Sequential process for the fabrication of a 3D muscle bundle attached to a compliant and a rigid cantilever, for measurement of optically stimulated contractile force. Process adapted from the sacrificial molding process described elsewhere[1]

Two days after cell seeding, the medium in the culture was switched to myogenic differentiation medium DM+ (DMEM + 4% horse serum + PS + AA), supplemented with 50ng/ml mouse IGF-1. By day 4 after switching, we may start observing some twitches with optogenetic stimulation. But by day 8-12, the optical stimulation leads to tetanic contractions, a sign of mature muscle (**Fig.** 18). The f-actin disruptions are conducted on day 12 (after switching) unless otherwise stated.

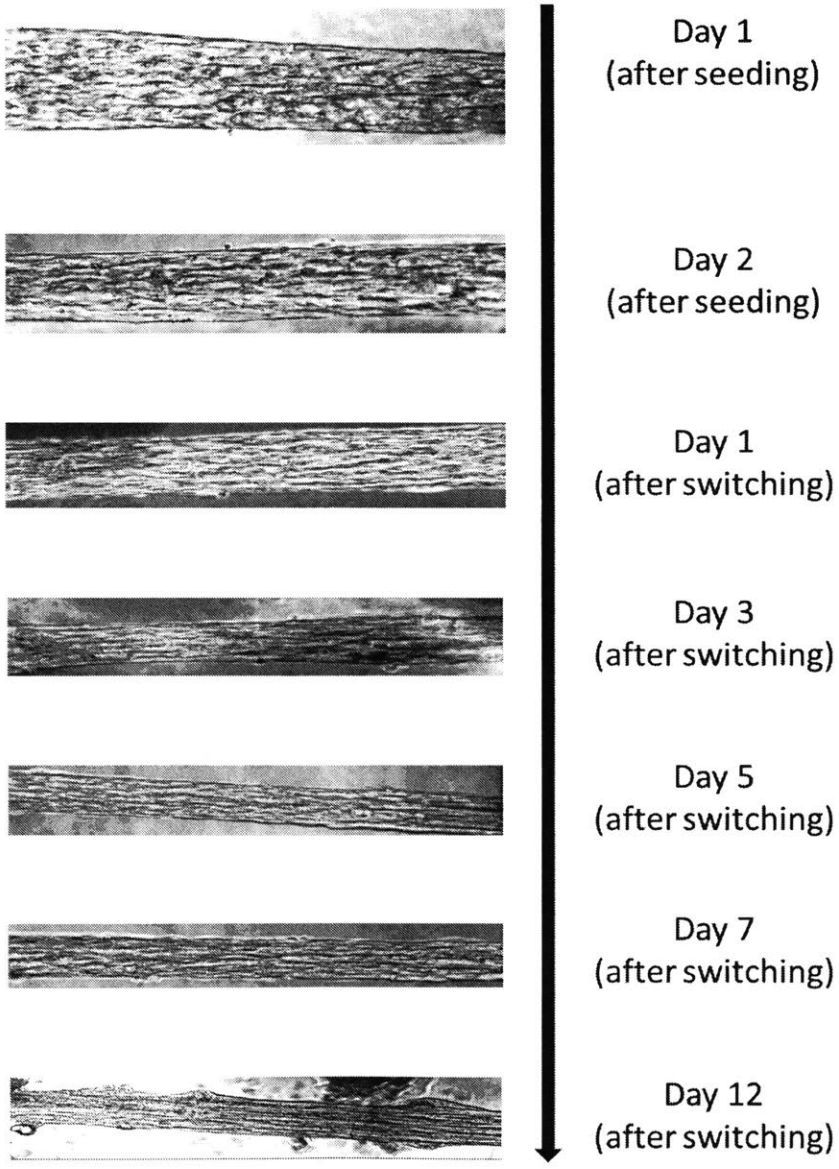

Fig. 16: Phase contrast images of the development of the muscle fiber bundle. The myoblast/ECM gel compacts soon after cell seeding and compacts successively over the course

of the differentiation. In this case, the culture was switched to differentiation medium 2 days after cell seeding and the final assay (force, stiffness etc.) was conducted on day 12 after switching.

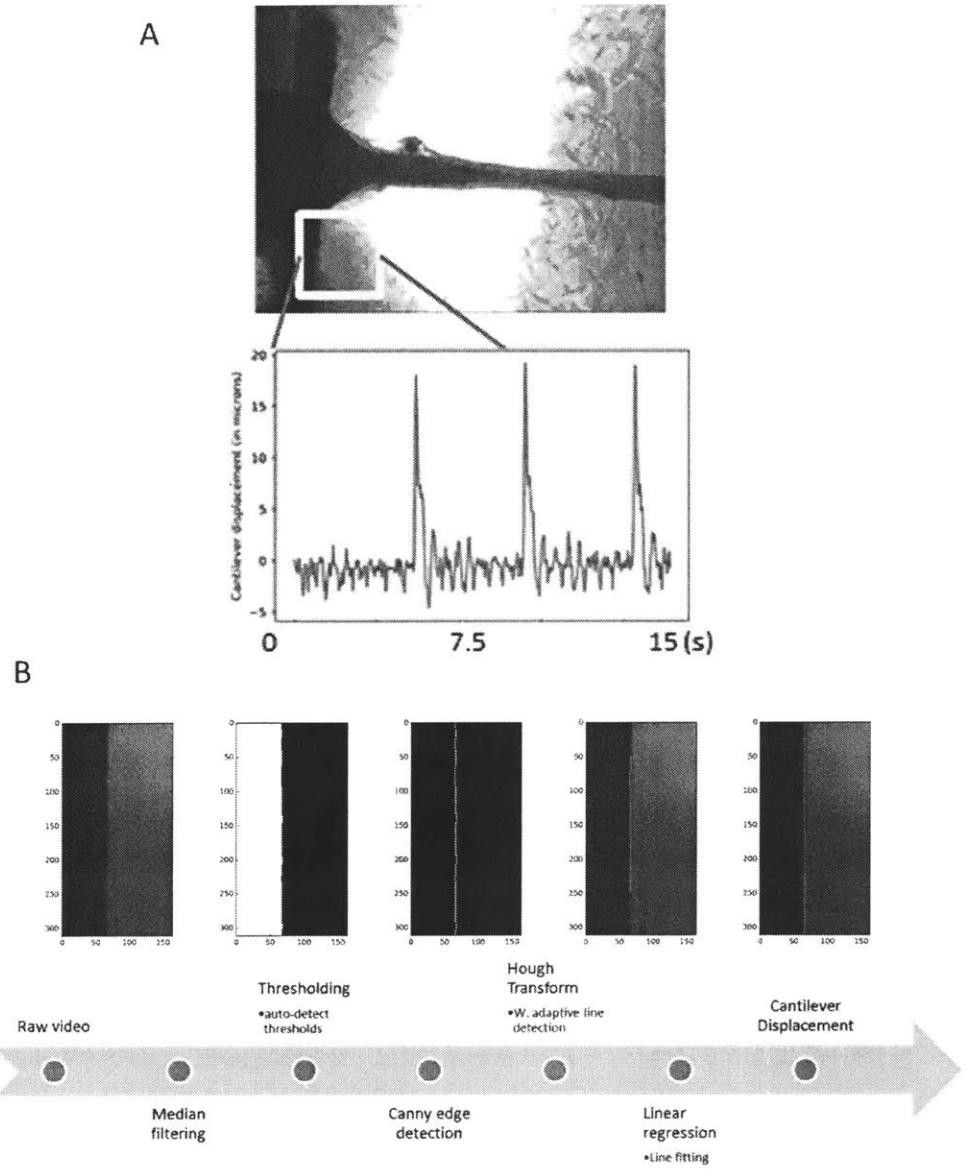

Fig. 17: Image processing pipeline to detect (A) cantilever active movement. (B) A typical pipeline is shown with the final output of the algorithm being the position of the edge of the cantilever as shown in red overlaid on top of the raw image. The green lines are many lines output by the Hough transform algorithm which detects many lines along the cantilever edge. A linear regression is then performed to estimate a single edge based on all these edged

(shown in red). The position of this cantilever is tracked over time to estimate the displacement (both the x-location and slope of the line are considered).

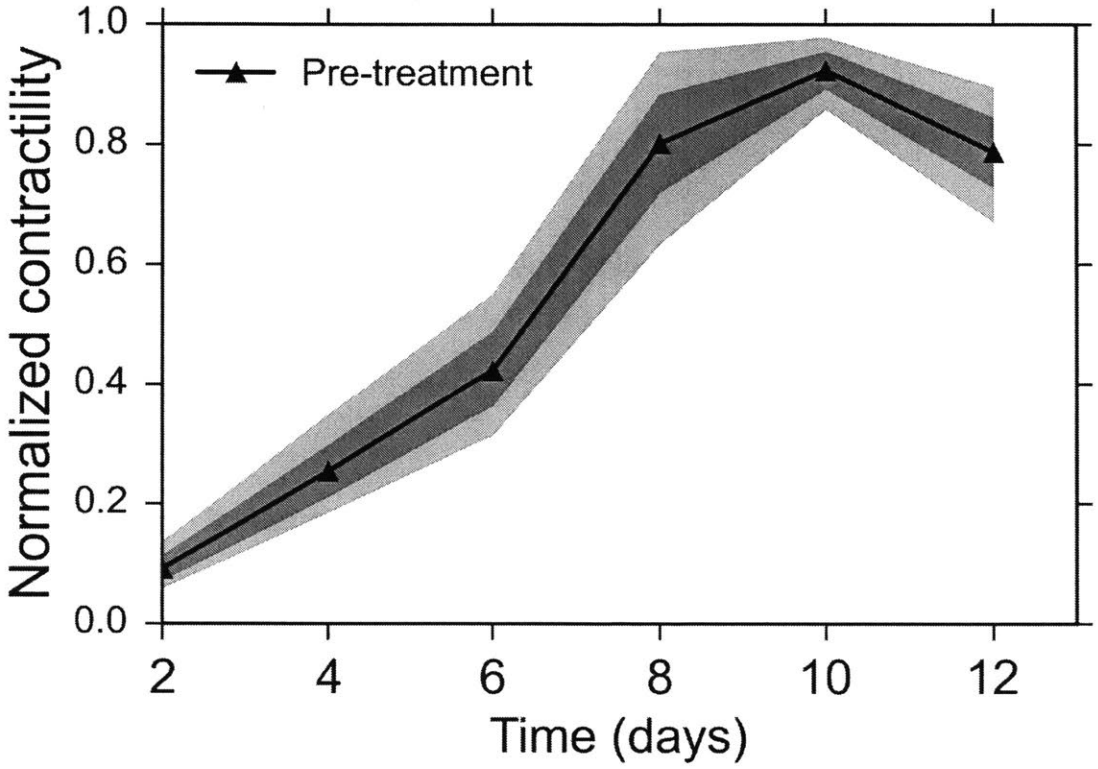

Fig. 18: Time-course of active contraction of C2C12 based 3D muscle tissues. The contractility seems to saturate (or change slower) after day 8 and peak contraction is reached between day 8-12. The two colored envelopes represent the 68% and 95% confidence intervals. n = 10 independent muscle fibers were used for this experiment. The contractility of each muscle fiber was normalized with respect to its respective maximum during the time-course of differentiation.

2.3.2.3 Optical stimulation and active force quantification

The muscle fibers were simultaneously imaged with phase contrast microscope and optically stimulated with a 5ms ON, 30Hz blue light pulse using the 10X objective. Blue light was supplied through Zeiss filter set #38 (BP 470/40). The optical stimulations of the differentiated myofibers was conducted through a 10X objective, yielding an irradiance of 7.5mW mm^{-2} and controlled via the TTL port of the Lumencor engine through an Arduino Uno board. Videos of the stimulation were acquired at 30 frames/s or higher by focusing on a small pixel area (~ 150-300 by 300 pixels) at the edge of the compliant cantilever as shown in **Fig.**

17. The high frame rate is to ensure that we catch the peak, at which the cantilever stays for more than 1 frame.

The video was processed frame by frame using software written with Python OpenCV libraries (Appendix 2). Essentially an edge detection algorithm using the Hough line finding algorithm implemented on OpenCV was used to find the cantilever edge. The edge was tracked over time to find the peak displacement.

2.3.3 Results and Discussion

2.3.3.1 3D mouse muscle contractility increases with f-actin disruption

The 3D engineered muscle tissue was treated with CytoD 3μM or DMSO 12 days after differentiation. Changes in contraction with CytoD application were observed as early as a 2 minutes, but statistically significant differences between the CytoD and DMSO controls are observed by 15 minutes ($p < 0.05$) and thereafter as illustrated in **Fig.** 19.

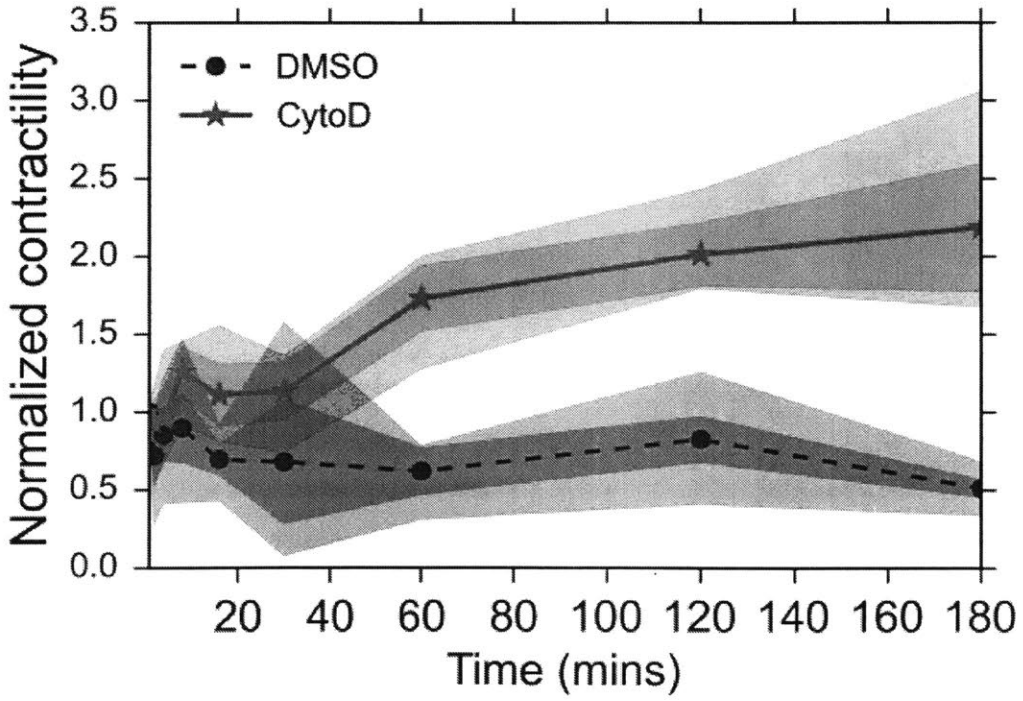

Fig. 19: Time-course of active contraction changes of C2C12 based 3D muscle tissues, within 3 hours. Statistically significant differences ($p < 0.05$) between the CytoD (n=5) and the DMSO (n=5) are observed as early as 15 minutes

In line with the results from the 2D myotube experiments, we find that the muscle active force also increases with f-actin disruption to ~2-fold. However, unlike the 2D experiments in which cell substrate adhesion changed, resulting in increased displacements, the 3D experiment has a muscle tissue with an intact connection to the kapton cantilever even after CytoD application. The fact that there is a dramatic increase in the force in this 3D *in vitro* model add more evidence to support our hypothesis that *f-actin disruption improves skeletal muscle contraction.*

We also notice a dose dependent response to CytoD as shown in **Fig.** 20. The active contractile force monotonically increases with increasing doses of CytoD. Blebbistatin, a myosin inhibitor was used as a positive control that is expected to completely inhibit the active force. As expected 50μM of Blebbistatin led to a 0 (non-measurable) optically stimulated active force within 5 minutes of application.

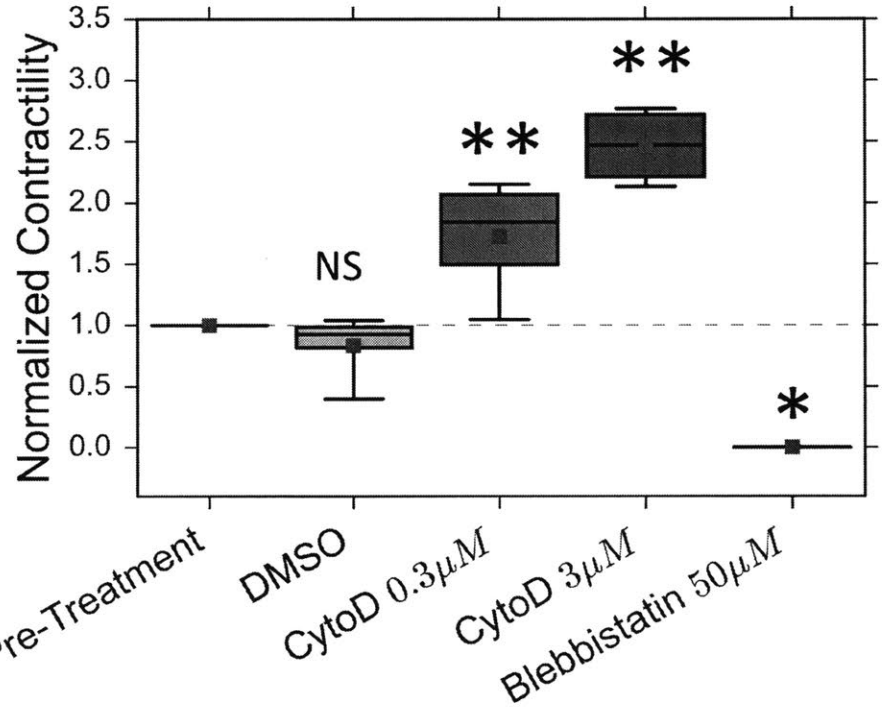

Fig. 20 Dose response test of 3D muscle active contractility with Cytochalasin D. The contractions are measure prior to treatment (Pre-Treatment) as well as 2 hours after CytoD or DMSO treatment. Normalization is with respect to the contraction prior to treatment. In the case of Blebbistatin, treatment with 50μM of this myosin inhibitor completely nullified the active force within 5 minutes of treatment. ** One-tailed Mann-Whitney test p = 0.00539. NS, p > 0.05 One-tailed Mann-Whitney test. * p = 0.0105 One-tailed Mann-Whitney U-test

Furthermore, to prove that the active force improvement is due to f-actin disruption and is not due to other non-specific side-effects of CytoD, we tested the effect of Latrunculin A. LatA is a G-actin sequestering molecule which depolymerizes f-actin also, but with a mechanism different from CytoD, thereby serving as an effective control for non-specific effects of CytoD. Interestingly, LatA treatment also elicits a muscle phenotype with improved contractility as shown in **Fig.** 21, further supporting our current hypothesis that f-actin disruption improves skeletal muscle contraction.

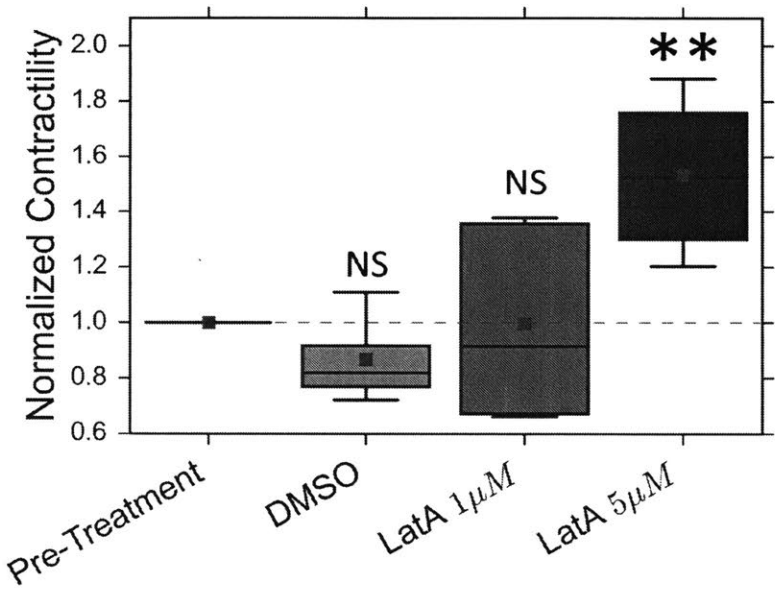

Fig. 21 Dose response test of 3D muscle active contractility with Latrunculin A. The contractions are measure prior to treatment (Pre-Treatment) as well as 2 hours after LatA or DMSO treatment. Normalization is with respect to the contraction prior to treatment.

The results of the 2 preceding sections (Secs. 2.2 and 2.3), showing an improvement in skeletal muscle contraction (displacement in 2D or force in 3D) with f-actin disruption, support the hypothesis that f-actin mechanically impedes contraction.

2.4 Potential drawbacks of f-actin disruption

2.4.1 Evolutionary advantages of f-actin

It is clear that f-actin disruption seems beneficial to muscle contraction at least in the short term (2-3 hours of f-actin disruption). However, as skeletal muscle structure is surprisingly conserved across vertebrates and several invertebrates [85,86], there is a natural followup

question: "If f-actin disruption is so beneficial to the primary function of muscle, namely contraction, why did the natural evolution of muscle not optimize for this by itself?" There are numerous biological regulators of f-actin such as cofilin, gelsolin, formins etc. If having lower amount of f-actin was evolutionarily beneficial, it is likely that such an optimization would have happened through natural selection.

There are several possible drawbacks of f-actin disruption, the biggest ones include:

1. Increased cell death
2. Loss of structural integrity of the myotubes
3. Lower fatigue resistance
4. Changes to autophagosomal activity

2.4.2 Increased cell death

2.4.2.1 Hypothesis: f-actin disruption leads to apoptosis and/or cell death

f-actin networks are thought to be essential for the function of most cells. It is plausible that f-actin disruption induces apoptosis or kills the muscle cells, or at least some fraction of the cells, given the presumed importance of f-actin.

2.4.2.2 Experiment: Caspase3 qPCR and Live/Dead assay

For RT-PCR, the myotubes were formed on a 2D matrigel coated surface exactly as described earlier in Section 2.2., except in a 6 well plate instead of the IBIDI-plate. On day 12 after differentiation, we treated the myotubes with CytoD (0.3μM) or DMSO for 2 hours and collected mRNA from the cells using TRIzol (Invitrogen) reagent for RT-PCR analysis. Reverse transcription was performed using SuperScript VILO cDNA synthesis kit (Invitrogen). Primer sequences are shown in Appendix 1. Real-time RT-PCR was performed with an Applied Biosystems 7900HT Fat Real-Time PCR System, using Power SYBR Green Master kit. mRNA of 18s-rRNA was used as the housekeeping gene in all experiments. The RT-PCR experiment was repeated at least 3 times for cDNA prepared from three batches.

For the live/dead assay, the myotubes were formed on a 2D matrigel coated surface exactly as described earlier in Section 2.2. , except in a 96 well plate instead of the IBIDI-plate. On day 12 after differentiation, we added 50μL of matrigel (Corning, growth factor reduced) on top of the cells, to keep the cells in place, and negate the effect of any cells detaching from the surface.

Once matrigel polymerized, 70μL of DM medium containing CytoD or DMSO was added to the cells, so that the final concentration of CytoD was 0.3μM. After 52 hours of incubation, the cells were stained with the ReadyProbes™ Cell Viability Imaging Kit (blue/green). The blue Hoechst dye stained for all nuclei. The green dye only entered cells with compromised plasma membrane integrity. N = 6 wells were used for each condition. The number of blue and green cells were counted to quantify overall cell viability.

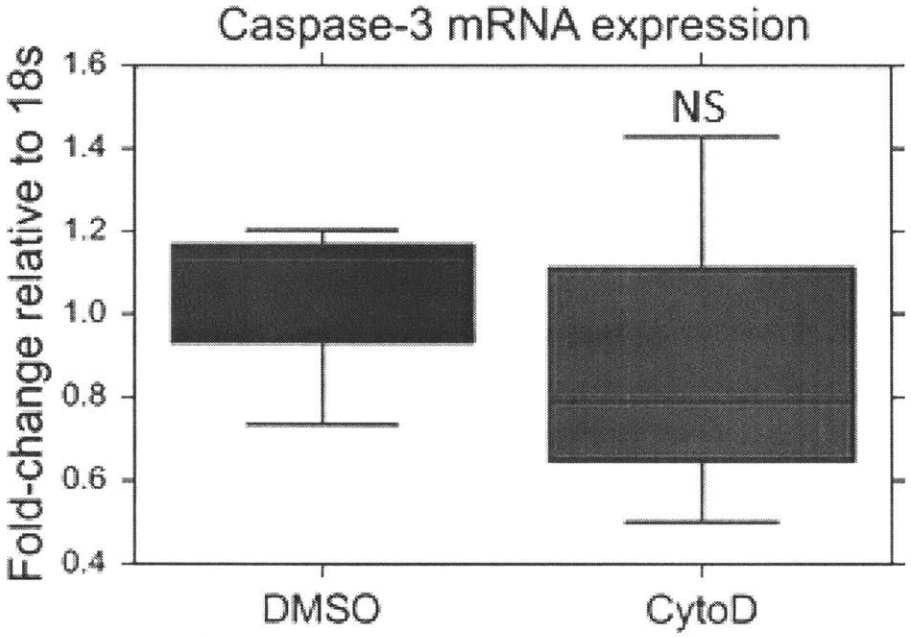

Fig. 22 Caspase-3 mRNA quantification (n=3) after 2 hours of CytoD 0.3μM or DMSO treatment. p = 0.37. A one-tailed 2-sample t-test was used for statistical significance testing.

2.4.2.3 Result: Mild f-actin disruption does not increase apoptosis or cell death

Running the above assays shows that treatment with 0.3μM CytoD for 2 hours does not induce apoptotic gene Caspase-3 significantly differently from controls (**Fig.** 22). Likewise, the viability of the cells was not altered significantly by CytoD treatment (52 hours) either as shown in **Fig.** 23. Overall these results imply that mild f-actin disruption does not induce apoptosis or kill cells at the same concentrations (0.3μM) that an increased force is observed.

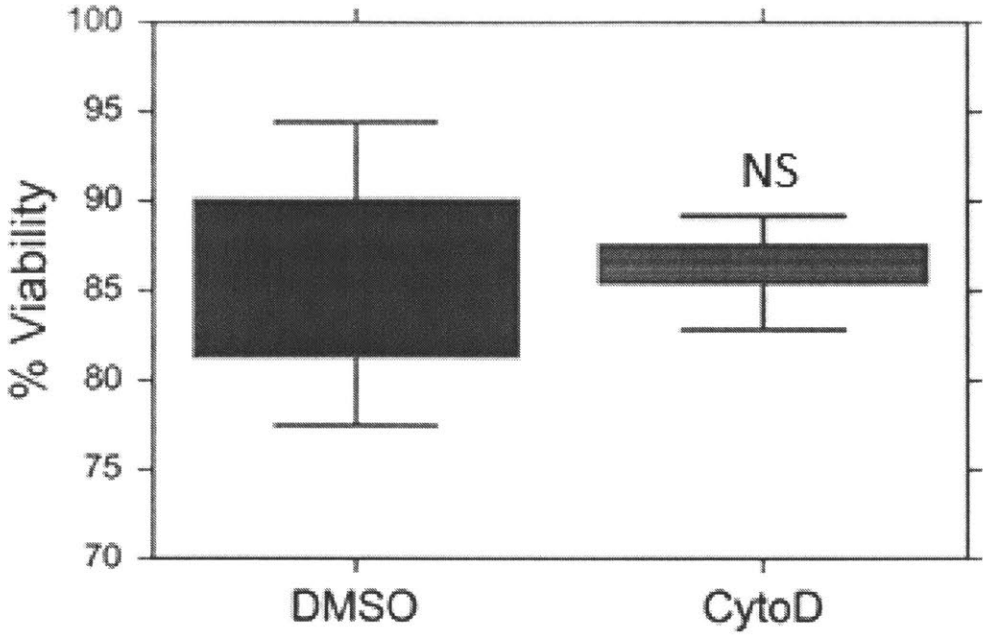

Fig. 23 Cell viability changes (n=6) after 52 hours of CytoD 0.3μM or DMSO treatment. p = 0.46 A one-tailed 2-sample t-test was used for statistical significance testing.

2.4.3 Structural integrity of myotubes

2.4.3.1 Hypothesis: f-actin disruption worsens sarcolemmal integrity

Perhaps cell death or apoptosis does not occur with mild f-actin disruption. However, f-actin networks are known to be one of the primary cytoskeletal structural scaffold for all cells, lending structural stability to the cells. So presumably disrupting f-actin has a downside in that the cell mechanically collapses due to lack of structural integrity. Lack of structural integrity is observed at the monolayer level when treated with high doses of CytoD (3μM). Monolayers of C2C12 myotubes detach from 2D surfaces and form a balled up cluster after treatment with high doses of CytoD (3μM), as described in Section 2.2. However, at lower doses of Cytod (0.3μM) they do not typically lift off, even though an increased force is observed in response to these doses. Does the cell lose its structural integrity at these low doses? F-actin is also known to bolster the mechanical integrity of the plasma membrane. So it is plausible that f-actin disruption results in a leaky plasma membrane. If the plasma membrane is leaky, it is likely that cytoskeletal proteins leak out in to the medium. In vivo, this is a situation referred to as

skeletal muscle injury, which often leads proteins such as Creatine Kinase (CK) to leak at detectable levels in to the patient's blood. In this section, we also test for Creatine Kinase activity in the supernatant as a proxy for general cytoplasmic protein leakage because there are very sensitive assays to detect low doses of CK, and because CK is not a component of the culture medium.

2.4.3.2 Experiment: Creatine Kinase assay using exercising myotubes

We grew 2D myotubes exactly as described earlier in Section 2.2. , except in 96 well plates. On day 12 after differentiation, we treated the myotubes with CytoD (0.3μM) or DMSO. Each well was loaded with 100μL of medium containing CytoD or DMSO. Just as the treatment began, we setup an optical stimulation rig underneath the myotubes. 8 LED lights (455 nm, 700 mA, Mouser Electronics) were aligned below the well plate and this module was placed in a 37C incubator. The myotubes were stimulated for 2 minutes continuously at 5Hz with a 5ms ON pulse width and repeated every 30 minutes. The voltage drop across each LED was 3.2 V emitting an average of luminous flux of approximately 15-18 lm. We chose these parameters as another work from our lab [87] showed that stimulation more often for prolonged period led to significant fatigue induced damage of the myotubes. After 52 hours of stimulation (just over 2 days), we collected 5μL of medium from each well and added it to a 96 well plate with the Creatine Kinase Assay buffer from the Creatine Kinase Assay kit (Biovision). n=6 wells was used for this test. 5μL supernatent from Triton 0.1% treated myotubes was used as a potential positive control for the presence of Creatine Kinase in the cells. NADH standards were added to make a standard curve. The reaction was initiated by adding the Creatine Kinase reaction buffer to the wells and incubated at 37C. The assay is colorimetric and a microplate reader was used to quantify the absorption of each sample at 450 nm. Measurements were taken every 5 minutes for 30minutes and the rate of change in absorption quantified between the various samples, compared to the NADH standard curve to estimate the Creatine Kinase activity in the CytoD 0.3μM, DMSO and Triton 0.1% treated samples.

2.4.3.3 Result: Mild f-actin disruption leaves the sarcolemmal integrity intact

As the results indicate, the CK activity in the supernatant medium was not significantly different from DMSO control (**Fig.** 24). It was however 4-fold lower than triton 0.1% treated positive controls. This indicates that sarcolemmal integrity at the stimulation parameters used was intact compared to triton 0.1% treated positive controls. The baseline level of CK activity even in the DMSO controls was non-zero because of the presence of some baseline level of dead cells in culture. Such dead cells are normal in cultures containing differentiated myoblasts.

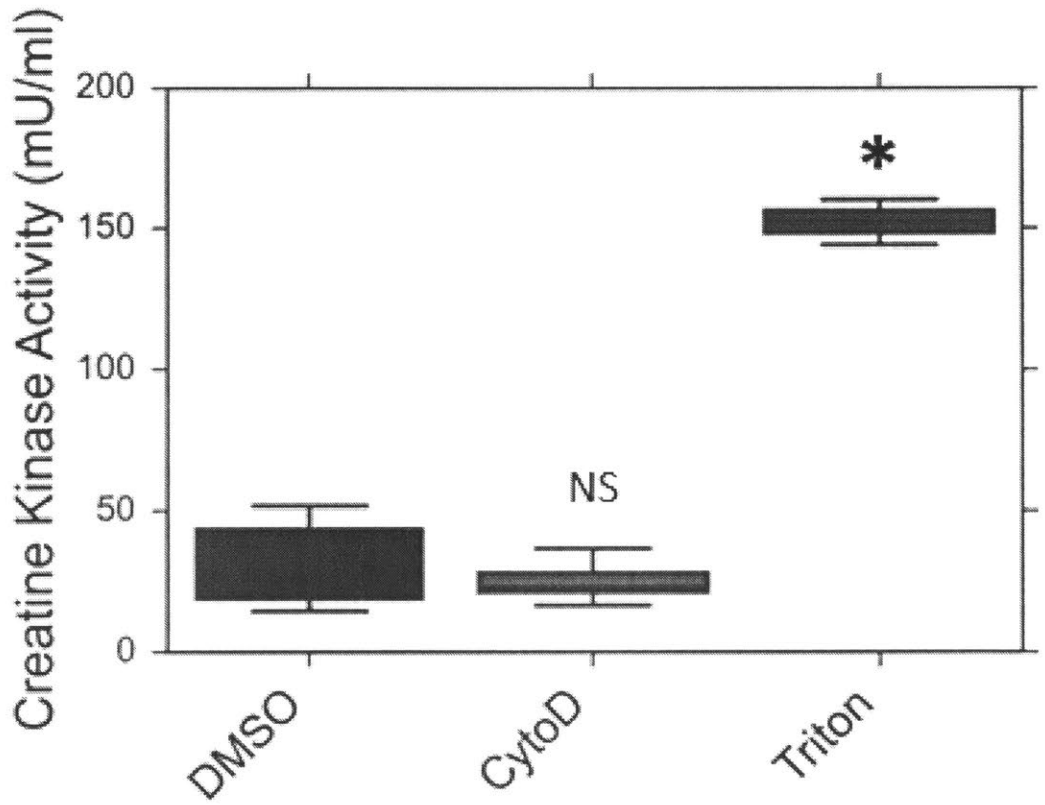

Fig. 24 CytoD treatment likely leaves the plasma membrane intact. It does not significantly change the activity of Creatine Kinase in the supernatant of the optically stimulated C2C12 myotubes relative to DMSO treated and optically stimulated controls. However, as expected for positive controls, Triton 0.1% treated samples as expected, show a significant 4-fold increase in CK activity relative to DMSO controls, indicating the presence of CK in the cells. A one-tailed 2-sample t-test was used for statistical significance testing. NS ($p = 0.16$) for CytoD (n=6) vs DMSO(n=6). * $p = 7.5*10^{-7}$ for Triton (n=3) vs DMSO(n=6)

2.4.4 *Lowered fatigue resistance*

2.4.4.1 *Hypothesis: f-actin disruption lowers the fatigue index*

The F-actin cytoskeleton could in theory act as a restoring force or spring-like element that helps reduce relaxation times after an active muscle contraction. Disrupting the f-actin could potentially affect the number of times the muscle can contract and relax freely. So we tested if the fatigue resistance of skeletal muscle is affected by f-actin disruption

2.4.4.2 *Experiment: fatigue loading of 3D muscle for 15 minutes*

We fabricated 3D muscle fibers attached to cantilevers and differentiated for 12 days. At this point, they were treated with DMSO, CytoD 0.3μM or CytoD 3μM for 2 hours. 2 hours after treatment, the muscle fibers were subjected to a fatigue loading stimulus of 5ms ON blue light pulse at 30Hz repeated once every 4 seconds, for 15 minutes total. The optical stimulation parameters we used are identical to that described in 2.3.2.3. Videos were recorded at 30 frames per second and analyzed as described earlier (see Sec. 2.3). The average force, normalized to the pre-fatigue force was computed each minute and the change over time of this average was tracked over the 15 minutes of stimulation.

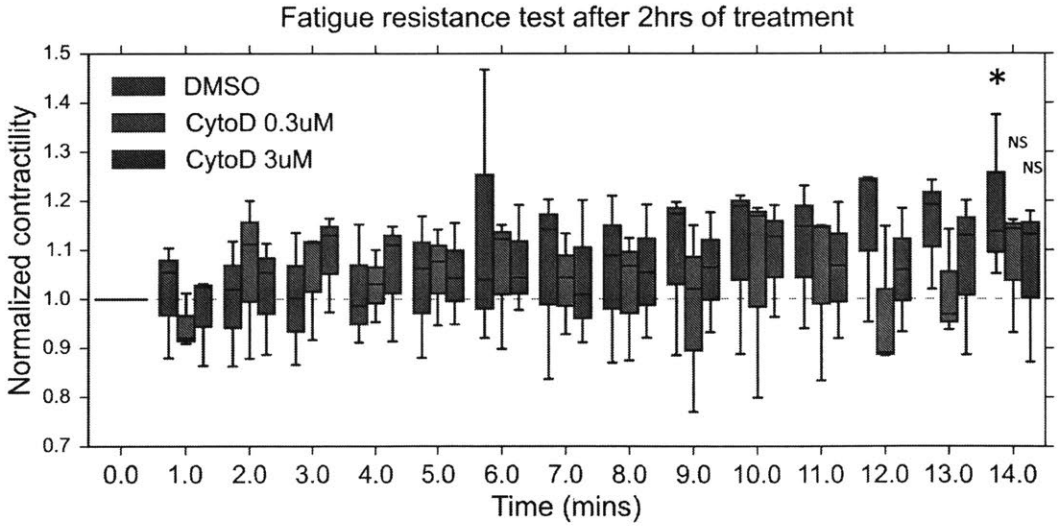

Fig. 25 Effect of a fatigue loading optical stimulus on muscle active contractility with (or without) f-actin disruption using CytoD (or DMSO). DMSO controls show a self-strengthening behavior after 15minutes of fatigue load, while CytoD treated tissues do not. A one-tailed Mann Whitney U-test was used for statistical significance testing. NS ($p>0.05$). *($p=0.032$). N=3 samples were used for each condition.

2.4.4.3 Result: Small change in fatigue resistance at short term

We found CytoD treatment does not lead significant fatigue at this short term, but that relative to DMSO-treated controls, which showed a small but significant strengthening behavior (14% increase in force after 15 minutes of fatigue), the CytoD treated tissues did not show any such increase (**Fig.** 25). This difference is not necessarily deleterious to muscle in terms of not having a self-strengthening behavior. But it does offer some clues as to the functional role that f-actin may have during periods of continuous exercise. Future studies should be designed to look at the response to fatigue loads over longer time periods.

2.4.5 Intracellular organelle or protein damage

2.4.5.1 Hypothesis: f-actin disruption increases autophagy

There are many intracellular organelles and proteins which are associated with f-actin and perhaps disrupting f-actin may damage these organelles or proteins. If impaired, the cell typically dissolves these dysfunctional organelles or proteins using autophagy.

Autophagy is an intracellular degradation system that traffics intracellular material, typically waste or dysfunctional, in to a phagophore, resulting in a double-membrane vesicle called an autophagosome. The autophagosome then fuses with lysosomes to then degrade the internal material. In this experiment, we test if *mild f-actin disruption with CytoD 0.3μM (or lower), which is a concentration sufficient to cause an improvement in force, increases autophagy*. If so, clearly f-actin disruption is harmful to the cell.

2.4.5.2 Experiment: CytoID test of myotubes

We use the CytoID Autophagy detection kit (Enzo lifesciences) to monitor autophagy in the cells as an indicator of intracellular damage. Briefly, the test uses the CytoID reagent, a fluorescent dye that selectively labels accumulated autophagic vacuoles. The dye was optimized to exhibit bright fluorescence upon incorporation into pre-autophagosomes, autophagosomes, and autolysosomes (autophagolysosomes). This assay helps monitor the extent of autophagy in the cells.

Similar to previous sections, we differentiate C2C12 myoblasts to myotubes in a 96 well plate. We use normal C2C12 cells (non-channel rhodopsin) as the CytoID assay requires blue light excitation. We did not want optogenetic stimulation to affect the assay. We then treat the cells with either CytoD (0.3μM and 0.03μM) or DMSO for 2 hours, and then with the CytoID reagent for 30 minutes at 37C, and then measure the fluorescence signal. To 0.01% Hoechst was also added along with the CytoID reagent to count the number of nuclei. N=3 images were taken for each case, each image containing cells with a total of ~10-20 nuclei. The overall green intensity in each image was computed and normalized with respect to the number of nuclei in that image to obtain the average green intensity per nucleus. All of these normalized intensities (16 bit values) were then normalized with respect to the DMSO mean intensity. The results were analyzed for significant differences.

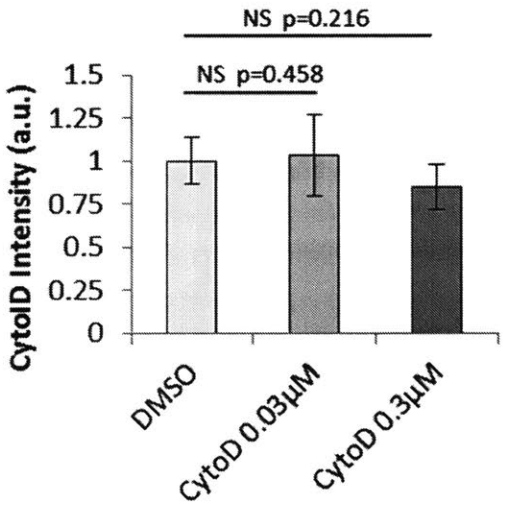

Fig. 26 F-actin disruption with CytoD does not affect autophagy as indicated by the CytoID fluorescent based assay. N=3 samples were used for each condition. A 2-sample one-tailed t-test was used for statistical significance testing.

2.4.5.3 Result: No change in autophagy

As shown in **Fig.** 26, there was no statistically significantly observed increase in autophagy due to mild f-actin disruption, indicating that there may not be significant protein/organelle damage at least within the 2 hours of the f-actin disruption tested.

2.5 Conclusion and next steps

The results with our ex vivo muscle assay, 2D myotube based assay and 3D in vitro engineered muscle tissue based assays indicate that f-actin disruption is very beneficial to creating higher active forces (~2-fold) with no observable deleterious effects . With mild f-actin disruption (CytoD 0.3μM) for 2 hours, there was no measurable effect on gene expression of Caspase-3 (apoptotic marker), cell viability, or protein/organelle damage (autophagy). Even with longer term stimulation (52 hours) in exercising myotubes, there is no significant change in structural integrity (CK assay). The only possible downside is a slight decrease in fatigue resistance observed under a fatigue load. Further studies are warranted to understand this tradeoff (higher force vs lower fatigue resistance) better.

So far, our experiments have been primarily functional in the sense of answering: ***what*** *does f-actin disruption do functionally to the force, to fatigue etc.?* In order to understand *how f-actin disruption leads to a functional improvement*, we first need to understand ***which actin filaments are affected by CytoD***. This is the topic of the next chapter.

Chapter 3: Cytoskeletal changes underlying f-actin disruption

3.1 Introduction

In this chapter, we try to pin-point the cytoskeletal changes that f-actin disruption due to CytoD treatment causes in order to derive further mechanistic insights. We aim to answer the following questions:

- Is the functional improvement due to f-actin disruption transient and reversible?
- Which f-actin fibers are disrupted?
- How are the sarcomeric f-actin filaments affects?
- Are there specific sub-categories of f-actin that drive the majority of the functional improvement we observe?

In order to address some of the questions in this chapter, we use a combination of experiments such as 1) functional active force assays with dose response and longer term f-actin disruption as well as reversal of f-actin disruption, 2) live 3D confocal intracellular f-actin visualization, 3) fluorescence recovery after photobleaching (FRAP) with transfected GFP-actin as well as 4) the use of more targeted small molecule actin inhibitors.

3.2 Reversibility of force changes due to f-actin disruption

3.2.1 Hypothesis: CytoD associated force improvement is reversible

The experiments presented in chapter 2 are short term in nature. In all the experiments, we test the effect of CytoD application on muscle active force improvement in the short term (~2 hours). However, does this force improvement persist beyond 2 hours? Furthermore, what happens when we wash out CytoD? The binding of CytoD is typically considered to be reversible, leading to the expectation that after washout of CytoD, the disrupted f-actin may repolymerize. Does this repolymerization restore the f-actin cytoskeleton to its original microstructure? How does that affect the functional performance of the muscle tissue? Does the active force drop again? These are complex questions. In order to start prying apart these questions, we start by testing the hypothesis that *CytoD associated force improvement is reversible* with our functional assay measuring muscle active force generation.

3.2.2 Experimental methods

As described in section 2.3, we grow and differentiate C2C12-ChR based skeletal muscle tissues on cantilevers for 12 days and then perform a dose response test to CytoD at 0.3μM and 3μM, along with DMSO as a control. We measure the active force on day 12, apply the treatment for a day, while measuring the changes in active force 2 hours and 1 day after the treatment. Finally, we washout the medium with fresh DM+ medium (without CytoD or DMSO), wait for a day to recover and then measure the force again. For each muscle fiber that goes through this sequence of tests, we normalize the force with respect to the corresponding force prior to treatment. A one-tailed paired t-test was conducted to assess statistical significance for each of the comparisons.

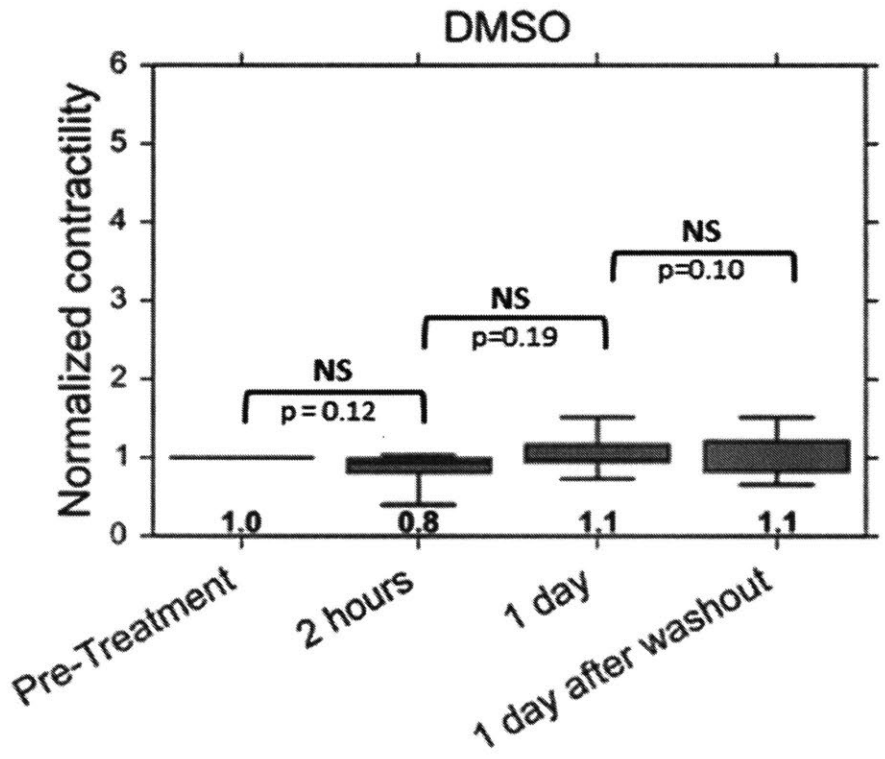

Fig. 27 The DMSO control tissues show no significant change in active muscle contractility. Shown are the effects of DMSO application to C2C12 skeletal muscle active contractility 2 hours after treatment, 1 day after treatment, as well as 1 day after washout (which is 2 days after the treatment was initiated). The active force measured at different times for each device are normalized to the corresponding pre-treatment force (n=5). Statistical significance tests were conducted using a paired one-tailed t-test to check if any potential increases are significant.

3.2.3 Results and conclusions

3.2.3.1 DMSO treatment

As expected DMSO-treated tissues show no statistically significant change (**Fig.** 27) either with treatment or washout, with the average force largely being similar throughout the 2 days of the experiment (1 day treatment and 1 day to recover after washout).

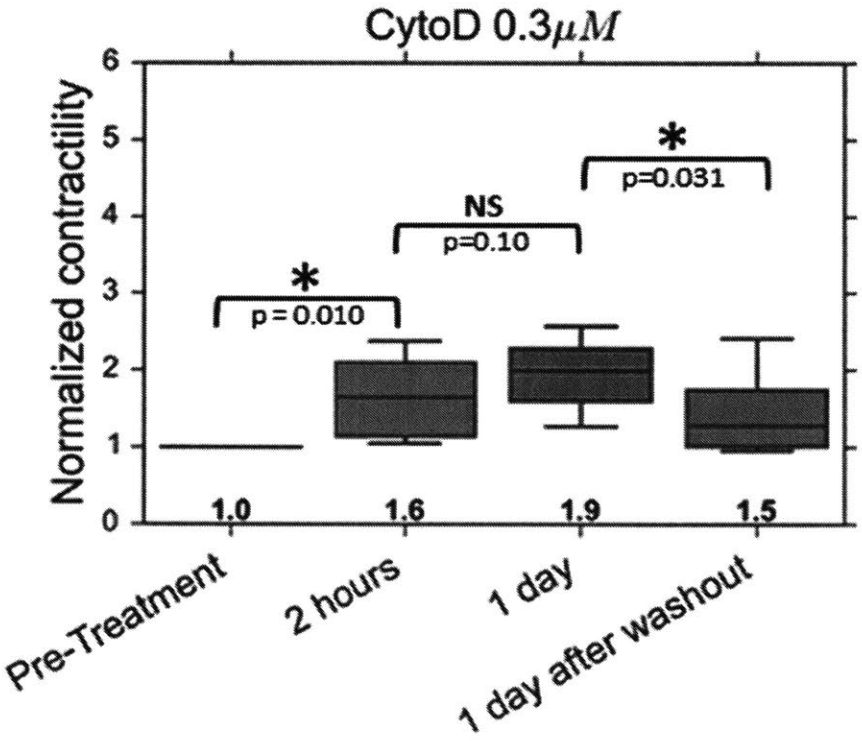

Fig. 28 Mild f-actin disruption with CytoD 0.3μM shows a significant increase in active muscle contractility within 2 hours (1.6X) and a smaller (but not statistically significant) increase a day after treatment. The plot shown is the effect of CytoD 0.3μM application to C2C12 skeletal muscle active contractility 2 hours after treatment, 1 day after treatment, as well as 1 day after washout (which is 2 days after the treatment was initiated). The active force measured at different times for each device are normalized to the corresponding pre-treatment force (n=7). Statistical significance tests were conducted using a paired one-tailed t-test to check if any potential increases are significant. There is a statistically significant drop in active contraction 1 day after washout of CytoD 0.3μM indicating at least partial reversibility of CytoD's effect, partial because the force is still 50% greater than force prior to treatment (statistically significant).

3.2.3.2 CytoD 0.3μM treatment

Mild f-actin disruption with lower CytoD dose (0.3μM) appears to lead to a sustainable improvement in the force. Long term exposure (1 day) to a lower CytoD dose (0.3μM) increases the active force only slightly (not statistically significant) compared to the peak of 1.6X (reached 2 hours after exposure) (**Fig.** 28) and in any case does not lead to a decline of force. To probe the reversibility of this CytoD associated improvement, we washed out the CytoD 1 day after exposure and measured the muscle active force, 1 day after washout. Interestingly, the muscle force declines over 20% 1 day after washout (statistically significant). However, this recovery towards the pre-treatment level is incomplete, as the force is still 50% higher than the force prior to treatment.

This leads us to 2 hypotheses about the manner in which CytoD affects f-actin:

1) 0.3μM CytoD does not depolymerize the sarcomeric f-actin even with prolonged exposure (1 day), as 0.3μM CytoD seems beneficial to muscle active force development. We will further test this hypothesis in Section 3.3 (Spoiler: it does not depolymerize mature sarcomeric f-actin)

2) The CytoD treatment does seem to be partially irreversible, as even after washout of CytoD, the force remains high.

a) This could either mean that the washout wasn't effective in that some of the CytoD still remained in the muscle fibers. (We actually rule out this hypothesis later in section 3.2.3.4, by testing the completeness of washout using a fluorescent version of CytoD)
b) Or it could also mean that there has been some permanent cytoskeletal or biological change due to CytoD application that does not reverse.

3.2.3.3 CytoD 3μM treatment

It seems likely that irreversibility is due to cytoskeletal changes in f-actin disruption that do not fully recover. If so, increasing the concentration of CytoD to 3μM for a more severe f-actin disruption may have a disproportionate effect on the irreversibility.

Severe f-actin disruption with 3μM CytoD turns out to be deleterious with 1 day of exposure. In fact there is a statistically significant (**Fig.** 29) 50% drop in the force relative to the peak force 2 hours after exposure. However, this force is not zero. In fact it is larger than the level of pre-treatment (by 40%, barely significant p = 0.051, 1-tailed paired t-test).

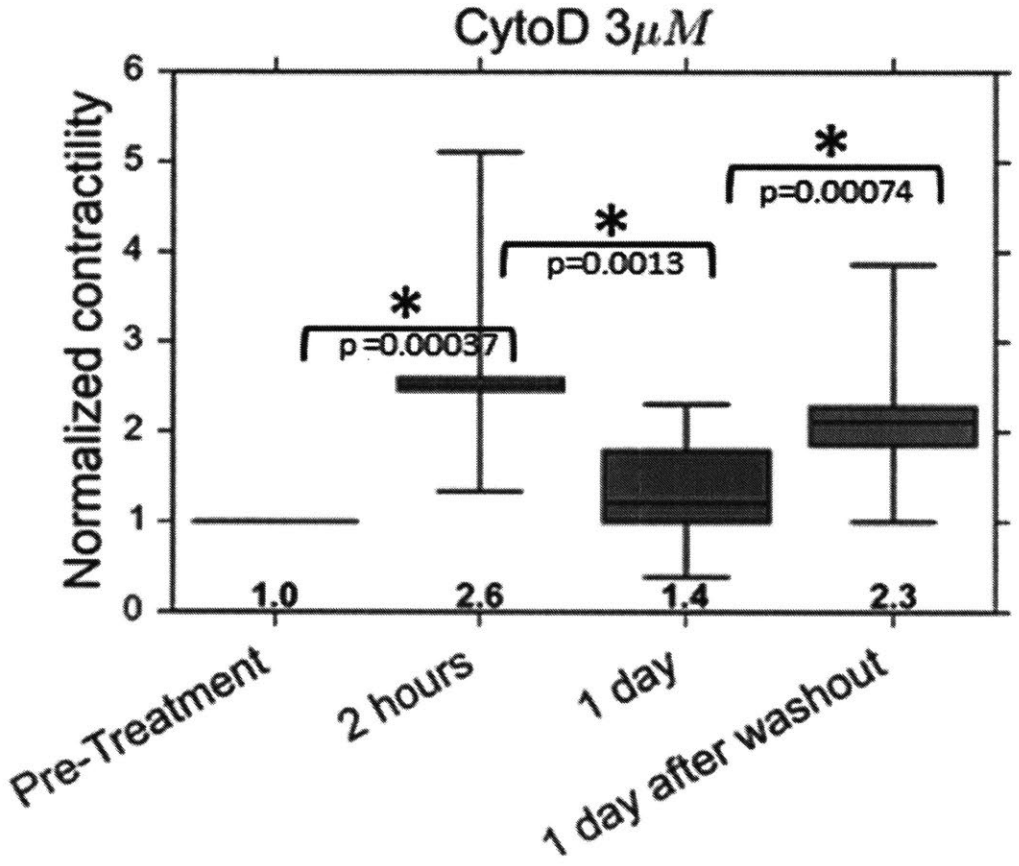

Fig. 29 Strong f-actin disruption with Cyto 3μM shows a significant increase in active muscle contractility within 2 hours (2.6X), a deleterious decrease relative to the peak of nearly 50% down to 1.4X and a recovery to nearly the level of the 2 hour peak (2.3X) within a day of CytoD washout. The plot shown is the effect of Cyto 3μM application to C2C12 skeletal muscle active contractility 2 hours after treatment, 1 day after treatment, as well as 1 day after washout (which is 2 days after the treatment was initiated). The active force measured at different times for each device are normalized to the corresponding pre-treatment force (n=10). Statistical significance tests were conducted using a paired one-tailed t-test to check if any potential increases are significant. There is a statistically significant drop in active contraction 1 day after washout of Cytod 0.3μM indicating at least partial reversibility of CytoD's effect, partial because the force is still 50% greater than force prior to treatment (statistically significant).

This further strengthens our hypothesis that CytoD application does not depolymerize the sarcomeric f-actin, at least not completely. The rationale is that even though there is a force decline with long term exposure (1 day) relative to the 2 hr peak with 3μM CytoD, the fact that it is non-zero implies the presence of functional sarcomeres. Interestingly though, 1 day after washout of 3μM CytoD, the active force recovers to the level of the peak.

This leads to the hypothesis that there are non-sarcomeric f-actin structures within muscle cells that aid sarcomeric contraction . Furthermore, the force recovery after washout suggests that such f-actin structures likely recover once CytoD is washed out. Both of these points support each of our first set of hypotheses (Chap 1) that the presence of some of these non-sarcomeric f-actin structures may be beneficial to force transmission, while other non-sarcomeric f-actin structures may mechanically impede contraction. The fact that we find evidence of both these behaviors under different conditions points to the presence of different kinds of non-sarcomeric f-actin filaments that may have different roles (we hone in on the specific nature of these filaments in Sec. 3.6).

Lastly, the reversibility of the force recovery in this case implies that it is unlikely that the sarcomeric f-actin is depolymerized, as assembly of sarcomeres typically takes several days to weeks[88,89,90] in C2C12 based muscle systems. Also, it is intriguing that the variability of responses to 3μM CytoD after 2 hours is much higher than the effect of 0.3μM CytoD, implying that the higher dose CytoD likely affects a wider range of f-actin structures.

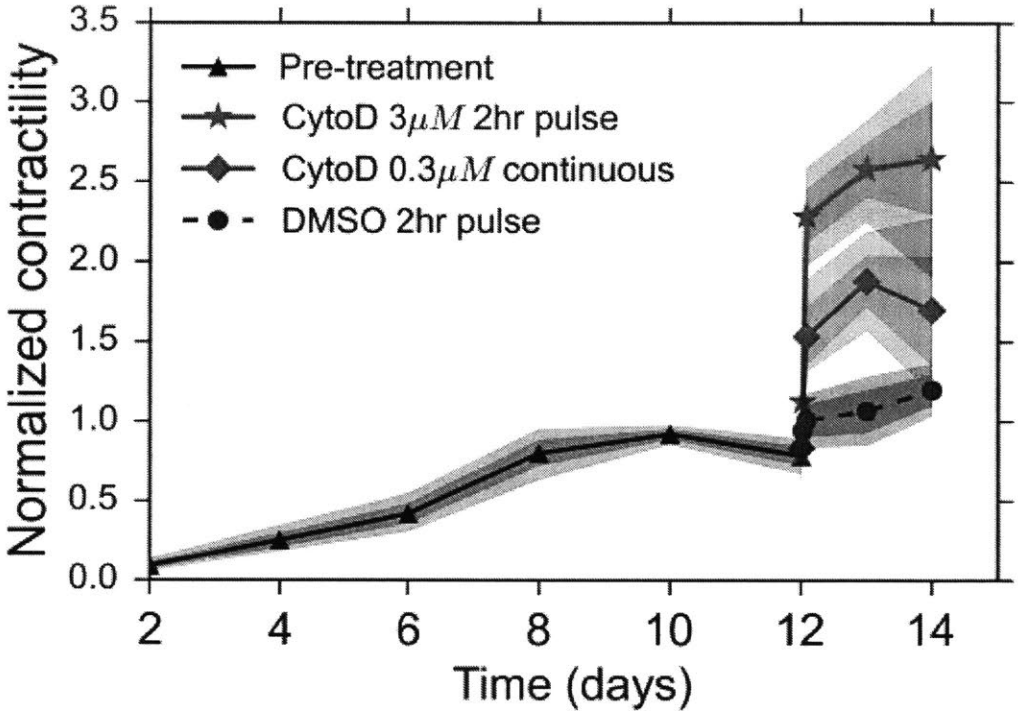

Fig. 30 Comparison of the effect of CytoD for longer term (2hrs to 2 days) on muscle contractility relative to the forces during muscle differentiation. In the case of CytoD 3μM and DMSO, a 2 hour pulse was applied and then washed out to test the recovery and reversibility long term. This was compared with a continuous mild f-actin disruption with CytoD 0.3μM for days. Clearly, both the high dose (3μM) pulse of CytoD and the low dose continuoud treatment both led to sustainable improvement in active contraction beyond the DMSO pulse control and relative to the maximum force during differentiation (all fibers were normalized with respect to their respective peaks during days 2-12 of differentiation. The colored envelopes around each means curve (black, blue, green and red) represent 68% and 95% confidence intervals.

3.2.3.4 Pulsed high-dose CytoD & continuous low-dose CytoD treatment

Given that high dose CytoD affects the muscle deleteriously after long term exposure (1 day), we tested if a short pulse of CytoD 3μM for 2 hours, followed by a washout could lead to a persistent improvement. Interestingly it does as shown in **Fig.** 30. Furthermore, for two days after the washout, we find that the active force improvement persists.

Just as before, this could be due to permanent cytoskeletal rearrangement during those 2 hours or incomplete washout of CytoD.

We rule out the possibility of incomplete CytoD washout by testing CytoD washout characteristics using a fluorescent version of CytoD, called CytoD EverFluor-TMR (Setareh

Biotech). We test its penetration in to a C2C12-based 3D muscle fiber and washout using fluorescence imaging. Normal C2C12 cells without ChR2-tdTomato was used to minimize red background because this CytoD EverFluor-TMR emits red fluorescence. The experiment was to treat the muscle fibers with CytoD for 2 hours and then washout the CytoD, all while imaging the fluorescence intensity at 6 locations along the muscle fiber and the background, before and after treatment/washout.

As seen from Figs. 31 and 32, there is a significant drop in CytoD-EverFluor intensity after washout (almost imperceptible in the first row of images in **Fig.** 31). As shown in the quantification of **Fig.**32, the peak intensity of CytoD 2 hours after treatment is ~1000-fold higher than the pre-treatment background intensity. 1 day after washout, this gap between the muscle fiber intensity and the no CytoD background drops to ~5-fold, i.e., there is a ~200-fold drop in fluorescent CytoD intensity relative to the 2 hour peak. Likewise, there is a 700-fold drop after 2 days of washout.

Given this, it is unlikely that CytoD washout was incomplete. So the likely hypothesis that may explain the persistence in force even 2 days after washout is some sort of cytoskeletal rearrangement. Finally, we also plot the force evolution when the muscle fiber was continuously treated with low dose CytoD (0.3μM) and we find that the force improvement lies in between the DMSO controls and the high-dose pulsed CytoD treatment. However, importantly, even 2 days in to this stimulation, the muscle force improvement seems to persist, reemphasizing our earlier point that with mild f-actin disruption, long term treatment may not be disruptive.

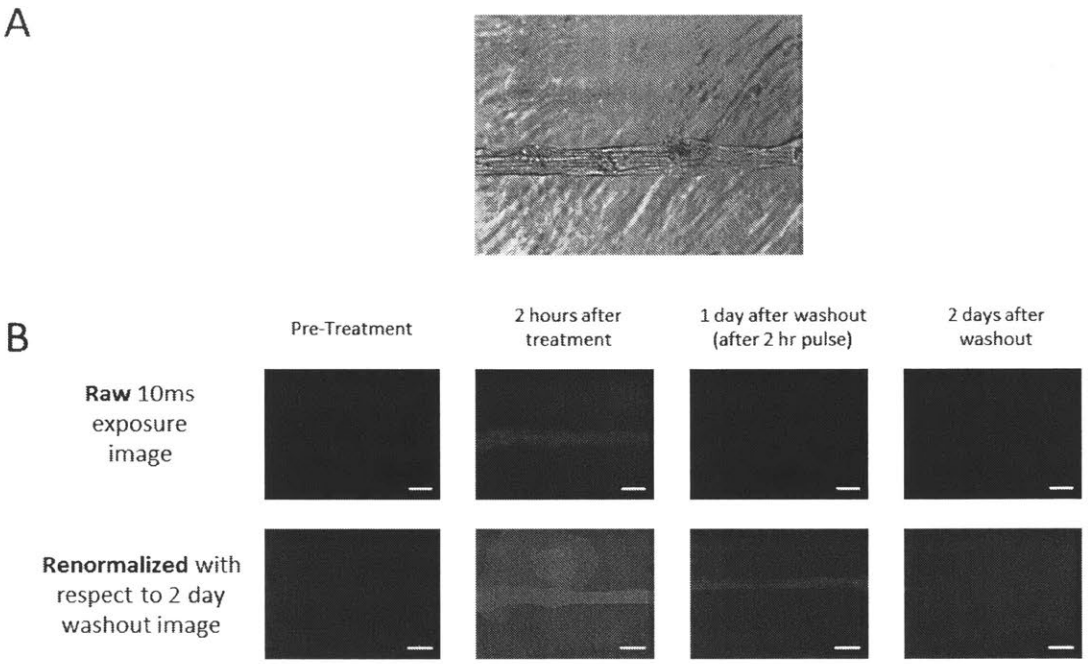

Fig. 31 Fluorescence intensity of CytoD EverFluor-TMR measured 2 hours after treatment and after washout. (A) a phase contrast image showing a typical 3D muscle fiber. (B) The first row of images contains the raw images used for quantification purposes in **Fig.** 32. The second row contains histogram normalized versions of images in the first row. The normalization with respect to the 2 day washout image in order to make the visibility of the muscle fiber clear, while still maintaining the relative intensity. Clearly there is a significant drop in intensity, almost imperceptible by 1 or 2 days after washout. Scale bar 300μm

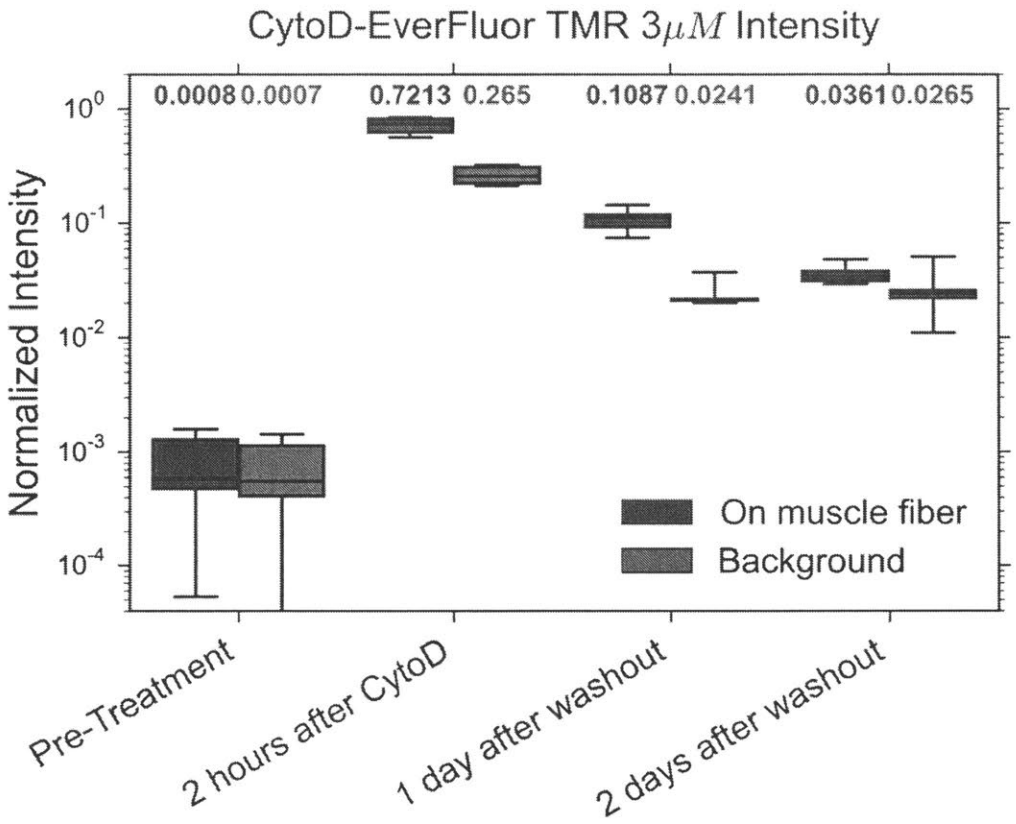

Fig. 32 Fluorescence intensity of CytoD EverFluor-TMR measured 2 hours after treatment and after washout. All the intensities were normalized between 0 and 1 with respect to the maximum average intensity measured as well as the minimum (throughout the experiment). The background intensity could vary from day to day, due to changes in environmental conditions as well as variations in the laser. So the intensity values corresponding to zero CytoD concentration are ~ $6*10^{-4}$ for both the pre-treatment and 2 hour cases. In the 2 hour image, the background is high because it contain CytoD-EverFluor. However, the intensity of the muscle fiber is even higher than that as it seems that CytoD reacts with f-actin and accumulates inside the muscle. 2 hours after treatment, the average intensity on the muscle fiber is ~1000-fold larger than the pre-treatment background. One day 1 after washout, the muscle intensity drops to being 5-fold larger than background (~200-fold reduction) and on day 2, it drops to being 1.4-fold larger than background (i.e. a ~700-fold reduction compared to the 2 hour peak)

3.2.3.5 Conclusion and next steps

Overall, it seems that f-actin disruption with CytoD follows a complex pattern. The functional assays in the previous sections 3.2.3.2-3.2.3.3 lead us to the following hypotheses:

1) Sarcomeric f-actin is not affected by low dose CytoD (or CytoD penetration in to tissues in incomplete)
    - From the previous section, we found that even long term (2days) exposure to high CytoD does not affect the active contractile force negatively. This could either mean that sarcomeric f-actin is not disrupted by CytoD application or that CytoD does not completely penetrate the tissue. We test both these hypotheses in sec 3.3 and 3.4.
2) Low dose CytoD disrupts some of the dynamic f-actin which may recover quickly after washout. We test this hypothesis in sec 3.5.
3) There are some stable f-actin filaments that help sarcomeric contraction. We test this hypothesis in sec 3.6.

3.3 Dynamics of CytoD penetration

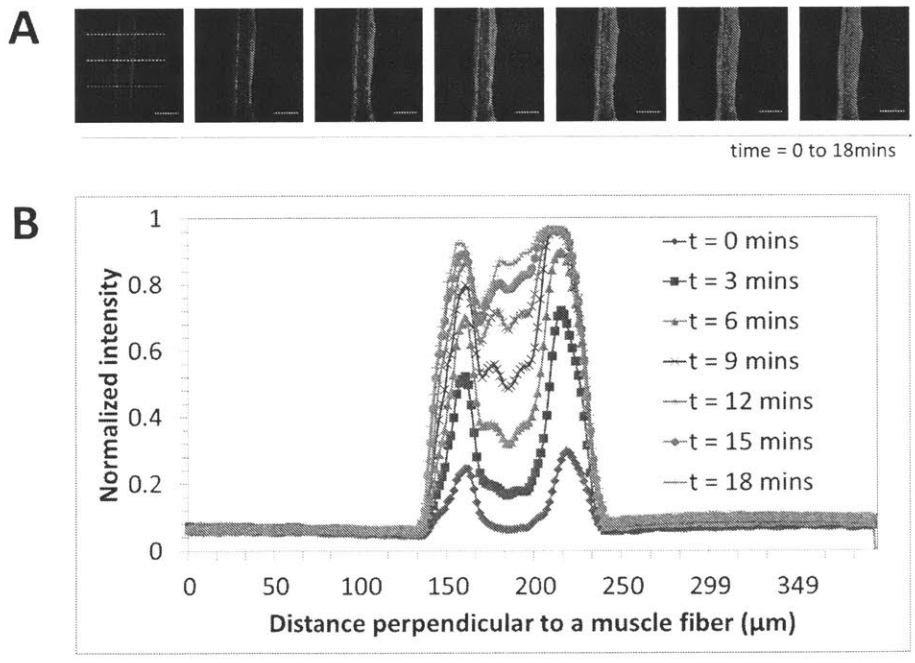

Fig. 33: Diffusion of Cytochalasin D – Everfluor conjugate through a muscle fiber. (A) Confocal fluorescence timelapse images of the Cytochalasin D – Everfluor conjugate

penetrating the 3D muscle tissue. Scale bar in images is 100μm. (B) Quantification of the fluorescence intensity variation, with time. All intensities are normalized with respect to the same maximum 16-bit greyscale spectrum. Every line at any given time point represents the average intensity across the muscle fiber averaged over 30 cross sections along the length of the muscle.. 3 of the cross sections are shown in the first image in (A).

3.3.1 Hypothesis: CytoD fully penetrates the muscle 3D tissue within a day

The fact that long term exposure to CytoD still doesn't eliminate active contractility leads us to believe either that CytoD does not penetrate the tissue fully, or (if it does) it does not depolymerize the sarcomeric f-actin. In this section we test the former of these 2 hypotheses.

3.3.2 Experimental methods

As described in section 2.3, we engineer a C2C12-based 3D muscle fiber using normal C2C12 (non ChR2-tdTomato), differentiate it for 12 days. The engineered muscle fibers after 12 days of differentiation are ~80μm in diameter. We then test the dynamics of penetration of Cyto-EverFluor TMR, a red fluorescent version of CytoD at 0.3μM concentration using 3D confocal timelapse microscopy with a confocal laser scanning microscope (FV-1000, Olympus, Japan).

3.3.3 Results and conclusions

As illustrated in **Fig.** 33, we focus on a confocal slice in the middle of the muscle fiber. As shown in **Fig.** 33, we find that within 20 minutes, the CytoD penetration saturates at the outer edges and has begun to plateau within the center of the muscle fiber. Part of the reason the intensity in the center is lower is also due to laser excitation and emission attenuation through a thick muscle tissue. It is clear from **Fig.** 33 that within 24 hours (the duration of the long term exposure), CytoD-EverFluor will penetrate the entire muscle (in fact the timescale seems to be 10s of minutes for am ~80μm diameter muscle fiber). CytoD-EverFluor (M.W. 887 g/mol) has a slightly higher molecular weight of CytoD (M.W. 507 g/mol), which makes it likely that CytoD diffuses through the tissue faster (ignoring charge effects).

Overall, this experiments rules out the possibility that CytoD does not reach all the muscle cells during the long term exposure (1 day). In fact, from **Fig.**33., it seems that even 2 hours after treatment, the entire muscle must be saturated with CytoD.

3.4 Visualization of f-actin breakdown

3.4.1 Hypothesis: Sarcomeric f-actin is not broken down by CytoD

From the results of Sec 3.3, it is clear that all muscle cells must be exposed to CytoD by the 2 hour timeframe. For the CytoD to not eliminate the active contraction, we hypothesize that it must not depolymerize the sarcomeric f-actin within this time frame. To reframe this, we also wanted to understand what changes occur in the f-actin cytoskeletal structure within 2 hours of exposure to CytoD. This is because, our experiments in Chapter 2 showed significant increases in active force starting at 30minutes and plateauing close to 2 hours. So we designed an experiment to answer the following questions:

1) Are the sarcomeric f-actin filaments depolymerized by CytoD 0.3μM in 2 hours?
2) Are the non-sarcomeric f-actin filaments depolymerized by CytoD 0.3μM in 2 hours?

3.4.2 Experimental methods

We use Sir-Actin (Cytoskeleton Inc.), a fluorescent far-red small molecule dye that binds to f-actin filaments and helps visualize structural changes in f-actin. According to established protocols with Sir-Actin (Cytoskeleton Inc., Spirochrome), we use the dye at very low concentrations (100nM) so as to not affect the f-actin dynamics because of the dye.

We differentiate C2C12-ChR cells on matrigel coated IBIDI-plates in 2D (as described in section 2.2), differentiate the cells in DM+ for 12 days. At this point, we check for tetanic contractions using the blue light from a fluorescence lamp (see section 2.2). If the cells are contractile and tetanic (a sign of mature C2C12s), we expose the cells to DM+ containing 100nM of Sir-Actin dye, incubating at 37C overnight.

At this point, we use aspirate the medium from the top of the cells, add 150μL of matrigel (Corning), allow matrigel polymerization for 20 minutes at 37C in the incubator, and then add 2ml medium on top, also containing Sir-Actin. The purpose of the matrigel is to provide some ECM for the cells to stick to in order to prevent complete cellular collapse during the imaging with CytoD. We then found a variety of cells in the 2D IBIDI-surface. Some cells contained mature sarcomeres, with primarily sarcomeric f-actin, while others contain immature sarcomeric f-actin filaments. Others still had partially differentiated myotubes (without a clear sarcomeric f-actin pattern). This provides a great test bed to observe the effect of CytoD on

various kinds of f-actin filaments (sarcomeric, non-specific f-actin mesh, non-sarcomeric f-actin stress fibers etc). In real muscle fibers, there is a combination of these different kinds of f-actin filaments.

3.4.3 Results and discussion

The results indicate that sarcomeric f-actin filaments are not depolymerized by CytoD, while some of the non-sarcomeric f-actin filaments are depolymerized.

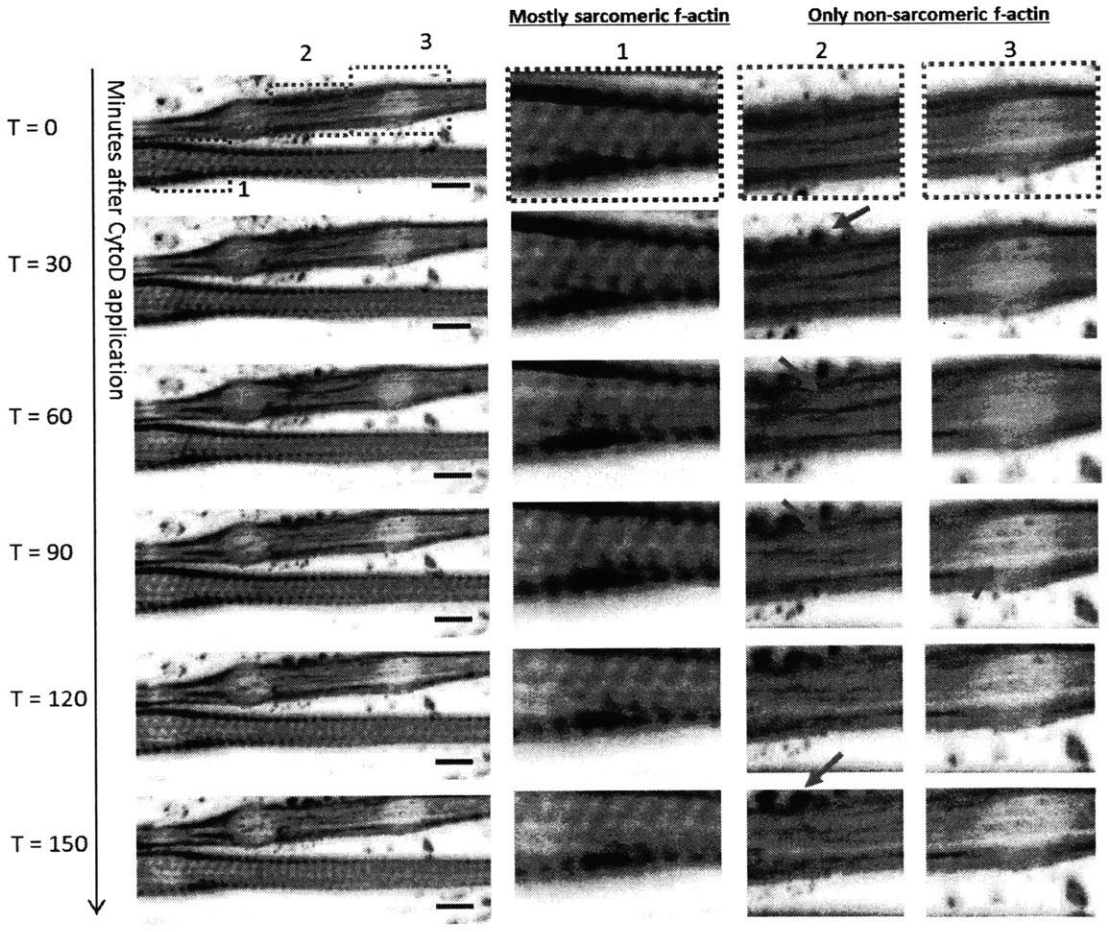

Fig. 34: Visualization of f-actin in mature and immature myotubes using Sir-Actin and confocal timelapse microscopy reveals that sarcomeric f-actin in mature myotubes is not depolymerized by CytoD 0.3μM. However, a small fraction of the non-sarcomeric f-actin is depolymerized with CytoD. For instance, in window 2: the arrows mark areas with f-actin clustering at T=30 and 150mins(dark rounded spots), which is typical when filamentous actin breakdown appears (also see **Fig.** 36B for more obvious clustering). Also shown using arrows in window2 (between T=60 and 90mins) as well as in window 3 (T= 90mins) is the sudden appearance of a lighter background, indicating the disappearance of the dark f-actin. Scalebar is 10μm.

In order to parse this out, we performed confocal timelapse imaging simultaneously with a more mature myotube with sarcomeric f-actin filaments, as well as an immature myotube without sarcomeric f-actin. Myotubes with sarcomeric f-actin also have non-sarcomeric f-actin but as Sir-Actin stains all f-actin (as seen in **Fig.** 34), it is often difficult to pinpoint the non-sarcomeric f-actin in mature sarcomeric myotubes. This is the reason we also chose to image more immature myotubes which are typically found in 2D differentiated myotubes along with more mature myotubes. The prime assumption in this experiment being that the dynamics of the non-sarcomeric f-actin in the immature myotubes are similar to the non-sarcomeric f-factin found in mature myotubes.

In one of these imaging sessions, illustrated in **Fig.** 34, both a mature and immature myotube are found on the same frame, which makes a comparison easier. These myotubes were exposed to 3μM CytoD for 2.5 hours. As seen in **Fig.** 34, the sarcomeric f-actin structure remains even after 120 minutes of exposure to CytoD. However, within the same timeframe, there are several non-sarcomeric f-actin filaments shown to be depolymerized. We see several hallmarks of f-actin depolymerization in the non-sarcomeric f-actin filaments, such as f-actin clustering (annotated by pink arrows in **Fig.** 34), disappearance of uniform background f-actin which are likely sub-diffusion limit sized thin filaments that don't appear as distinct filaments (also annotated by pink arrows in **Fig.** 34) and severing of aggregated stress fiber like f-actin filaments (**Fig.** 36B).

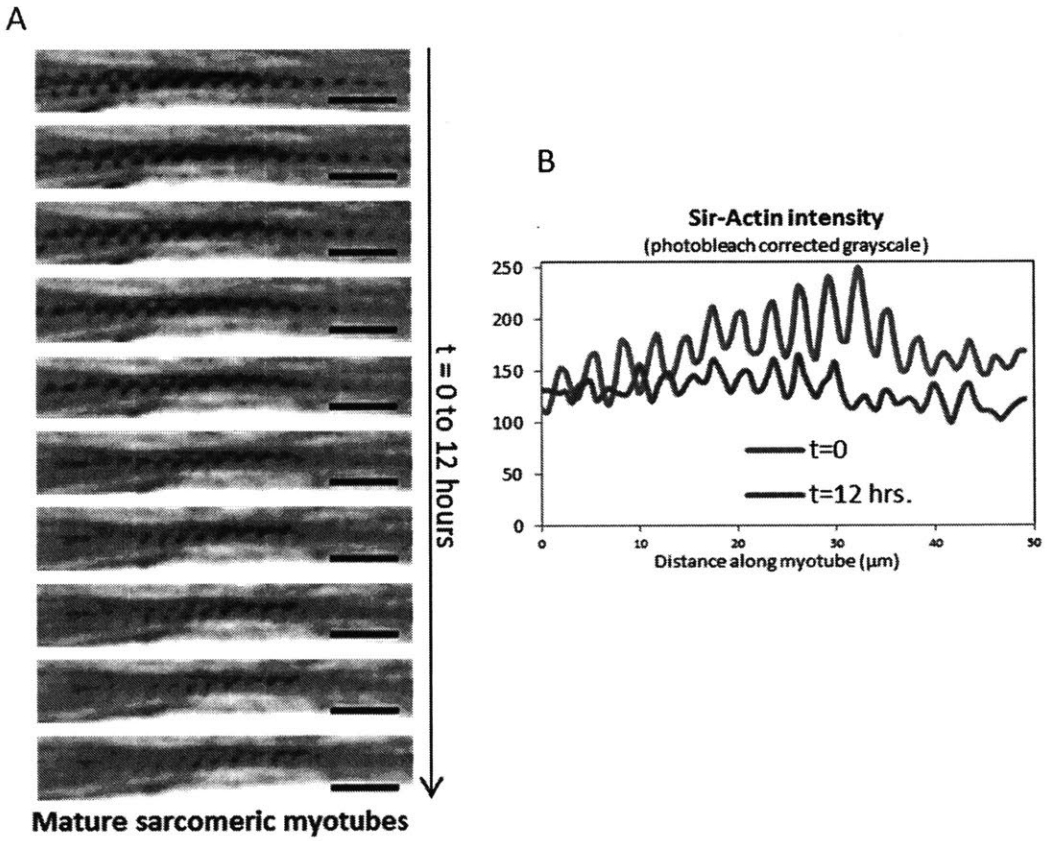

Fig. 35: Visualization of f-actin (Sir-Actin) in mature sarcomeric myotubes with CytoD 0.3μM application using confocal timelapse microscopy reveals that while sarcomeric f-actin in mature myotubes are not depolymerized by CytoD 0.3μM, the non-sarcomeric non-specific f-actin (darker) around the periodic f-actin structures do get depolymerized. This is also illustrated in the intensity line plot showing that the periodic structures remain after 12 hours, while the overall intensity level comes down, due to depolymerization of some of the non-specific, non-periodic background f-actin. The scalebar is 10μm.

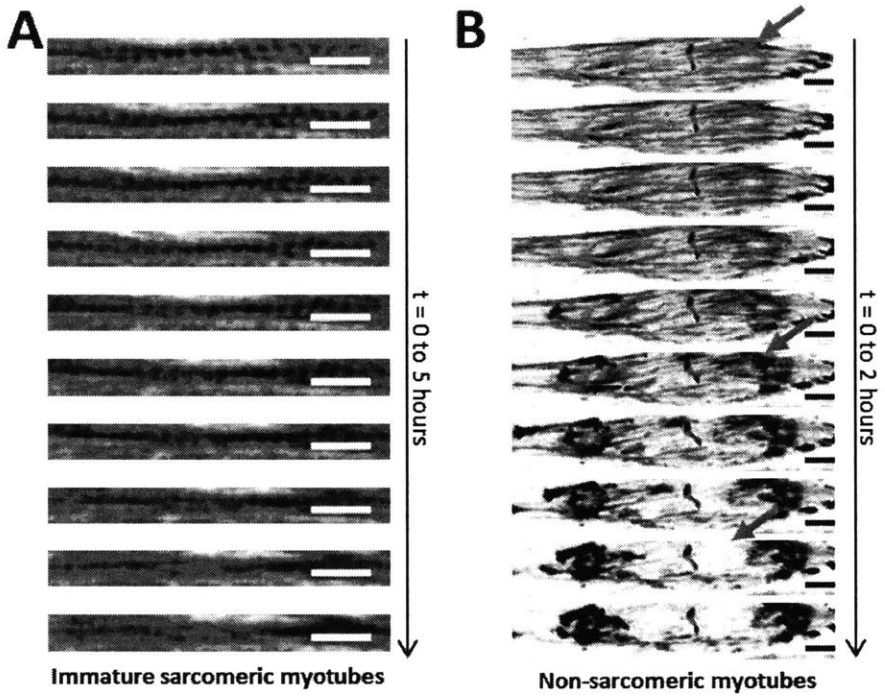

Fig. 36: Visualization of f-actin (Sir-Actin) in immature sarcomeric myotubes as well as immature non-sarcomeric myotubes with CytoD 0.3μM application using confocal timelapse microscopy reveals that (A) Even the periodic sarcomeric f-actin gets disrupted if the myotube organization is immature as seen in A with the imperfectly aligned developing sarcomeric structure. (B) Several of the stress-fiber like f-actin filaments in the non-sarcomeric immature myotubes are severed. As the pink arrows indicate, what starts off as an area with many stress-fiber like f-actin structures become f-actin clusters by ~1hr indicating snapping and balling up of the stress fiber-like f-actin. By ~2hrs, the CytoD treatment depletes that cytoskeletal area of most of the stress fiber-like structures, leaving an almost plain white image. Scalebar is 10μm.

We performed further investigation observing f-actin in myotubes that are at different stages of differentiation for longer durations of CytoD 0.3μM exposure (up to 12 hours). **Fig.** 35 shows that when the sarcomeric myotubes are mature, the sarcomeric f-actin is not depolymerized by CytoD. However in these mature myotubes, the non-specific background f-actin (dark non-periodic areas around the sarcomeric structures) structures are depolymerized (**Fig.** 35). Interestingly, such disappearance of the non-specific background actin, with an intact sarcomeric pattern has been observed earlier[91] in cardiomyocytes treated with Latrunculin B, yet another actin depolymerizing agent. These dark structures however slowly depolymerize in the timescale of about 8 hours, which indicates that some of these f-actin structures are

likely much more stable than f-actin in pre-sarcomeric immature myotubes (**Fig.** 36B). There are cytoskeletal changes that occur in the non-sarcomeric f-acin in these myotubes within 2 hours. However these changes are much more subtle (can be seen in videos and in **Fig.** 34 if carefully observed) because they and are underwhelmed by the tremendous amount of sarcomeric f-actin.

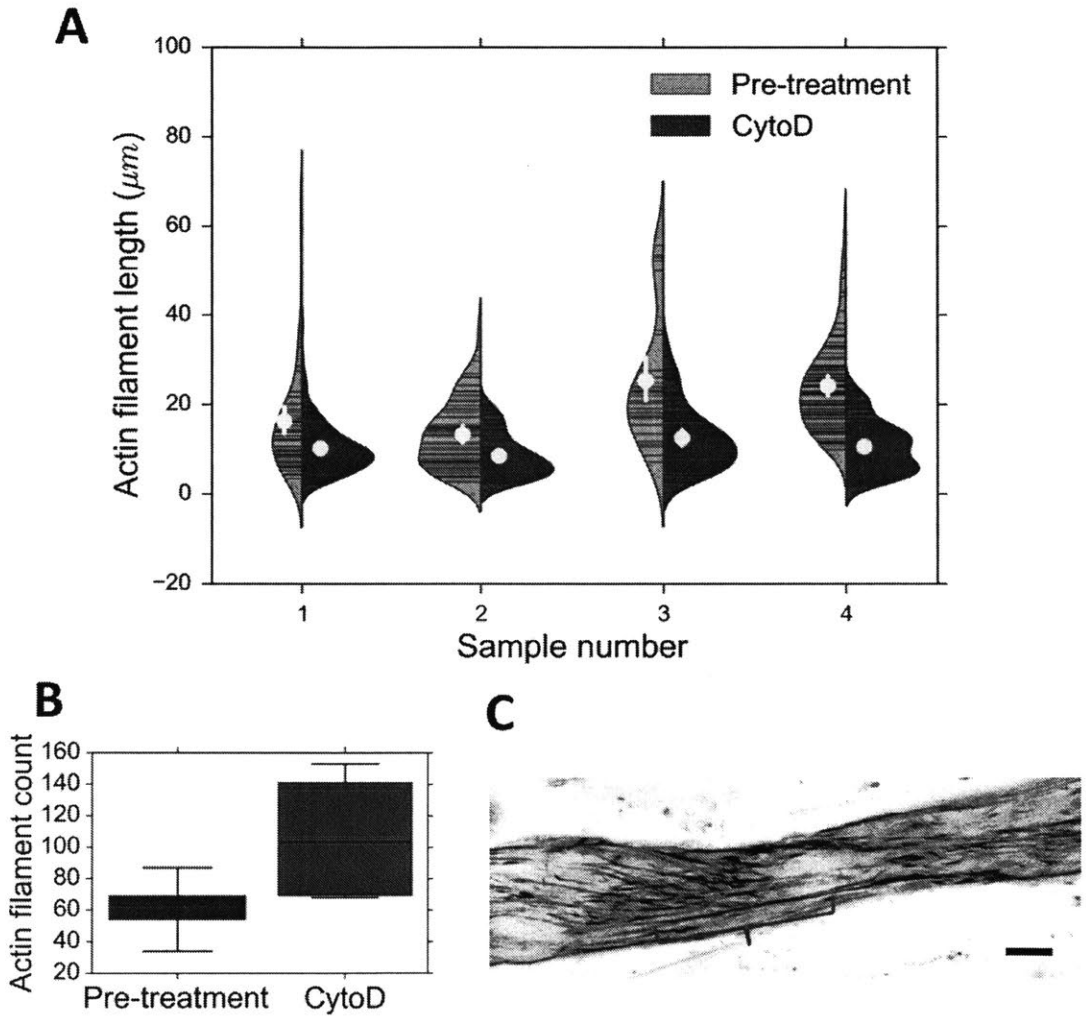

Fig. 37: (A) Quantification of the non-sarcomeric stress-fiber like f-actin breakdown in pre-sarcomeric immature myotubes shows that the distribution of linear f-actin filaments gets skewed towards shorter filaments with CytoD treatment (B) There seem to be many more stress-fiber like f-actin filaments with CytoD treatment. i.e. CytoD treatment converts a few long f-actin filaments into many more shorter filaments. (C) Quantification is performed by manually counting stress-fiber like f-actin structures and measuring their length using the length tool of ImageJ software. An example of an stress-fiber like actin filament in shown with a red curly brace showing the extent of the filamentous. The beginning and ends were chosen

(subjectively) based on the location where there appears to be a branching of the bundled stress-fiber like f-actin or a clear stop.

In immature myotubes, the immature sarcomeric f-actin structures do get disrupted by CytoD as shown in **Fig.** 36A. This also follows from earlier efforts[92] which show that immature sarcomeric f-actin filaments, also called pre-myofibrils are not capped (unprotected ends), while mature sarcomeric f-actin filaments, myofibrils have capped (protected) ends, with the protein CapZ capping the barbed end of f-actin and tropomodulin capping the pointed end. So it follows that mature sarcomeric f-actin is indeed protected from CytoD, which induces depolymerization typically by binding to the barbed end of f-actin. Lastly, f-actin filaments in pre-sarcomeric immature myotubes are disrupted quickly in 1-2 hours by CytoD (**Fig.**36B). Furthermore, a quantification of this non-sarcomeric f-actin reveals that the number of f-actin filaments increases while the size of each filament reduces upon CytoD treatment. This trend clearly reflects the f-actin depolymerization trend qualitatively illustrated earlier in **Fig.** 34 and 36.

3.4.4 Conclusions and next steps

It is clear that CytoD doesn't disrupt the sarcomeric f-actin in mature myotubes, while it does disrupt the non-sarcomeric stress fiber like f-actin filaments often severing a few long f-actin filaments into many short ones. Severing the stress fiber like f-actin filaments seems counter-intuitive to the mechanism of actin of CytoD which induces thin filament depolymerization by binding to the barbed end. We hypothesize that this is an indirect effect due to adhesions holding the stress fiber like f-actin intact being disrupted. From observations of timelapse videos of this severing phenomenon, it almost seems like a rope that is in tension suddenly snapping leading to thinner ropes which also release some tension. There are many categories of f-actin as discussed later in Sec. 3.6. So far, it is still unclear which f-actin filaments are being disrupted by CytoD.

In order to perform a more detailed characterization of this, we perform 2 kinds of studies:

1) A study of the dynamics of f-actin polymerization and turnover using fluorescence recovery after photobleaching (FRAP). This is the topic of Section 3.5

2) The use of more specific f-actin inhibitors to understand which f-actin filaments impede muscle contraction and which ones help. We discuss these experiments in Section 3.6

3.5 The shifting polymerization dynamics of f-actin

3.5.1 Hypothesis: CytoD depolymerizes the fast-turnover f-actin filaments

There are several ways to classify f-actin structures within a cell: long stable stress fiber like f-actin vs short rapidly turning over mesh-like f-actin, f-actin capped by capping proteins such as tropomodulin and CapZ vs others that are not, sarcomeric f-actin vs non-sarcomeric f-actin etc. In order to classify all these different kinds of filaments broadly in to 2 quantifiable categories, we use the fluorescence recovery after photobleaching (FRAP) experiment with GFP-tagged monomeric actin.

By bleaching a window of these monomers, and observing the recovery times, we can compute the actin turnover timescales. In this case, we categorize all the fluorescent actin present into 3 regimes: free monomeric actin, dynamic (fast turnover) f-actin and immobile stable f-actin. The choice of "3 regimes" is on purpose[1] in this case, as we would like to subcategorize the filamentous actin in to those that turnover in the 10s-1min timescale, and those that turnover much slower (eg. > 10min timescale). The former we define here as dynamic f-actin and the later as stable f-actin.

As illustrated in **Fig.** 38, the FRAP experiments involving fluorescently tagged actin monomers are complex to interpret due to the different processes that contribute to the fluorescence recovery. The early phase of the recovery is rapid and dominated by the diffusion of the GFP-

[1] When analyzing GFP-actin FRAP experiments, one needs to use a minimum of 2 separate phases to account for the various timescales of fluorescence recovery: rapid recovery due to monomer diffusion and slower recovery due to filamentous actin. However, the filamentous actin phase could potentially be subdivided in to many categories (n>7). There are many sub categories of f-actin (sec 3.6) which all have their characteristic timescales. Depending on the experimental question, for instance in investigating differences between two specific sub-divisions within the dynamic filaments, we may have to fit multiple exponentials to the same ~1min timescale data as well. For example see 93 Fritzsche, M. *et al.* Cytoskeletal actin dynamics shape a ramifying actin network underpinning immunological synapse formation. *Science Advances* **3** (2017).. But that is a 2rd order level of detail that would be good, but something we are not investigating in this study. We are just looking at the average turnover rate of all filaments that recover in the ~10sec to 1min timescale, and thus sub-categorize the filamentous actin into dynamic filaments (~10s to 1min timescale) and stable filaments (whose recovery time is in the 10s of minutes i.e. much longer than the duration of this experiment which is 3 minutes long).

tagged monomeric actin due to its size relative to the GFP tagged f-actin diffusing in from other areas [94]. This is typically complete within a few seconds depending on the area of the bleach window. In the next phase, the recovery is dominated by incorporation of GFP monomers within the bleached dynamic f-actin filaments. This process has a timescale typically much slower than monomer diffusion and is in the 10s of seconds. Finally, there are bleached f-actin filaments that are so stable (slow turnover) due to capping proteins and/or stabilized by nebulins, tropomyosins, adducing, caldesmon and calponins that in the timescale of the experiment (2-3 minutes), they do not recover. This could involve a combination of sarcomeric and non-sarcomeric f-actin and we lump them together as the immobile fraction or stable f-actin in this experiment.

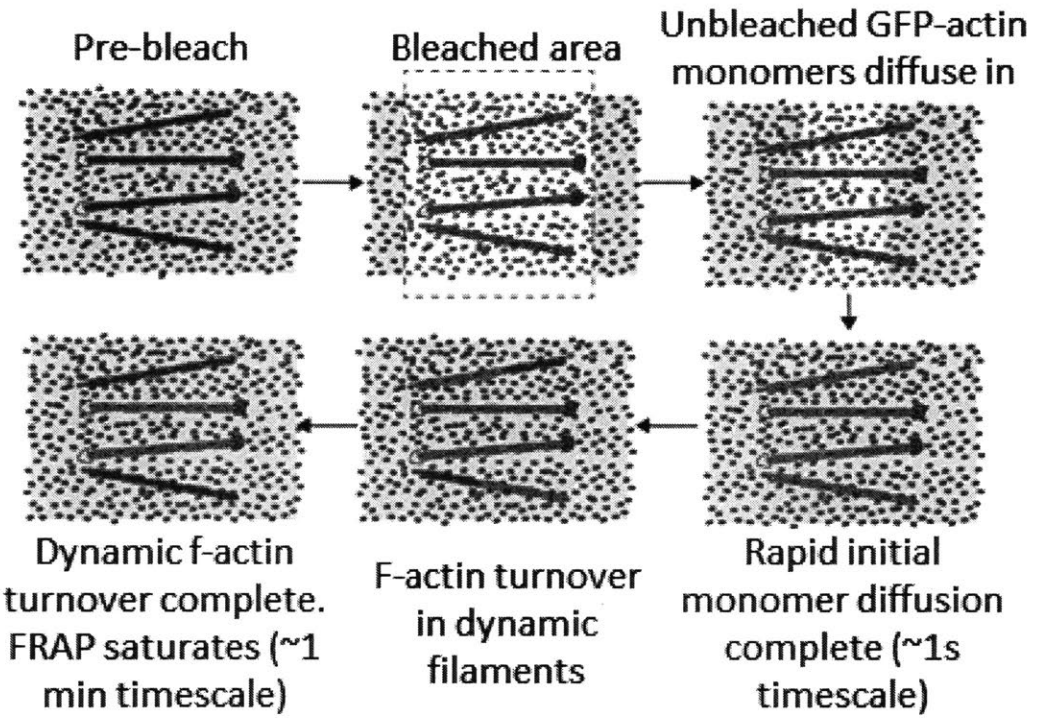

Fig. 38: Schematic of fluorescence recovery after photobleaching of GFP-tagged actin monomers. Monomer recovery occurs first and is the most rapid (GFP-tagged monomers indicated by the green particles and the background green used to doubly emphasize the location of unbleached GFP-tagged monomers). F-actin turnover driven recovery is slower than the diffusion of monomers (10X slower), and so can be considered to occur after monomer recovery is complete. This is schematically indicated by the grey (bleached) f-actin filaments acquiring some green particles (unbleached monomers) from the barbed/polymerizing end of f-actin. Some of the bleached f-actin filaments recover much more

slowly (10s of minutes) due to protective capping proteins. These are schematically shown to never recover (always grey after bleaching) in the timescale of the experiments conducted (2-3 minutes).

The timescales of the recovery of the 3 actin sub-compartments have an order of magnitude difference from each other (monomeric actin ~1s, dynamic f-actin 10s-1min, stable f-actin > 10mins). The contribution to the recovery curve of stable f-actin is limited as we only analyze the first 3 minutes of recovery. So an implicit assumption in the FRAP analysis is that the plateau of the exponential recovery curve fit to the dynamic f-actin recovery region marks the amount of stable f-actin (see **Fig.** 39). Furthermore as monomeric diffusion is an order of magnitude faster than dynamic f-actin turnover (see **Fig.** 39 and 40), we utilize this to temporally decouple the 2 processes and thereby simplify the interpretation of the FRAP recovery profile. We discuss further details in the next section.

3.5.2 Experimental methods

We grow and differentiate C2C12 myoblasts on an IBIDI-treated surface to form myotubes on 2D (see section 2.2). We use unmodified C2C12 cells for this as we want the cell not to be bluelight sensitive (as the C2C12-ChR2 cells are) because we want to have GFP-actin in these cells. One day before the FRAP assay (day 11 after differentiation), we added 100μL of Bacmam 2.0 Cell Light Actin-GFP reagent (ThermoFisher) in 1ml of DM+ to the cells for GFP-Actin transfection. Overnight incubation of this reagent leads to expression of a GFP-tagged actin construct delivered through a BL1 safe insect virus, Baculovirus.

After verifying the GFP-actin expression in the cells using a confocal line scanning microscope (FV-1000, Olympus, Japan) with a 60X oil immersion objective (NA 1.30), 150μL of matrigel was polymerized on top of the IBIDI plates so that cell adhesion to this ECM prevents dramatic cell movements when treated with CytoD. A bleach window was defined using the stimulus settings of the FV-1000 software such that the height of the window was slightly larger than the width of the myotube (**Fig.** 39). This is so that all diffusion of GFP-actin in to this window occurs from the left or right, making it effectively a 1D diffusion problem. Furthermore, the width of the window was chosen to be 2μm so that diffusion into this effective length scale is complete within 1s (timescale ~ L^2/D, with a D ~ $3*10^{-8}$cm^2/s for monomeric actin, timescale ~ (1μm)^2/($3*10^{-8}$cm^2/s) < 1s). Lastly the pinhole of the confocal was completely opened (800μm) so that the entire depth of the cell was bleached. We also ensured that there are no

out-of-plane cells that contribute to the recovery curves. This is possible as most cells are in a plane on 2D.

There are several imaging parameters listed below that need to be optimized depending on the desired FRAP study. The optimal parameters completely photobleach all the GFP across the cell in the bleach window, minimize photobleaching while capturing the recovery and capture the recovery at an appropriate frame rate and duration so as to capture the phenomenon of interest. More details about these choices follow.

1. Photobleaching
    a. Laser intensity, laser duration time for photobleaching
2. Recovery
    a. Laser intensity
    b. Pixel resolution of capture
    c. Size of the photobleaching window
    d. Frame rate of recovery capture
    e. Duration of capture

The photobleaching parameters (laser intensity, duration) described below were chosen to as to completely bleach all the GFP to the level of the background so that any recovery of fluorescence in the window of recovery occurs due to diffusion of GFP-tagged monomers from outside of the window (as shown in **Fig.** 38 and 39) and consequent incorporation in to the f-actin. Bleaching of the window was performed with the DAPI, FITC and TRITC lasers all set at 80% of the maximum power, with bleach settings being 200μs/pixel, 1px = 0.1μm in the XY plane, and with 5 frames of sequential bleaching. The pre-bleach image was acquired, followed by 5 bleaches within the bleach window and then the post-bleach recovery profile (of average intensity within the bleach window) was obtained. Each pixel was exposed for 2μs in line scanning mode and the effective framerate of acquisition this depends on the overall number of pixels imaged used in imaging.

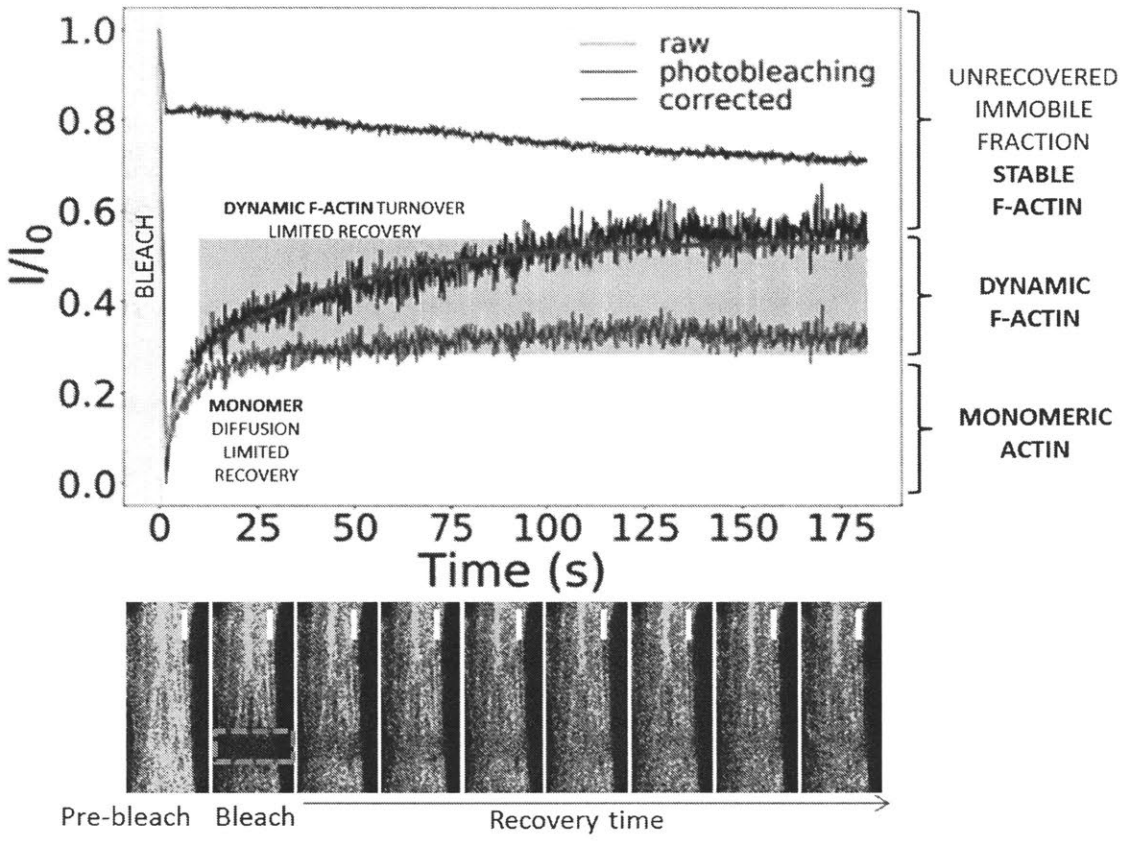

Fig. 39: A typical FRAP recovery curve and pictures from an actual experiment. C2C12 myotubes with GFP-actin monomers are bleached with a rectangular window covering the entire width of the cell throughout the entire depth. Scalebar is 10μm. By plotting the intensity recovery within the bleach window over time and by using the remaining image to compute the rate of photobleaching we obtain a corrected recovery curve, which has a rapid diffusion limited recovery in the ~1s timescale followed by a slower turnover limited recovery.

The parameters for capturing the fluorescence recovery are chosen as follows:

As shown in **Fig.** 39 with the FRAP recovery data from one cell sample, photobleaching does occur. We lowered the laser power to ~2%, used a pixel resolution of 1px = 0.1μm in the XY plane and an exposure time to 2μs/px in order to minimize photobleaching, while 1px = 0.1μm in the XY plane optimizing for maximal signal. Using too low a laser intensity (<2%) is not optimal as it would decrease signal:noise too much even though photobleaching would be even smaller. With the above parameters we kept photobleaching during recovery to < 20%. We correct for the effect of photobleaching on the fluorescence recovery curve by computing

the change in average intensity of the non-bleached areas. By quantifying photobleaching during acquisition in areas outside the bleach window (**Fig.** 39), we use this information to normalize the raw recovery curve.

The choice of frame rate and duration of capture are also optimized based the following criteria. The upper bound to the frame rate is limited by the pixel exposure time, pixel resolution and number of pixels because we use a line scanning confocal microscope. The upper bound is also dependent on the duration of recovery capture and photobleaching. Using a high frame rate limits the duration of capture, which significantly affects which phenomena we capture. For eg. to capture diffusion, we may only need a few seconds of capture (see above, diffusion within a bleach window having a length scale of 1um has a 1s timescale). However, to capture f-actin turnover which has a timescale between ~10s-1min, we may need to capture several minutes of data. The lower bound of the frame rate depends on the Nyquist criterion. To capture the different recovery regimes, we use different frame rates based on the Nyquist criterion (frequency of information capture must be > 2*frequency of phenomenon observed). For instance, rapid diffusion may require a much higher frame rate than slower f-actin turnover. In order to capture the initial rapid diffusion limited fluorescence recovery, this optimization resulted in an effective frame rate of ~33Hz and duration of ~5s. For the f-actin turnover, we acquired images of larger areas leading to an effective frame rate of ~5Hz (which is sufficient to capture recovery curves with timescale of 10s of seconds) and duration of ~180s. Alternatively, we could have captured the entire recovery curve with the highest possible frame rate to capture all phenomena. But this would have minimized the pixel area (and thereby increase noise in the measurement). Due to our use of a line scanning confocal microscope, imaging a larger area leads to lower frame rates. Moreover, using the highest frame rate, also dramatically increases the rate of photo-bleaching and this limits the duration of capture. Hence the high frame rate used for short timescale diffusion limited recovery (<1s), cannot be used to capture the dynamic f-actin recovery (which has a 3 minute duration).

Overall, it must be clear from the discussion above that choosing parameters for FRAP is a complex multi-dimensional optimization problem involving several competing tradeoffs. The final choice of our parameters is empirical and these choices may not necessarily represent the global optimum. However, the key to performing a valid comparison between the control (DMSO treated) and the condition (CytoD treated) is to ensure that the FRAP parameters used for both cases are identical, thereby preventing any internal bias. The exact choice of

parameters (frame rate 5Hz vs 2Hz, duration of 120s vs 180s) introduces a global selection bias in terms of analyzing the recovery of specific f-actin filaments with a certain range of timescales captured by the specific parameters. But as long as the parameters are fixed between the control and condition cases, there is no internal comparison bias.

In this experiment, we sub-categorize the total GFP-actin in to GFP-actin present as monomers, incorporated in dynamic f-actin (turnover timescale ~1 minute) and stable f-actin (bleached stable filaments don't recover in the timescale of minutes). By using a total capture time of 3 minutes, we ignore the recovery of stable f-actin filaments (including sarcomeric f-actin) that recover in the timescale of 10s of minutes. Moreover, the monomeric actin recovery is complete within the first few seconds (see description below).

So , in order to compute the timescale of dynamic f-actin turnover, the fluorescence recovery profile from 10s to 180s was fit with an exponential curve such as (a-b*e^(-t/tc)) similar to works described elsewhere[95]. In this equation, 'a' is the total recovered fraction at t -> ∞, which is the sum of the monomer associated recovery and dynamic actin associated recovery. a-b represents the monomer fraction (this approximation works because the monomer recovery timescale of ~1s << 180s, so effectively (a-b*e^(-t/tc)) evaluated at t=0 is a-b which gives the fraction of monomer recovery). Hence, (a-(a-b)) = b is the fraction of dynamic f-actin. tc is the timescale of dynamic f-actin turnover. Lastly, (1-a) is the immobile fraction, which represents the stable f-actin, stable in the sense that it recovers at a timescale t_{stable} >> ~1min timescale of this experiment. The choice of 10s is an engineering approximation. If the timescale of diffusion is 1s, then 10s represents 10 timescales in an exponential recovery, which is 99.995% of completeness of diffusion recovery. So to find the dynamic actin turnover time, fitting an exponential to the curve after 10s ensures that the diffusion timescale does not affect the estimated turnover time. We use 5-9 cells typically for each condition (DMSO, CytoD 0.3μM, CytoD 3μM) and compute the FRAP recovery curves before and 1 hour after treatment for each of these cells. These experiments are paired because we observed the same cell before and after treatment. Based on the curve fitting exercise described above we compute the relative ratios of G-actin, dynamic F-actin and stable F-actin as well as the turnover timescale of dynamic F-actin, both before and after the treatments.

In **Fig.** 41 we have plotted these numbers as a ratio of (actin fraction after treatment)/(actin fraction before treatment for the same cell) for each of G-actin, dynamic and stable F-actin.

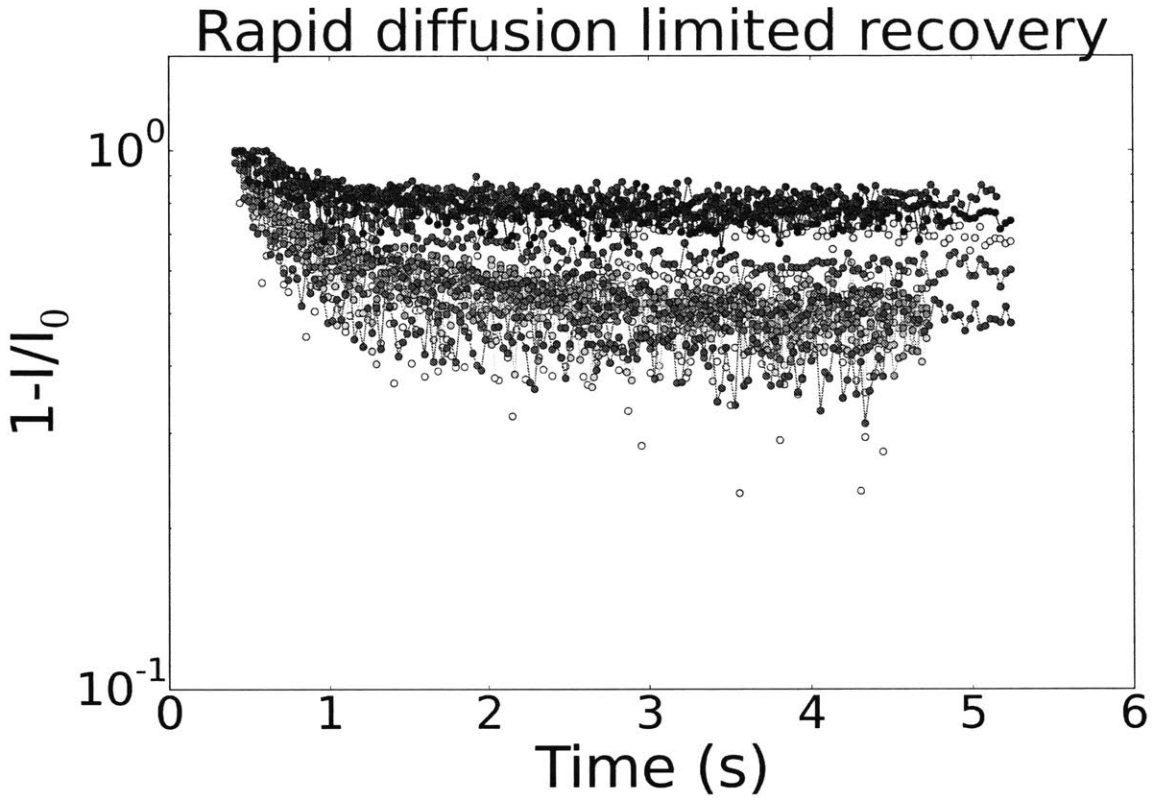

Fig. 40: The first few seconds of the FRAP recovery curve, plotted based on 19 individual FRAP experiments conducted at different regions along 3 different myotubes. The rapid initial rise is driven purely by diffusion of monomers. We use this recovery profile to compute the timescale of diffusion.

3.5.3 Results and discussion

We used a framerate of 33Hz to acquire the first 5 seconds of images, which gave us the rapid diffusion recovery (**Fig.** 40). By fitting this curve to an exponential curve (1-e^(-t/Tdiff)), we obtained the diffusion timeconstant (Tdiff ~ L^2/D). This let us estimate the order of magnitude of the diffusion constant D ~ $1.05*10^{-8}$ +/- $2.4*10^{-9}$ cm^2/s. This value is similar in magnitude to monomeric actin diffusion constants of ~$3*10^{-8}cm^2/s$ reported in literature[94], which validates our assumptions about the initial rapid diffusion with ~1s timescale.

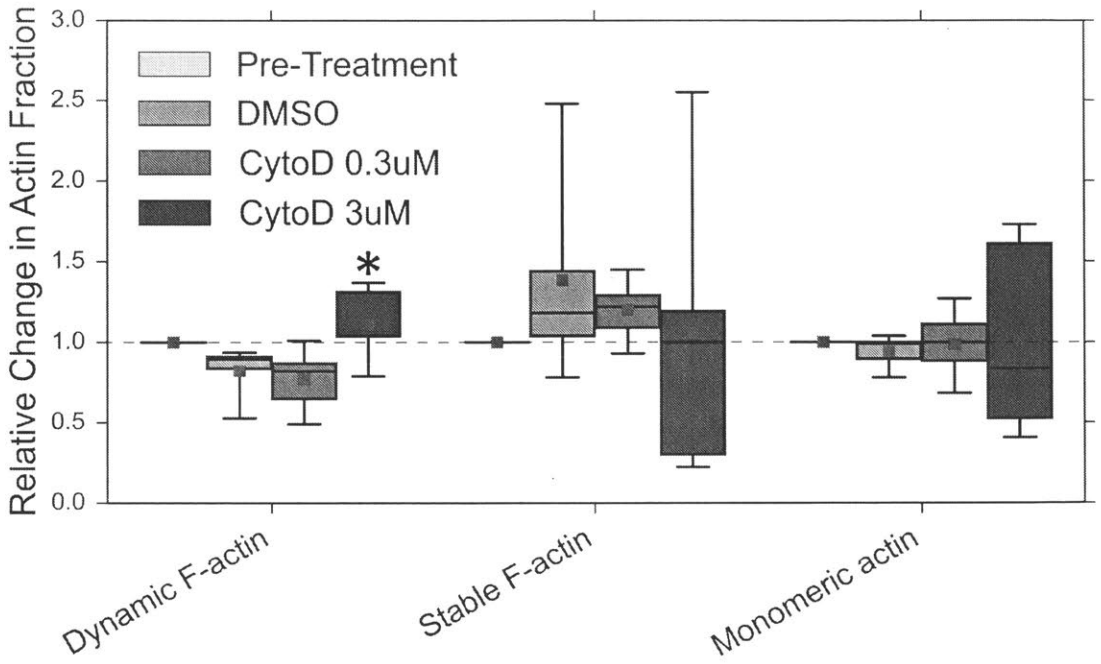

Fig. 41: Relative change ratio of the fractions of the various actin compartments(actin monomer, dynamic f-actin and stable f-actin). The Y-axis represents the ratio of (Dynamic F-actin fraction after treatment)/(Dynamic F-actin fraction before treatment) etc for the various compartments – Dynamic (corresponding to 'b' in the fit equation (a-b*e^(-t/tc))), stable F-actin (corresponding to '1-a') as well as Monomeric actin ('a-b'). The various treatment conditions (DMSO, CytoD) are shown in shades of green. The red dots represent the mean values. * p = 0.029 with a one-tailed unpaired 2-sample t-test with respect to the DMSO controls. N=5 was used for DMSO and CytoD 3μM conditions. N = 9 was used for the CytoD 0.3μM condition.

Treatment with CytoD did not lead to statistically significant changes among the various actin fractions. Largely this makes sense because even the f-actin visualizations with Sir-Actin did not show a very significant breakdown of f-actin everywhere. The changes were more subtle. The only exception to this being the dynamic f-actin change ratio which is statistically significantly higher with CytoD 3μM than DMSO controls. In general there is a trend towards decreasing stable actin and increasing dynamic f-actin with higher concentrations of CytoD (**Fig.** 41). Also, CytoD breaks down many long f-actin filaments (**Fig.** 37) which explains the trend of reducing stable actin with many of these filaments becoming dynamic at higher CytoD doses.

As there is not a significant change in most of the actin fractions, we wanted to identify if the distribution of filaments within the dynamic f-actin pool may have changed. CytoD is most likely to affect filaments that turnover fast.

In order to answer this question, we compute the average turnover time of the dynamic f-actin which represents the population average of the turnover times of all the dynamic f-actin filaments in the cell. We represent this as a ratio normalizing the timescales of f-actin turnover of each cell with respect to the corresponding timescale prior to treatment of that cell. As shown in **Fig.** 42, there is a significant increase in the timescale of dynamic f-actin turnover with CytoD concentration. For this to be possible, CytoD must be converting the dynamic f-actin filaments with relatively fast turnover time to ones with a slower turnover rate. This seems plausible given the mechanism of action of CytoD that is known to bind to the barbed end, preventing polymerization. So it follows that this binding slightly reduces the turnover speed (increases turnover time). Furthermore, as the relative fraction of dynamic f-actin doesn't vary significantly at low CytoD doses (**Fig.** 41), this suggests that there are not too many CytoD sensitive filaments. This is also reflected from our FRAP experiments illustrated **Fig.** 41 showing that the monomer fraction does not change significantly. If there was a significant amount of CytoD sensitive filaments among the dynamic f-actin filaments, the monomer fraction must have increased significantly (which did not). At the same time, several non-sarcomeric stress fiber like f-actin filaments get severed and exhibit a shortening characteristic of a severed "rope" in tension as illustrated in Figs. 34, 36 and 37.

To summarize, *CytoD treatment leads to depolymerization of a small fraction of dynamic f-actin filaments which leads to shortening and severing of several stress-fiber like non-sarcomeric f-actin filaments.* This effect of severing of stress-fiber like f-actin is not characteristic of the known mechanism of CytoD. It must be an indirect effect of CytoD. The working hypothesis is that the CytoD sensitive filaments stabilize the long stress-fiber like non-sarcomeric filaments. *Most interestingly, this effect is sufficient in some manner to improve the contraction significantly.* This could perhaps be due to the reduced mechanical hindrance of these f-actin filaments. We explore the mechanism of this improvement further in Chapter 4..

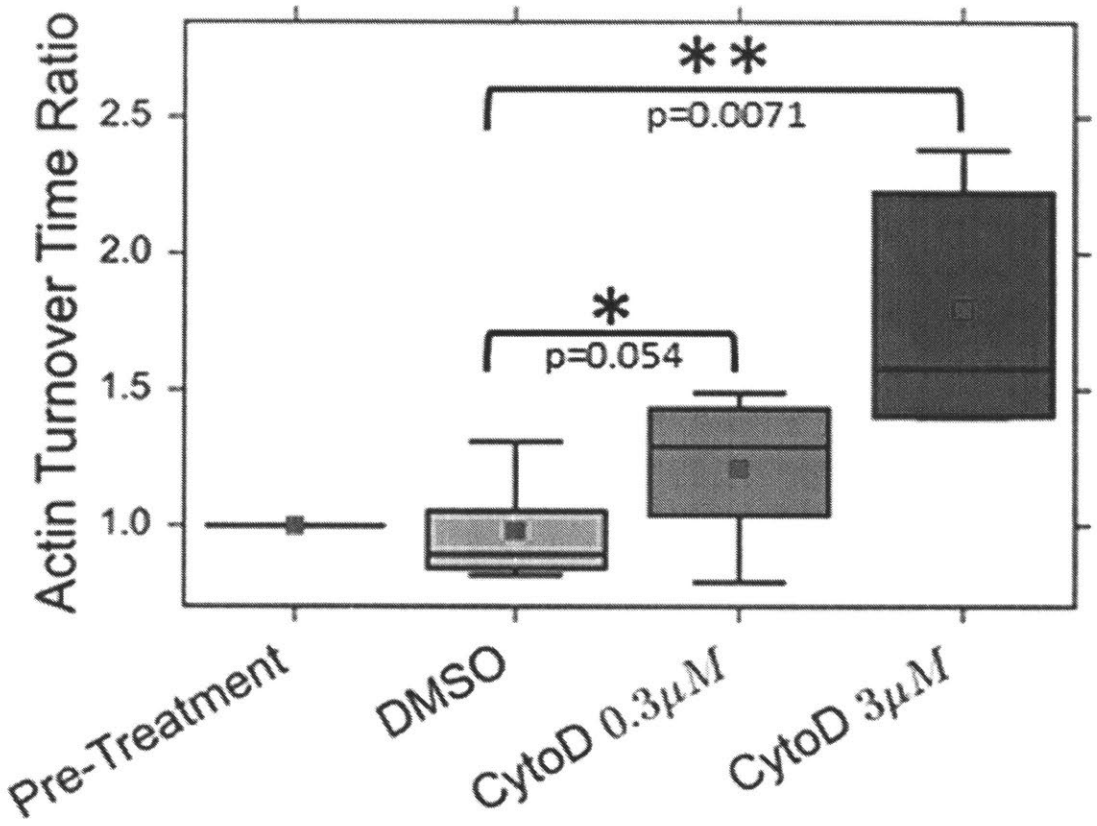

Fig. 42: Relative change ratio of the timescales of dynamic f-actin turnover with the various treatments. Significance tests were 1-tailed t-tests. The turnover time change with CytoD 0.3μM is barely statistically significant, while the change due to CytoD 3μM is highly statistically significant relative to the DMSO treated controls. A one-tailed unpaired 2-sample t-test with respect to the DMSO controls was used to test for statistical significance. N=5 was used for DMSO and CytoD 3μM conditions. N = 9 was used for the CytoD 0.3μM condition.

3.6 Targeting f-actin subcompartments

Our tests so far are limited to CytoD (majority of tests) and Latrunculin A(Chapter 2), which both disrupt f-actin and show a functional improvement in muscle contraction. CytoD is somewhat specific in the kind of f-actin it targets (dynamic f-actin with an uncapped or weakly-capped barbed end), leading to slightly "less dynamic" (slower turnover) dynamic f-actin filaments, which are slightly shorter and more in number.

However, Latrunculin A is not nearly as specific. As Latrunculin A acts by actin monomer sequestration, it is quite likely to affect all f-actin filaments that exchange monomers with the

monomeric pool, which is the vast majority of all f-actin subtypes. Not only is it likely to affect the dynamic f-actin pool that is involved in active exchange of monomers with the monomeric pool, but it also likely affects spontaneous actin nucleation, branched f-actin formation, formin-mediated actin assembly etc. by sequestering monomers. Clearly it is not specific.

In all the experiments so far, we have disrupted only the CytoD sensitive dynamic (uncapped) f-actin filaments. In this section, we would like to answer the following questions, which require targeting other f-actin sub-compartments with specific small molecule inhibitors:

- Is the improvement of muscle contraction an effect that is limited to disruption of just the CytoD sensitive dynamic f-actin filaments?
- Would disrupting other f-actin subdomains also lead to a functional improvement?

Identifying more specific f-actin sub-compartments whose disruption may be functionally beneficial could be a starting point towards developing more targeted actin disrupting therapeutics as well as understanding the mechanism underlying the functional improvement.

3.6.1 Introduction to the different non-sarcomeric f-actin subtypes

There are a large variety of non-sarcomeric f-actin structures within cells, typically formed and defined by their association to a range of actin binding proteins (italicized below). The 3 primary structures of non-sarcomeric f-actin that initially form are:

1) Short linear f-actin filaments typically formed by spontaneous nucleation and elongation of ATP bound G-actin monomers.
2) Long linear f-actin filaments nucleated through *formins* that are typically used in the contractile ring during cell division or in stress fibers. The formins protect the barbed end of f-actin from capping proteins which leads to increased lengths of the filaments formed through formins. *Profillin* also aids in improving the speed of this.
3) Branched f-actin formed by branching nucleators such as *Arp2/3* and its regulators such as *WASP and the SCAR/WAVE complex.*

There are many ways in which these 3 types of f-actin are modified and rearranged, which could lead to several different secondary structures or localization of these structures to different parts of the cell. These include [96]:

a) Cortical f-actin bound typically to membrane and membrane proteins through actin-binding proteins such as *α-actinin, annexin II, α-catenin, BPAG, dystrophin, ERM proteins, plectin, spectrin, Sla2 (HIP1R), talin, tensin, utrophin and vinculin*
b) Stable f-actin stabilized, scaffolded or chaperoned by proteins such as adducin, caldesmon, calponin, nebulin and tropomyosin
c) Capped f-actin through barbed end capping proteins such as *CapZ, formins and tensin*, as well as pointed end capping proteins such as *ARP2/3 and tropomodulin*
d) Tensile f-actin involved in creating cytoskeletal tension through *myosin.*
e) Actin linked to other cytoskeletal filaments. Eg. Actin linked to intermediate filaments (IF) through *spectrin*, to microtubules (MT) through *tau* as well as to IF and MT through *plectin, BPAG, MACF and MAP2.*
f) Cross-linked f-actin through cross-linking proteins such as *α-actinin, spectrin and transgelin*
g) Bundled f-actin through crosslinking proteins
    a. in microvilli such as *fimbrin, scruin, cillin and espin*
    b. in filopodia such as *fascin and α-actinin* (and)
    c. in stress fibers such as *α-actinin and fascin*

The ideal experiment would be to fabricate a 3D muscle fiber on our cantilever setup (Chapter 2), measure its contractility and then perform an acute disruption of any one of the specific proteins above to measure the change in contractility. If beneficial (or otherwise), such an experiment would elucidate the role of these various f-actin filaments in force transmission.

While the tools of modern molecular biology such as Si-RNA, CRISPR based gene regulation could be used to develop knock down models (at the RNA level), or CRISPR based gene editing to make knock out models, these tools are still not ideal for acute *in situ* disruption experiments due to differences in delivery, slower time of action etc. So we limit this study to small molecules that may be targeted towards specific actin subdomains to understand their influence on muscle active contractility.

The following are the small molecule inhibitors that specifically disrupt 4 categories of f-actin:

1) **Uncapped dynamic f-actin**: **Cytochalasin D** is known to bind to the barbed end of f-actin typically depolymerizing the dynamic filaments which shorten from their pointed end.
2) **Long linear f-actin filaments:** **SMIFH2** is a specific small molecule inhibitor of formins. It is known to interact with FH2: formin homology domain 2, which typically prevents formation of long linear f-actin (by blocking formin mediated actin assembly), and/or disrupts long f-actin associated with formins.
3) **Branched f-actin:** **CK666** is a specific small molecule disruptor of the ARP2/3 complex, which effectively prevents the formation of branched f-actin
4) **Stable tropomyosin stabilized non-sarcomeric f-actin: TR100 and ATM3507** are small molecule inhibitors of the non-sarcomeric tropomyosin isoform Tpm3.1, which could be used to disrupt f-actin filaments associated with Tpm3.1.

As we have investigated the effect of CytoD in detail, this section is focused on inhibitors for the other three actin subdomains. We differentiate C2C12-ChR2 cells in 3D as before on our cantilever device and measure the active formation before and after treatment with different doses of the various inhibitors.

3.6.2 Inhibiting formin-mediated actin assembly

As shown in **Fig.** 43, treatment with SMIFH2 leads to a statistically significant improvement in active contraction at the high concentrations. Inhibiting formins typically leads to halting of formin mediated f-actin assembly of long f-actin filaments. This must mean the average f-actin length in the cell must be smaller with SMIFH2 treatment. This is very interesting because even CytoD treatment leads to shorter f-actin filaments albeit, with a different mechanism. The force improvement observed due to SMIFH2 supports the hypothesis that some f-actin filaments impede contraction.

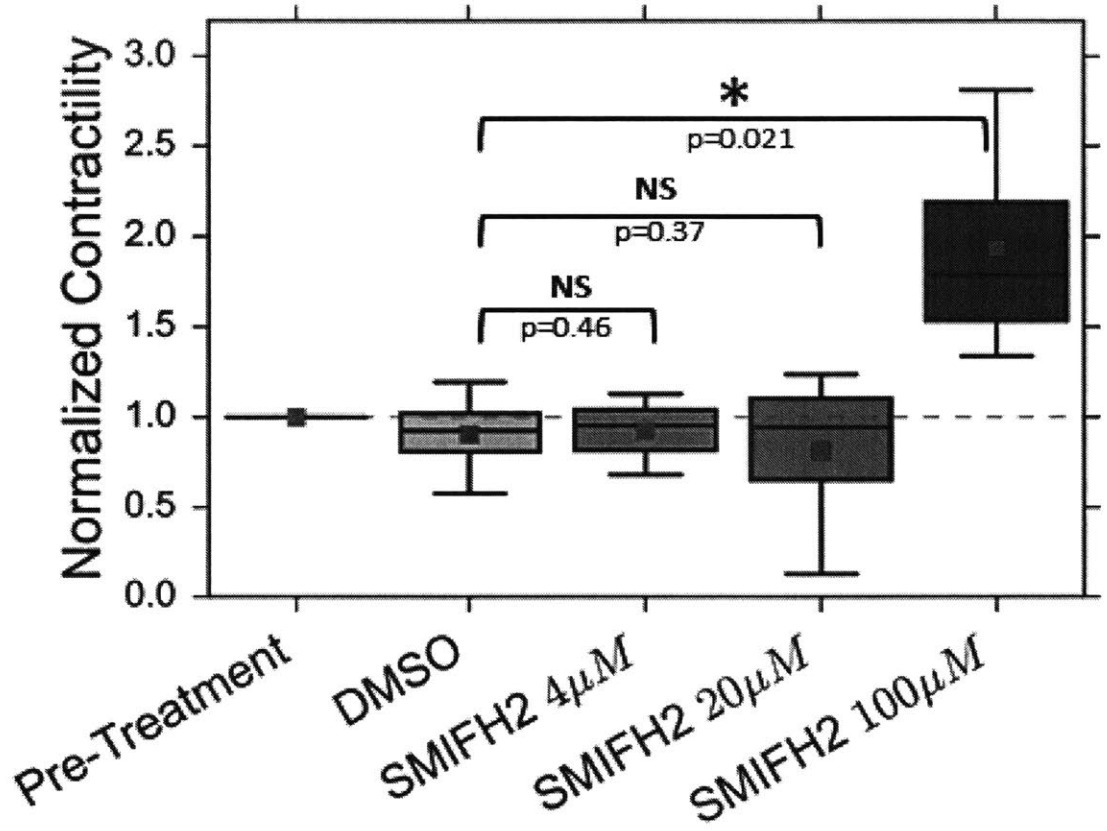

Fig. 43: Treatment with 100μM SMIFH2[97], a small molecule inhibitor of formin homology domain 2 improves active skeletal muscle contractility within 2 hours of treatment. This is likely due to inhibition of the FH2 domain of formins which leads to disruption of formin associated f-actin filaments and/or inhibition of formation of such filaments as formin is an f-actin nucleator. At SMIFH2 doses of 20μM or lower, no improvement in contraction was observed. Statistical significance testing was performed with a one-tailed unpaired 2-sample t-test with respect to the DMSO controls.

3.6.3 Disruption of Arp2/3 mediated branched f-actin

As shown in **Fig.** 44, treatment with CK666 (at 100μM), an Arp2/3 complex inhibitor leads to a gradual drop in the active contraction to nearly 50% 1 day after treatment. No functional improvement was observed. This leads us to conclude that the branched Arp2/3 mediated f-actin actually helps sarcomeric force transmission in muscle. This is the first data point in support of the hypothesis that f-actin (specifically the Arp2/3 mediated filaments) may have an important role in force transmission (Sec. 1.3, hypothesis 1). Future works are warranted to further explore the mechanistic role of these branched filaments in the force transmission.

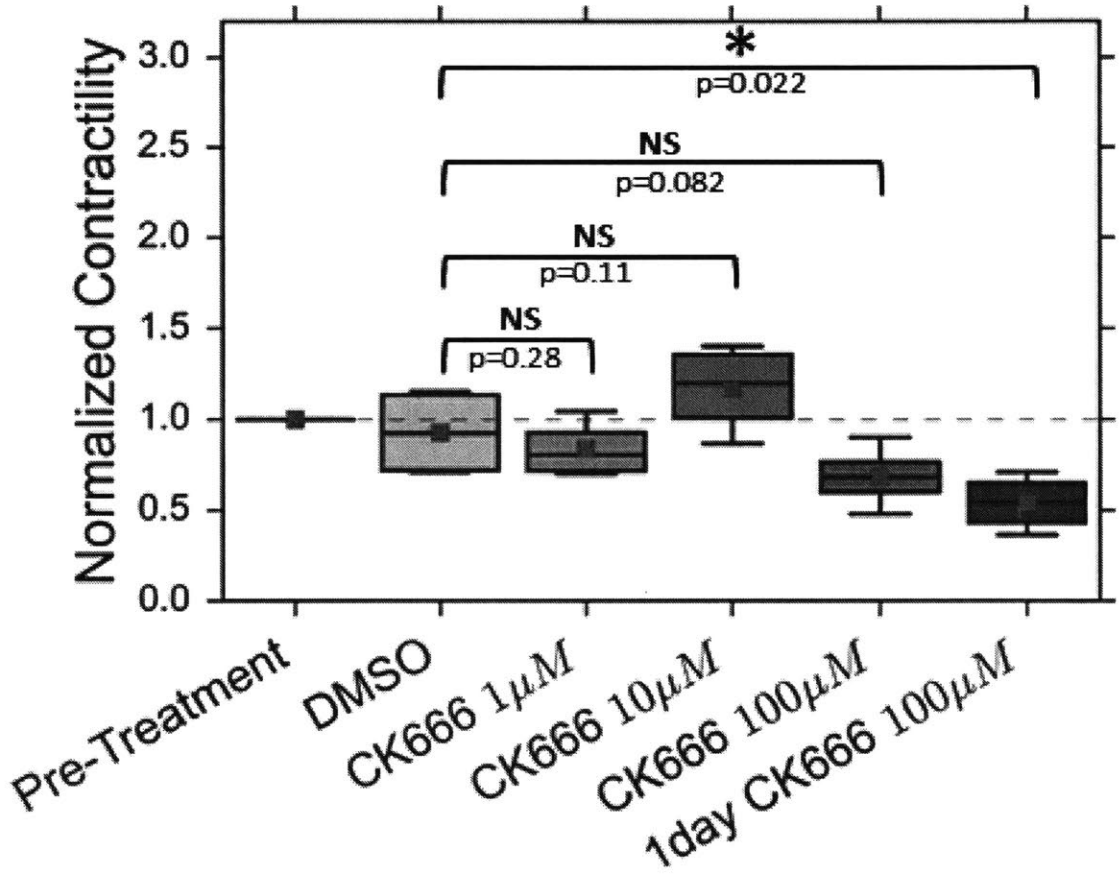

Fig. 44: Treatment with CK666 100μM, an inhibitor of the Arp2/3 complex leads to a gradual decline of contractility. The data for the change in contraction 2 hours (not-significant) and 1 day (statistically significant) after treatment with CK666 100μM are shown. This makes it plausible that the branched Arp2/3 mediated f-actin filaments do help in sarcomeric force transmission. At SMIFH2 doses of 20μM or lower, no statistically significant change in contraction was observed after 2 hours (shown) of contraction or after 1 day (not shown).

Statistical significance testing was performed with a one-tailed unpaired 2-sample t-test with respect to the DMSO controls.

3.6.4 Tropomyosin stabilized stable f-actin

We treated another set of 3D differentiated muscles on cantilevers with the anti-tropomyosin compounds TR100 and ATM3507 [98,99] (gifts from Dr. Peter Gunning) in order to investigate the role of tropomyosin stabilized f-actin in force transmission. Both these compounds are targeted towards the non-sarcomeric tropomyosin isoform Tpm3.1. As shown in **Fig.** 45 and 46, treatment leads to a dose dependent decline in the muscle active force. There is a ~60% decline in active force with 2 hours of exposure to TR100 50μM. Lower doses had no effect. In the case of ATM3507 50μM, there is a 90% decline within 2 hours, with lower doses showing slightly lower, yet significant declines.

TR100 and ATM3507 are compounds with such different structures that both bind to Tpm3.1, that the functional decline observed is clearly an effect of targeting the tropomyosins. Clearly f-actin filaments stabilized by the tropomyosin Tpm3.1 have an important role to play in sarcomeric force transmission. Interestingly, a similar result was also reported with mice which when treated with TR100 presented a muscle dystrophic phenotype [100]. This is the second data point in support of the hypothesis that f-actin (in this case the Tpm3.1 stabilized filaments) may have an important role in force transmission (Sec. 1.3, hypothesis 1).

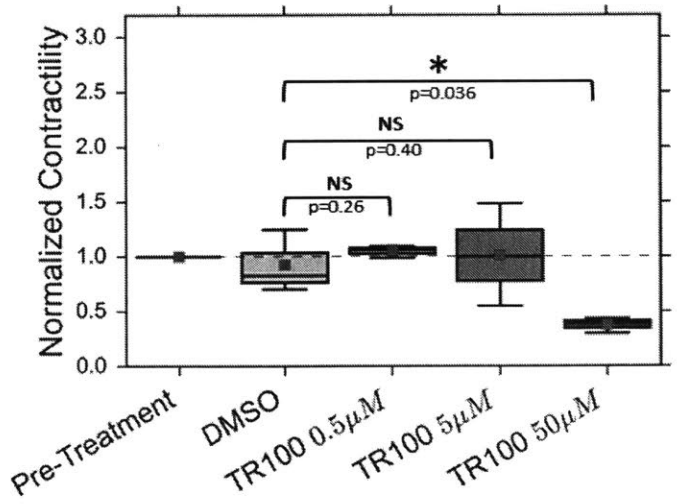

Fig. 45: Treatment with TR100, an anti-tropomyosin compound targeting the non-sarcomeric tropomyosin isoform Tpm3.1 leads to a decline in muscle contractility 2 hours after treatment.

Statistical significance testing was performed with a one-tailed unpaired 2-sample t-test with respect to the DMSO controls.

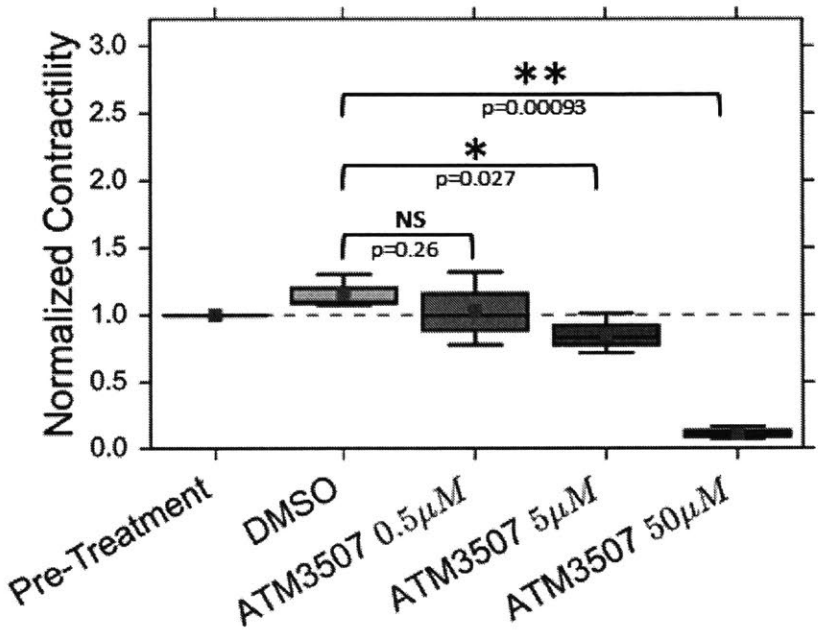

Fig. 46: Treatment with ATM3507, another anti-tropomyosin compound targeting the non-sarcomeric tropomyosin isoform Tpm3.1 leads to a decline in muscle contractility 2 hours after treatment. Statistical significance testing was performed with a one-tailed unpaired 2-sample t-test with respect to the DMSO controls.

3.6.5 Conclusions

We find that disrupting the dynamic f-actin (CytoD) or long linear f-actin by preventing formin mediated assembly could be beneficial to muscle contraction. In both these cases actin disruption leads to lower filament length. However, disruption of either Arp2/3 mediated branched f-actin or tropomyosin Tpm3.1 stabilized f-actin seems deleterious to muscle active force, indicating an essential role of these filaments (when intact) in muscle sarcomeric force transmission.

Chapter 4: Mechanical softening improves muscle force

4.1 Mechanical hypothesis

Our evidence so far supports both the hypotheses discussed in Sec 1.3. We have evidence in support of the hypothesis that certain f-actin filaments (the CytoD sensitive dynamic f-actin and the formin-mediated filaments) mechanically impede skeletal muscle contraction (Sec. 2.2, 2.3, 3.2, 3.3, 3.4, 3.5, 3.6.2). However in Sec 3.6, we also found evidence in support of the other hypothesis that Arp2/3 mediated f-actin and Tpm3.1 stabilized f-actin may be required for skeletal muscle contraction. In this chapter, we don't explore these filaments (Arp2/3 mediated f-actin and Tpm3.1 stabilized f-actin) any further. We focus on unraveling the mechanical hypothesis underlying CytoD mediated f-actin disruption.

As f-actin is typically a protein providing structure and mechanical support to cells, perhaps the following mechanical analogy could provide a potential hypothesis: the muscle sarcomeric contraction system is a bio-mechanical motor facing both an internal (its own stiffness) and external resistance (the stiffness of the cantilever/anchor). By disrupting the f-actin cytoskeleton and shortening the non-sarcomeric f-actin filaments, we are likely creating a more loosely connected cytoskeleton, one whose mechanical stiffness could potentially be lower. If so, the muscle now needs to contract against less of a resistive stiffness. This could provide a possible causal relationship for the observed improvement.

Hypothesis: ***f-actin disruption with CytoD improves skeletal muscle contraction due to a lower internal mechanical resistance.*** For this hypothesis to be true beyond all the evidence collected so far (Sec. 2.2, 2.3, 3.2, 3.3, 3.4, 3.5, 3.6.2) , the following criteria must **all** be true:

1) No increase in muscle sarcomeric force producing proteins
2) The internal mechanical resistance has to be lower due to CytoD treatment
3) The timescale of mechanical resistance changes must match the timescale of force improvements
4) No change in energy consumed (increased force output could be explained potentially by increased energetic input)
5) No change in metabolic capacity of the mitochondria which processes the glucose to ATP, a molecule used in the majority of energetic process in muscle cells including sarcomeric force production.

6) Lastly, reversal of the phenomenon, namely stabilizing f-actin must lead to decreased active contraction

We test each of these hypotheses in the following sections.

4.2 Changes in sarcomeric force producing proteins

Based on the results in Chapter 2, we know that CytoD treatment leads to a force improvement within 30 minutes. This rapid response likely rules out excessive production of sarcomeric force associated proteins as the cause of the improved force. This is because sarcomeric protein assembly (myofibril formation) typically takes several hours (eg. in Xenopus myocytes [101]) to several days (eg. in C2C12 based systems [88,89]). Sometimes, in C2C12 based systems it could even take weeks under certain culture conditions[90]. It follows that in C2C12 based systems improved sarcomeric assembly should take much longer than the 30mins to 2hrs timescale in which the force improvement was observed. In order to confirm this, we use RT-PCR to look for changes at the gene expression level of the following sarcomeric proteins: myosin heavy chains MHC2B and MHC1, as well as myosin light chains MYL3 and MYL19 (**Fig.** 47). None of these genes change in expression significantly after 2 hours of CytoD 0.3μM treatment. Furthermore, the expression of 14 other genes (**Fig.** 47) that have important roles in protein synthesis, energetic metabolism, protein degradation, apoptosis and Ca^{2+} regulation were also not altered significantly after 2 hours of exposure to CytoD (**Fig.** 47). RT-PCR methods used are identical to methods described earlier (Chapter 2, Sec. 2.4.2). A full list of gene names and PCR primer sequences are in Appendix 1.

These results show that in the time window that we observe a force increase (30mins to 2hrs), we do not see significant changes in expression of almost several important genes involved in muscle force production and energetic metabolism etc. Further studies must be conducted in the future to understand gene expression changes that may occur due to long term f-actin disruption (timescale of days to weeks).

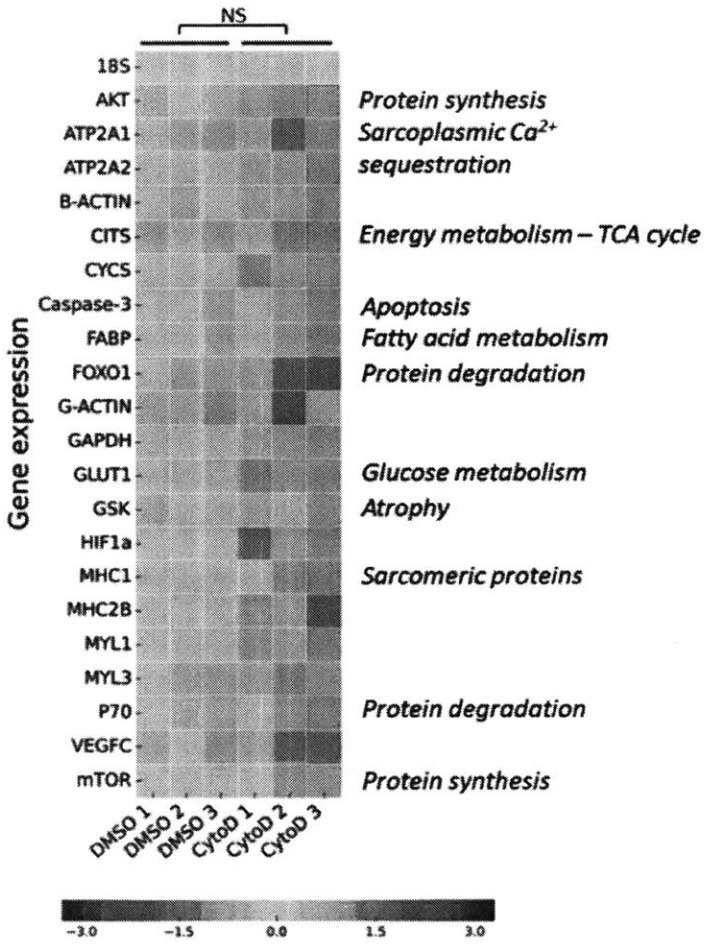

Fig. 47: Gene expression analysis using RT-PCR for 21 genes including housekeeping gene 18s rRNA, with CytoD 0.3μM application for 2 hours. The relative expression levels are colored with a $\log_2$ scale (10^{-3} to 10^{3}). No significant changes in gene expression were found. There were 3 samples used for both CytoD and the control (DMSO), labeled 1-3. A 2 sample t-test was used to obtain significance levels of the relative expression, with samples made in triplicate.

4.3 Changes in cell level stiffness with AFM

4.3.1 Hypothesis: CytoD lowers the apparent elastic modulus of myotubes

If CytoD treatment were to lower the internal mechanical resistance faced by a contraction cell, it follows that this change would be reflected through a change in the mechanical stiffness of the cell. One of the widely used methods to test this change at the level of a single myotube is atomic force microscopy.

4.3.2 Experimental methods

C2C12-ChR2 cells were differentiated on 10cm tissue culture treated polystyrene dishes for 12 days with the same protocol as described earlier. Once the myotubes were differentiated, we performed AFM indentation using a pyramid shaped cantilever on 30 cell locations on myotubes with application of DMSO or 3μM CytoD for 30 minutes in the 37C incubator.

AFM Force-distance measurements were acquired with a JPK Nanowizard-I (JPK instruments, Berlin, Germany) interfaced to an inverted optical fluorescence microscope (Zeiss). Pyramid shaped AFM cantilevers (MLCT, Bruker, Karlsruhe, Germany) were used. Cantilever spring constants were determined using the thermal noise method implemented in the AFM software (JPK SPM, JPK instruments). Prior to any cellular indentation tests, the sensitivity of the cantilever was set by measuring the slope of force-distance curves acquired on stiff regions of the petri dish. For measurements on cells, we used cantilevers with nominal spring constants of 0.01 $N.m^{-1}$). The cantilever tip was brought into contact with the cells using an approach speed of 5 um/s until reaching a target force of 10nN. This was followed by retraction of the cantilever. The approach force-indentation curve was fit (up to 1μm indentation depths to neglect effects of the substrate) with a Hertzian model to estimate the apparent elastic modulus. A Poisson's ratio of 0.5 was assumed for the purpose of this estimation.

4.3.3 Results and discussion

As shown in **Fig.** 48, the AFM indentation experiment clearly shows that the apparent elastic modulus of C2C12 myotubes decreases with AFM indentation. This conclusively proves that at the single myotube level, the mechanical stiffness drops with CytoD treatment.

The f-actin visualizations in Chapter 3 showed us that CytoD treatment led to severing, shortening and clustering (balling-up) of the stress fiber like f-actin filaments (Sec. 3.4). Furthermore, subtle changes to the background intensity stain of f-actin depolymerization were observed indicative of f-actin depolymerization (**Fig.** 34 and 35 in Sec. 3.4). However, FRAP analysis showed that the depolymerization was not so significant as to lead to a significant increase in relative fraction of monomeric actin (**Fig.** 41). In light of these subtle cytoskeletal changes, one may question if any of these changes would have led to a lowering of

internal mechanical resistance. The AFM indentation experiment conclusively shows that this is the case. The mechanical consequence of all these changes to the cytoskeletal f-actin structures is in fact ~50% lower stiffness.

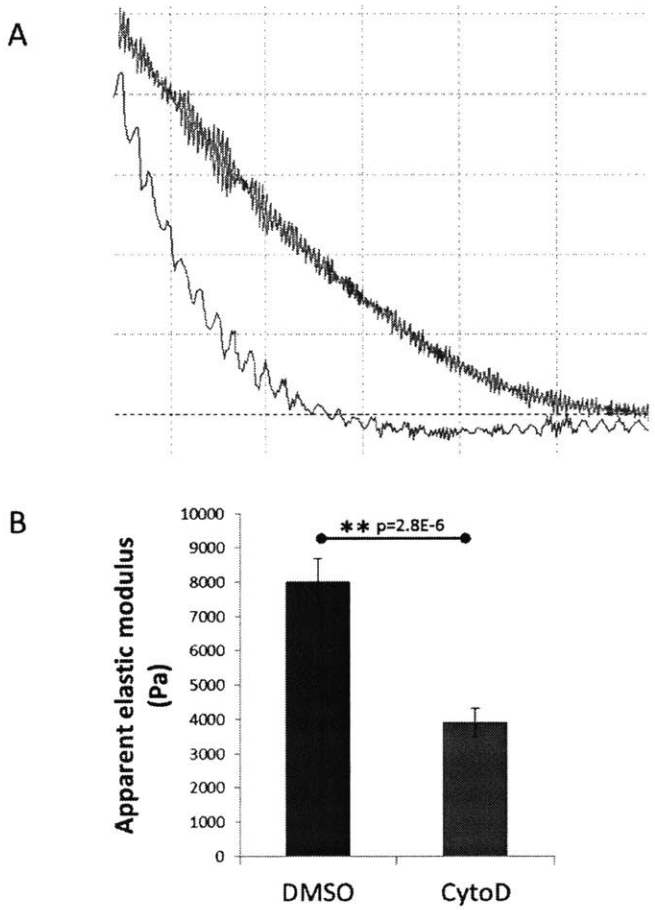

Fig. 48: AFM indentation of C2C12-based myotubes reveals a drop in mechanical stiffness. (A) AFM approach retraction curve (red) with a curve-fit (green) to the approach curve. A Hertz model was fit to the data to compute the apparent elastic modulus. (B) CytoD treatment clearly lowers the apparent elastic modulus relative to DMSO treated controls (AFM) by 50%. N=30 cell indentations were used for this test.

4.4 Changes in tissue level stiffness with a micro-tensile test

4.4.1 Hypothesis

In the last section, we proved that CytoD treatment does significantly lower the cell level stiffness of the myotubes in a 2D environment. However, in a 3D in vivo like environment, such as in the 3D engineered muscle construct, the cells likely have slightly different mechanical properties and might respond differently to cytoskeletal drugs such as CytoD. In this section, we test the hypothesis that the axial stiffness of the muscles also drops with CytoD treatment.

4.4.2 Experimental methods

To test this hypothesis, we constructed a micro-tensile test setup, adapting an apparatus similar to that described in Sec. 2.1 as shown in **Fig.** 49.

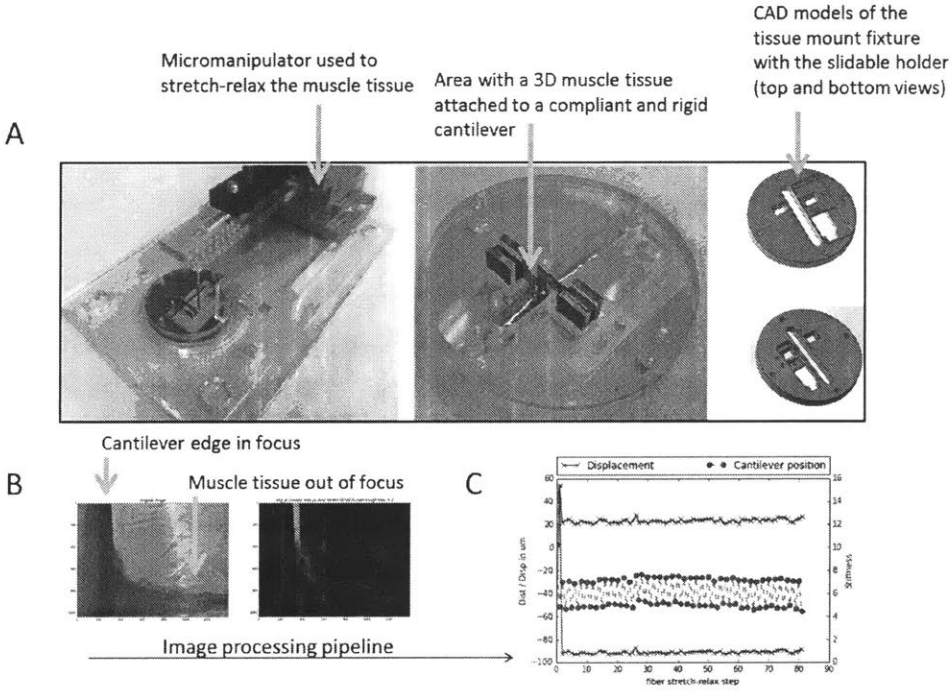

Fig. 49: Micro-tensile testing of a muscle tissue. (A) The setup used for testing of the axial stiffness of a muscle tissue. The typical muscle tissue used in this study is ~100μm in diameter, 3mm in length anchored between two clamped kapton cantilevers (orange in color), one relatively compliant and the other relatively rigid (as described earlier in Chapter 2). The setup allows simultaneous measurement of the active contraction by observing the movement of the compliant cantilever (see the text in Sec. 4.2.2). Furthermore, the slidable rigid cantilever allows the muscle to be stretched and relaxed by 50 μm steps, which also allows estimation of

the axial stiffness. For a sense of scale, the circular tissue mount fixture is ~6cm in diameter. The distance between the cantilevers in the fixture is 3mm. (B) The image processing pipeline used for stiffness computation. The first image represents the raw image of the initial position of the compliant cantilever edge. The second image represents difference image between the initial and final positions of the compliant cantilever as the rigid cantilever is moved to stretch the muscle tissue. The thickness of the bright rectangular zone is the displacement. An edge detection algorithm similar to the one described in Chapter 2 (see appendix 2) is used to detect the two edges of the bright strip. (C) Shows the cantilever position displacement (black), the cantilever displacement (red) and the normalized stiffness (blue).

C2C12-ChR2 cells were used to form and differentiate a 3D muscle fiber in situ on two kapton cantilevers (as in Sec. 2.3). One of the kapton cantilevers is compliant and has a stiffness of 0.34 N/m while the other is more rigid and has a stiffness of 8N/m. To this point, the setup and protocol is identical to the in vitro experiments described in Chapter 2. The main difference is that the rigid cantilever is attached to a slidable base (as indicated), which allows us to apply defined stretch relaxation steps each with a 10μm accuracy as it is connected to a micromanipulator. Thus this setup allows simultaneous measurements of stiffness and contractility changes.

The active contractility changes are computed exactly as described before, by observing the changes in deflection of the compliant cantilever. The axial stiffness changes are computed using a tensile testing methodology. Briefly, the micromanipulator was used to stretch the muscle tissue by moving the stiffer cantilever away from the muscle tissue by ΔL_{rigid} = 50μm. The corresponding change in position of the compliant cantilever was recorded $\Delta L_{compliant}$. This allows us to estimate the axial stiffness $k = \Delta Tension_{axial} / \Delta L_{muscle} = K_{cantilever} * \Delta L_{compliant} / (\Delta L_{rigid} - \Delta L_{compliant}) \sim \Delta L_{compliant} / (\Delta L_{rigid} - \Delta L_{compliant})$. In this equation, $K_{cantilever}$ is the stiffness of the compliant cantilever, which cancels in the comparison as it does not change with CytoD treatment. This was followed by a relaxation by 50μm and the corresponding change in position of the compliant cantilever recorded too. Such stretch relaxation steps were repeated several times (as illustrated by the red dots in **Fig.** 49) to obtain a consistent measure of the axial stiffness. We chose to perform 30 total stretch-relax steps based on preliminary testing that showed very little variation in the stiffness measured after a few initial steps (see an example of this data in **Fig.** 49C, which shows 80 stretch relax steps).

Given this metric, we treat the fully differentiated muscle tissue at day 12 with CytoD 3μM and then simultaneously observe the change in contraction and change in axial stiffness every 10 minutes for 1 hour.

4.4.3 Results

As seen in **Fig.** 50, the axial stiffness of the muscle (n=5) drops by about 50%. At the same time the active contraction rises by about 45%. Moreover the two changes (drop in stiffness and rise in contraction) occur on very similar timescales ~ 1 hour. This provides further support for the mechanical hypothesis that the drop in internal stiffness is the cause of the improved contraction.

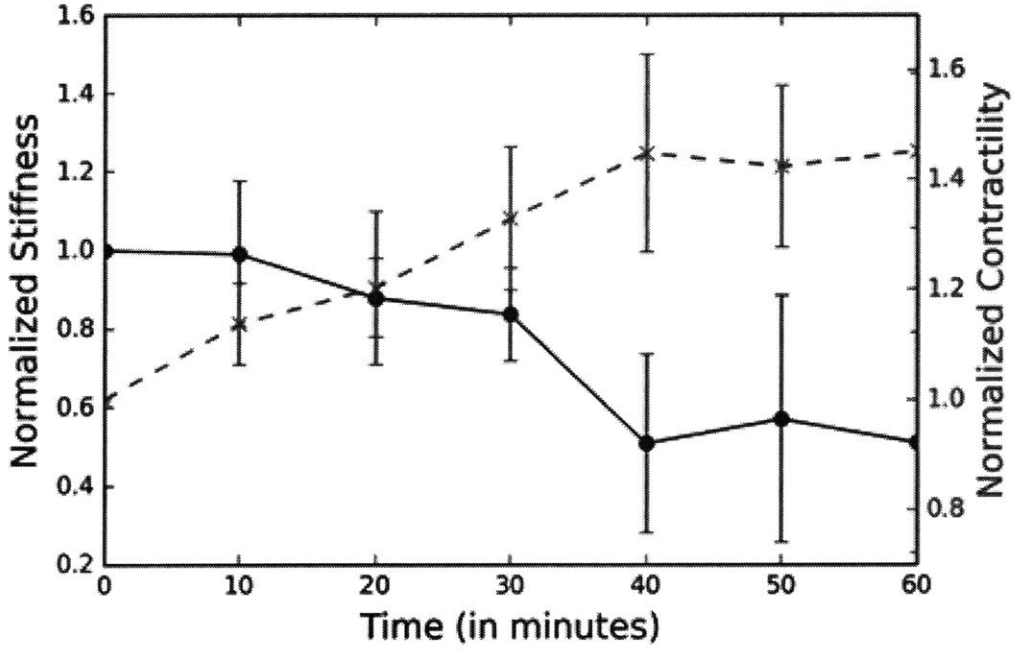

Fig. 50: CytoD treatment leads to a simultaneous decrease in axial tissue stiffness and improvement in active contraction as measured by the micro-tensile testing assay. The timescale of the 2 changes match each other well. (n=5) was used for this experiment.

4.5 Changes in energetic consumption

4.5.1 Hypothesis: CytoD treatment does not increase glucose consumption

In this chapter, we have been using the analogy of a mechanical motor as a model of the muscle tissue contraction. We been measuring changes in the active contraction, a measure of the output of the "muscle motor" as well as the change in stiffness, a measure of the energetic barrier imposed by the muscle internally to contract itself. In order for the increased active forces to be explained purely by decreasing internal resistance, the energetic consumption of the tissue shouldn't increase either. Going with the "muscle motor" analogy, drawing higher currents from the power source could also lead increased output of the motor. In order to rule out this possibility, we test the hypothesis that CytoD treatment does not increase energetic consumption. As a proxy of energetic consumption, we use changes in glucose concentrations in the culture medium as a measure of the energetic consumption.

4.5.2 Experimental methods

As before, we differentiate C2C12-ChR2 cells on matrigel coated 96 well plates for 12 days. We changed the culture medium 12 hours prior to CytoD treatment with 100μL of fresh DM+ containing 4.5mM glucose so that the cells are not metabolically starved. At this point, we aspirate the medium, add 50μL of matrigel on top of the cells so that the cells stay in place even if f-actin disruption dislodges it. Once the matrigel polymerizes (20minutes at 37C), we add 70μL of medium on top containing CytoD or DMSO (n=6) so that the final concentration of CytoD is 0.3μM. 52 hours after treatment, the supernatant medium was collected and the change in glucose concentration was estimated using the colorimetric test from the Glucose detection kit (GO assay, Sigma Aldrich). This was then normalized to the number of nuclei in each well to (correct for cell number variations from well to well in order to estimate the glucose consumption rate per cell per hour.

4.5.3 Results

As shown in **Fig.** 51, the baseline glucose consumption rate (GCR) did not change significantly due to CytoD treatment. This adds further evidence to the hypothesis that the energetic metabolism of the cells is not significantly altered by mild f-actin disruption.

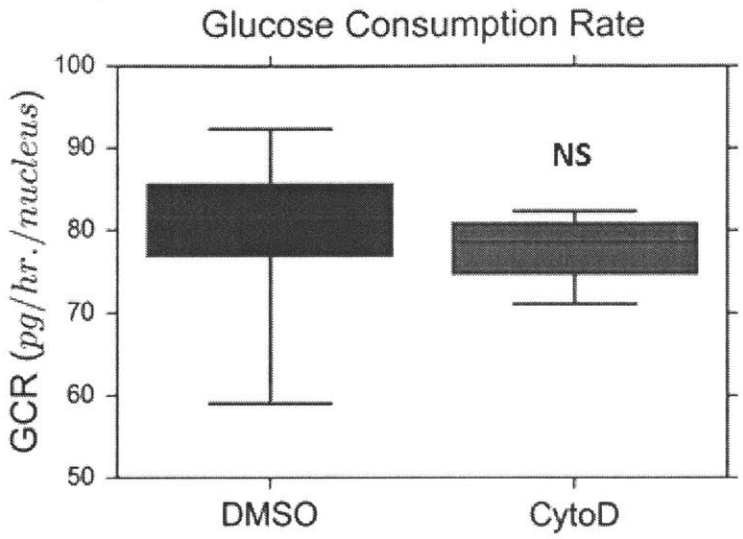

Fig. 51: CytoD (0.3μM) treatment does not significantly change the baseline glucose consumption rate of the differentiated C2C12 cells. A 1–tailed 2 sample t-test was used for statistical significance testing.

4.6 Changes in energetic signaling and metabolic activity

4.6.1 Hypotheses

From the last section, we found that there is no change in glucose consumption due to f-actin disruption. But perhaps the manner in which glucose is metabolized within cells or the pathways it activates might lead to a different cellular energetic state. In order to further probe changes to the energetic metabolism of these muscle cells due to f-actin disruption, we would like to test 3 hypotheses in this section:

Hypothesis 1: F-actin disruption does not affect AKT phosphorylation. Phosphorylation events happen within minutes and could potentially be within the timescale of the observed force changes in the cell (30mins to 2hrs.). Moreover, AKT phosphorylation is a master regulatory signal for a host of downstream biochemical pathways related to energetic activity.

Hypothesis 2: F-actin disruption does not change overall cellular metabolism. For overall cellular metabolic activity, wanted to test for changes in the TCA (Kreb's) cycle.

Hypothesis 3: F-actin disruption does not change mitochondrial activity.

Mitochondrial activity is important because it is the center of ATP production in the cell and ATP hydrolysis drives repeated muscle contraction.

If any one of these hypotheses are proven wrong, we can't rule out the possibility that changes in cellular energetic or metabolic activity contribute to the improved active force observed upon f-actin disruption.

4.6.2 Experimental methods

For hypothesis 1: Western blot of AKT phosphorylation.

C2C12-ChR2 cells were cultured in 6 well plates, differentiated as described earlier. After 12 days of differentiation, they were treated with DMSO, CytoD 0.3μM and CytoD 3μM for 2 hours. Cells were lysed with a cell lysis buffer containing RIPA buffer, a protease inhibitor cocktail (Cell Signalling) and PMSF. Proteins were quantified using the BCA assay and 20 μg of protein per condition was subjected to SDS/PAGE using 4-12% (wt/vol) gradient gels (Life technology, NuPAGE Novex, Bis-Tris), transferred to nitrocellulose membranes, and the relative concentrations assayed by immunoblotting. Experiments were conducted in triplicates. Primary antibodies were used for mouse anti-tubulin (Thermofisher, b-Tubulin loading control, 1:1000), mouse anti-actin (Thermofisher, b-actin loading control, 1:1000), AKT (1:1000 Cell Signaling), pAKT s473(1:500, Cell Signaling), pAKT t308(1:500, Cell Signaling). As for secondary antibodies, an anti-mouse IgG, HRP-linked Antibody (Cell Signaling) and an anti-rabbit IgG, HRP-linked Antibody (Cell Signaling) were used. HRP substrate was used for chemiluminescent analysis.

For hypothesis 2: MTT assay for mitochondrial succinate dehydrogenase activity.

For the MTT assay, the MTT Cell Growth Assay Kit (SigmaAldrich) was used. We cultured and differentiated C2C12 cells in 96 well plates for 12 days. n=4 wells was used for each condition. After 12days, they were treated with varying doses of CytoD or DMSO for 1 hour at 37C. After 1 hour, the MTT reagent was added to the different wells, followed by further incubation at 37C for 4 hours. The formazon formed was spun down using a plate centrifuge, the medium was aspirated and 100μL DMSO added to each well and mixed vigorously to fully dissolve the purple crystals. A plate reader was used for quantification.

For hypothesis 3: TMRE assay for changes in mitochondrial membrane potential.

The TMRE molecule is a cell permeant, positively-charged, red-orange dye that accumulates in active mitochondria due to the relative negative charge of the mitochondria. Depolarized or inactive mitochondria have decreased membrane potential, due to which they fail to sequester TMRE. Similar to the MTT assay, we differentiate C2C12 cells in 96 well plates, treat them with CytoD (0.3μM) and then use the TMRE reagent. At higher CytoD doses, the monolayer collapses and it becomes impossible to compare the relative fluorescence with respect to DMSO treated controls. N = 5 was used for this experiment. After 20 minutes of incubation with the TMRE reagent at 37C, we use a fluorescent readout to quantify the relative changes.

4.6.3 Results and conclusion

As seen in **Fig.** 52, AKT phosphorylation does not change with CytoD treatment. Likewise cellular metabolic activity (Kreb's cycle) tested through the mitochondrial succinate dehydrogenase activity doesn't change either (**Fig.** 53). Given that the mitochondrial enzymatic activity doesn't change with f-actin disruption, one might expect the average activity of mitochondria to not change either. This is reflected by the TMRE assay conducted (**Fig.** 54).

None of these 3 assays point towards energetic activity change. While these 3 results don't conclusively prove that the energetic state of the cell doesn't change, they do represent some of the earliest indicators of change in energetic activity of a cell. This evidence together with the gene expression data (Sec 4.2) also showing no significant change, does add significant support to our hypothesis of the force improvement due to f-actin disruption being purely mechanically driven.

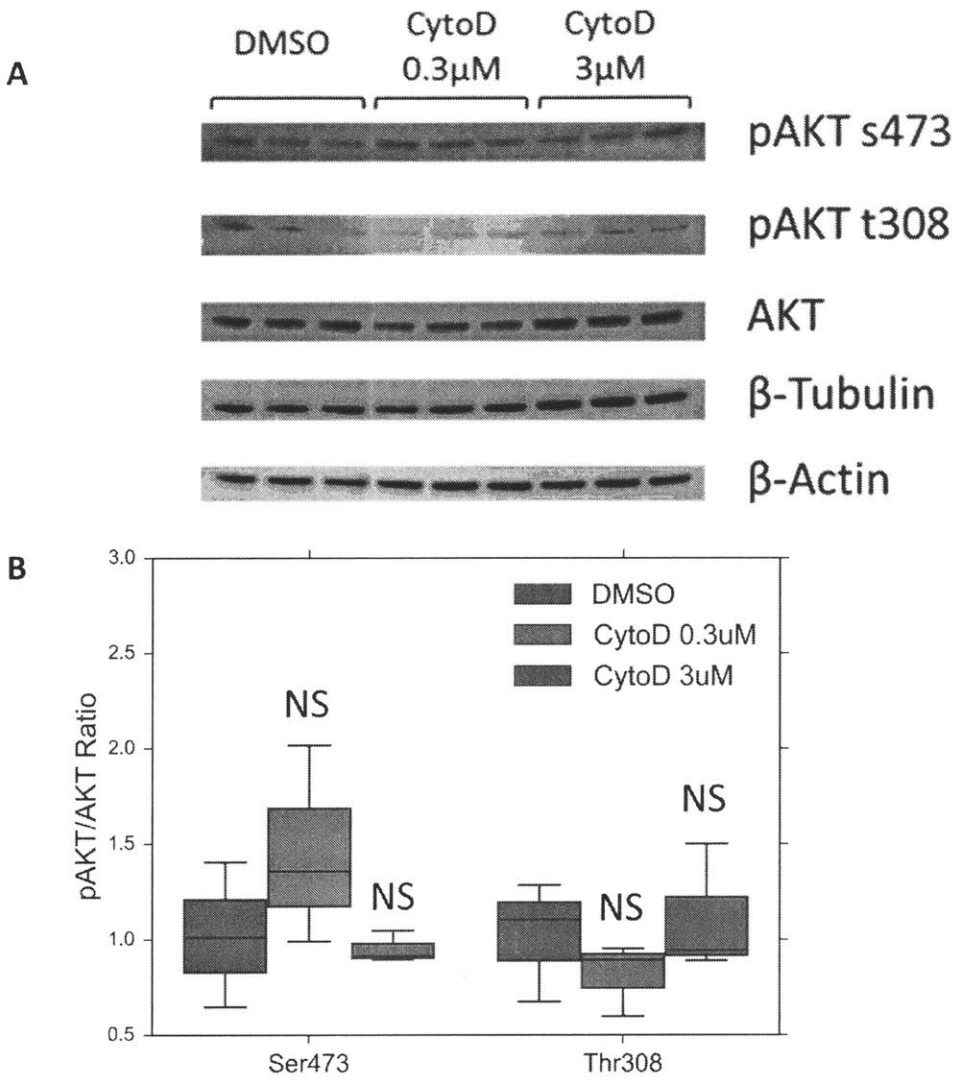

Fig. 52: CytoD treatment (0.3μM or 3μM) for 2 hours does not significantly change the phosphorylation of AKT at the 2 phosphorylation sites (Ser473 and Thr308). A) Western blots showing pAKT expression levels for both sites Ser473 and Thr308 along with AKT as a function of CytoD concentration. β-tubulin and β-actin are also shown as loading controls B) Averaged results showing the ratio of phosphorylated AKT to total AKT. A 2-sample 1-tailed t-test was used for statistical significance testing ($p > 0.05$). N=3 for all experiments.

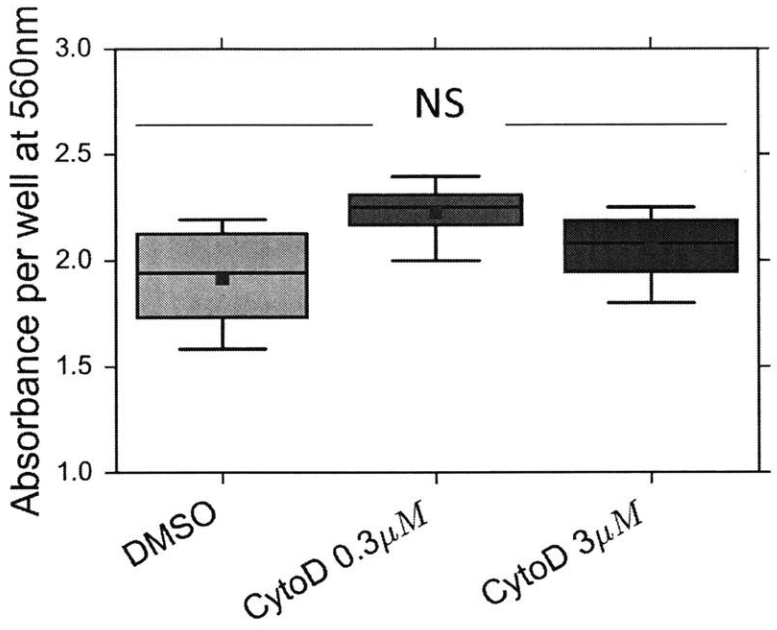

Fig. 53: CytoD treatment (0.3μM or 3μM) does not significantly change cellular metabolic activity as assessed by an MTT assay. See text for details about the time of exposure. A 2-sample 1-tailed t-test was used for statistical significance testing ($p > 0.05$). N=4 was used for these experiments.

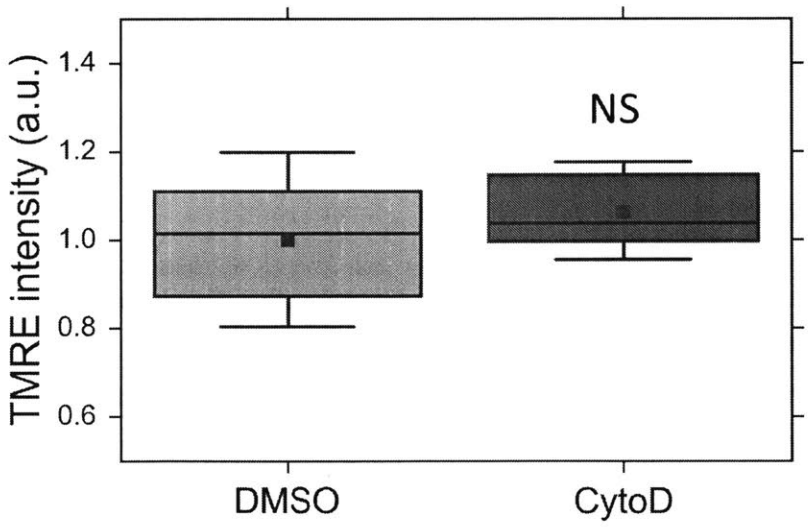

Fig. 54: CytoD treatment (0.3μM) does not significantly change mitochondrial activity as assessed by no significant changes in accumulation of TMRE a fluorescent dye that

accumulates only in active mitochondria. A 2-sample 1-tailed t-test was used for statistical significance testing NS ($p > 0.05$). N=3 was used for these experiments.

4.7 F-actin stabilization reverses the phenomenon

4.7.1 Hypothesis: Stabilizing f-actin decreases the active force

All our experimental data lack any evidence pointing towards a non-mechanical origin of the force improvement. If the mechanical hypothesis illustrated in **Fig.** 55 is true, then the reverse of this phenomenon, must also be true: ***Stabilizing f-actin decreases the active force.***

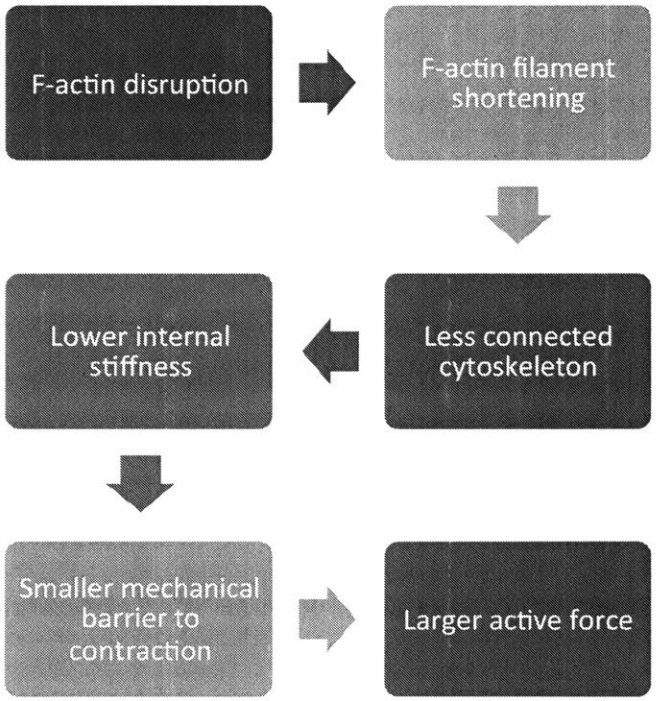

Fig. 55: Mechanical basis of active force improvement due to f-actin disruption in skeletal muscle.

4.7.2 Experimental methods

In order to test this hypothesis, we repeat our 3D C2C12 based muscle contractility assay of Chapter 2, with f-actin stabilizing chemicals jasplakinolide (Santa Cruz Biotech.) and phalloidin (Santa Cruz Biotech). Both are small molecules that bind competitively to the same site of f-actin. Phalloidin is known to bind to f-actin and stabilize it. Prior works [102] have shown that phalloidin treatment of reconstituted actin networks increase the network stiffness by a factor of 2. Jasplakinolide too is known to stabilize f-actin and also enhance f-actin polymerization by inducing nucleation. Furthermore, there is prior evidence [103] that jasplakinolide increases the mechanical stiffness of living cells (mouse embryonic fibroblasts). If our mechanical hypothesis is true, treatment with these chemicals must decrease the active force. We use a 5μM concentration of jasplakinolide as this concentration was shown earlier[104] to affect actin dynamics in quail myotubes. A high phalloidin concentration of 100μM is used because phalloidin is highly impermeable to cells. Prior works have shown that incubation of cardiomyocytes with this 100μM phalloidin affects the actin cytoskeletal dynamics[105]. DMSO is used as a control in both cases.

4.7.3 Results

As illustrated in **Fig.** 56 and 57, treatment with jasplakinolide and phalloidin do indeed decrease the active muscle force. Not unexpectedly jasplakinolide acts much more rapidly than phalloidin (perhaps due to its higher permeability into cells than Phalloidin). Prior works [104] investigating the actin cytoskeleton in myotubes show a rapid response to jasplakinolide as early as 30minutes. However, to the best of our knowledge, with phalloidin treatment in live cells, a response earlier than 5 hours of treatment has not been reported[105].

In any case, this is a demonstration that f-actin polymerization (or stabilization) decreases the active force. Together with all the previous results in this chapter, this result adds significant evidence to support the "mechanical" hypothesis shown in **Fig.** 55.

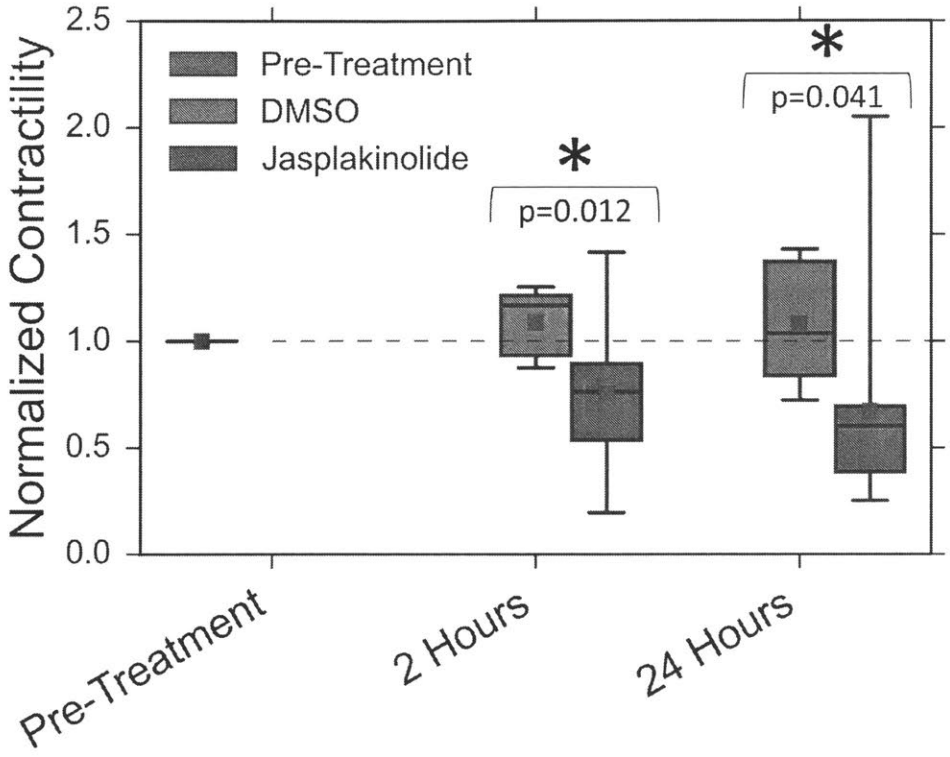

Fig. 56: Jasplakinolide 5μM treatment decreases active contractility of C2C12 based 3D engineered muscle by 25% within 2 hours of exposure and 33% within 24 hours of exposure. Statistical significance testing is based on the 1-tailed 2 sample t-test

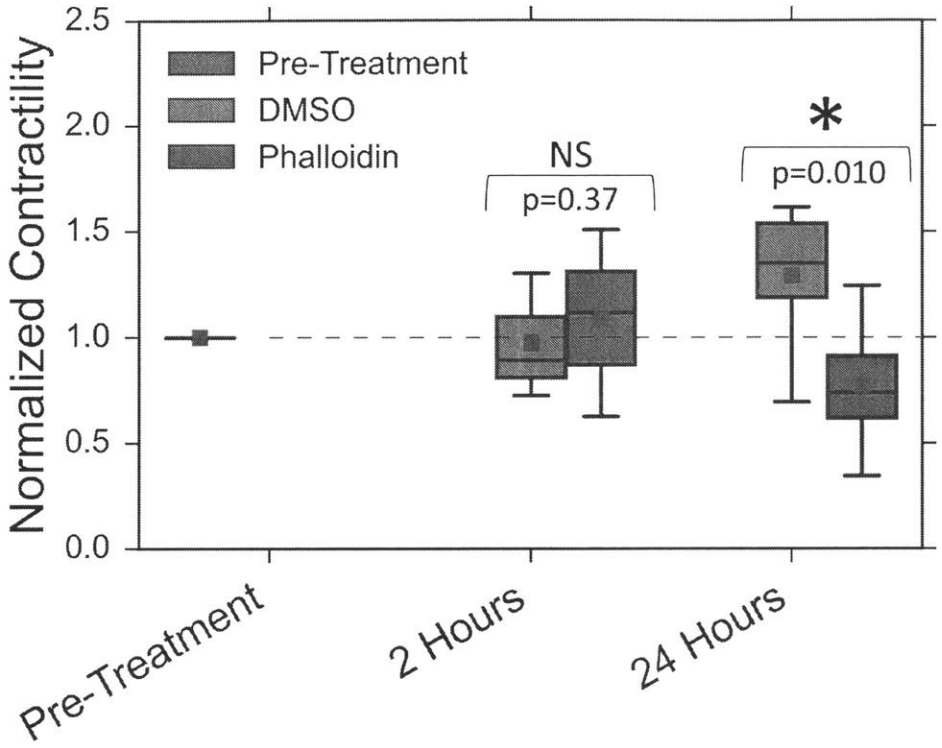

Fig. 57: Phalloidin 100μM treatment decreases active contractility of C2C12 based 3D engineered muscle by 25% within 24 hours of exposure. 2 hours after treatment, there was no significant change in contractility relative to DMSO treated controls. Statistical significance testing is based on the 1-tailed 2 sample t-test

4.8 Conclusion

In conclusion, all 6 criteria we listed in Sec. 4.1 that need to be satisfied for the mechanical hypothesis to be true have been met, adding significant evidence to support the mechanical hypothesis of the role of f-actin in muscle contraction. To recall:

Hypothesis	Experiment	Hypothesis True/False
No increase in muscle sarcomeric force producing proteins	RT-PCR	TRUE
The internal mechanical resistance has to be lower due to CytoD treatment	AFM, micro-tensile test	TRUE
The timescale of mechanical resistance changes must match the timescale of force improvements	micro-tensile test	TRUE
No change in energy consumed (increased force output could be explained potentially by increased energetic input)	Glucose consumption test	TRUE
No change in metabolic capacity of the mitochondria which processes the glucose to ATP, something used	AKT phosphorylation, MTT, TMRE	Not proven FALSE
Lastly, reversal of the phenomenon, namely stabilizing f-actin must lead to decreased active contraction	Jasplakinolide, Phalloidin effect on contractility	TRUE

Chapter 5: Summary, Applications and Future Studies

5.1 Summary

We started this thesis with two basic questions: 1) *What is the role of the non-sarcomeric f-actin in skeletal muscle sarcomeric force transmission? 2)* ***What would happen to the sarcomeric contractile force if the non-sarcomeric f-actin were disrupted****?* The 2 prevailing schools of thought in the field (prior to this thesis) pointed in opposite directions: (a) Disrupting non-sarcomeric f-actin is deleterious to muscle force transmission perhaps due to its role in linking the sarcomeres to the costameres or due to the f-actin serving as a scaffold to the sarcomeres of sorts. Or (b) Disrupting non-sarcomeric f-actin enhances muscle force transmission due to the reduction of internal mechanical resistance posed by the cytoskeleton to its own contraction. As in most complex systems, the thesis has revealed the answer to be: ***it depends on which f-actin sub-category.***

Depleting certain classes of non-sarcomeric f-actin filaments, namely the dynamic f-actin structures that are CytoD sensitive, as well as the formin-associated f-actin filaments, enhance skeletal muscle contraction. ***These actin filaments seem "detrimental" to muscle function***. This comes also with the added benefit of no significant changes to any of the following: mechanical integrity of the muscle cells, autophagy or apoptosis. In these filaments, we find that the likely mechanism of force improvement is due to mechanical softening of the cells that occurs due to f-actin depolymerization. This softening lowers the internal mechanical barrier to contraction. In order to rule out potential non-mechanical origins of the improvement in force, we measured changes in gene expression of sarcomeric proteins, energetic metabolism genes, protein production and degradation genes. We also measured changes in energetic activity that may have contributed to the force improvement as revealed by changes in AKT phosphorylation, glucose consumption, cellular metabolism and mitochondrial activity. None of these non-mechanical factors changed significantly with f-actin disruption, supporting our hypothesis that the force improvement is due to mechanical softening. Given the obvious contractile improvement observed upon their disruption, we investigated why these f-actin filaments were present to start with. We found that they may improve the fatigue resistance at the cost of reduced contraction.

On the other hand, depleting other non-sarcomeric f-actin structures that are ARP2/3 mediated or tropomyosin (Tpm3.1) stabilized were found to have a deleterious effect on skeletal muscle contraction. ***These actin filaments seem to be "beneficial" to muscle function.*** We hypothesize that these are among the filaments that help transmit the sarcomeric force to the costameres and eventually helping perform external work. Future studies are warranted to tease out this behavior further.

Both these are novel findings that have finally revealed the role of the non-sarcomeric f-actin, decades after the discovery of sarcomeric acto-myosin contraction in muscle. If these *in vitro* and *ex vivo* findings are proven to be true *in vivo*, we may open doors to a whole new family of f-actin based therapies of muscle disorders.

We conclude this thesis by demonstrating an application and proposing several new studies to translate these discoveries.

5.2 Changes in engineered biological robot walking

5.3 Hypothesis: f-actin disruption could improve skeletal muscle powered walking

In chapter 2, we have conclusively shown that f-actin disruption improves muscle active contractility as measured by the optogenetically induced peak twitch force. So what? What does this mean functionally for skeletal muscle function *in vivo*?

One hypothesis is that it could make *patients with weak skeletal muscles walk better*. Testing this method *in vivo* even in a live animal model is currently neither ethical (as most of the f-actin disrupting compounds that we use have significant cardiotoxicities) not feasible as it is not targeted well to just skeletal muscle. In order to test this hypothesis in an *in vitro* model simulating walking, we used a recently developed next generation functional assay for skeletal muscle powered walking[84].

5.3.1 Experimental model

The model is a C2C12 skeletal muscle based biological robot that uses a walking mechanism similar to an inchworm (which is one of the simplest examples of skeletal muscle powered motion). A hydrogel backbone is 3D printed that serves as the skeleton in "skeletal muscle".

Ring-shaped C2C12 based muscle rings are fabricated on ring shaped negative molds of ABS. These are then transferred to the skeleton.

Detailed step-by-step fabrication methods for the muscle powered biobot fabrication are described elsewhere [106]. But briefly, a commercial stereolithographic 3D printing apparatus (SLA 250/50; 3D Systems) was used to 3D print hydrogel based muscle ring molds (**Fig.** 58) with parts designed using CAD software (Solidworks). The biobot ring molds were fabricated on glass slides using a prepolymer solution composed of 20% (wt/vol) PEGDMA MW 1,000 g/mol (Polysciences) in PBS (Lonza) with 0.5% (wt/vol) 1-[4-(2-hydroxyethoxy)phenyl]-2-hydroxy-2-methyl-1-propanone-1-one photoinitiator (Irgacure2959; BASF) dissolved in DMSO. The walking bio-bot skeletons were fabricated on glass slides using a prepolymer solution composed of 20% (vol/vol) PEGDA MW 700 g/mol (Sigma-Aldrich) in PBS with 0.5% (wt/vol) Irgacure 2959 photoinitiator dissolved in DMSO. Following fabrication, molds and bio-bot skeletons were rinsed in PBS, sterilized in 100% ethanol (Decon Labs) for 1 h, and stored in PBS for at least 1 h before use. For parts that required chemical tethering to the underlying slides, the glass was pretreated with 2% (vol/vol) 3-(trimethoxysilyl) propyl methacrylate (Sigma-Aldrich) in 100% ethanol for 5 min, washed in 100% ethanol for 5 min, and baked at 110 °C for 3 min.

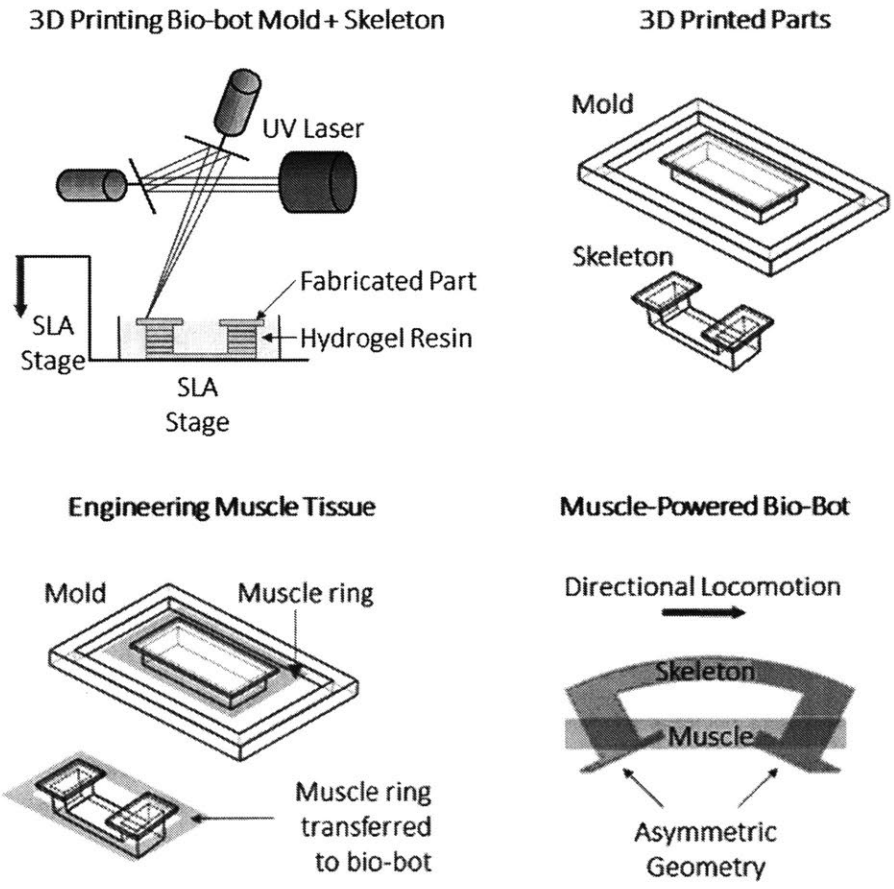

Fig. 58: Biobot fabrication process involving 3D printed hydrogel molds, molding optogenetic skeletal muscle and assembly of the bio-hybrid structure.

C2C12 based biobot rings were made by molding a cell gel solution in the ring molds. The composition of the cell gel is 10M/ml C2C12-ChR, with 30% matrigel in a 4mg/ml fibrin gel, made by cross linking fibrinogen (SigmaAldrich) with 2ui/ml thrombin. The muscle rings were transferred from the ring molds to the bio-bot walker molds using a pair of precision tweezers. They were incubated in GM+ (DMEM + 10% FBS + PS + ACA) for 3 days, and then switched to differentiation medium DM+ (DMEM + 4% HS + PS + AA + 50ng/ml mIGF1) for 12 days . After this, the bio-hybrid muscle/skeleton construct was dislodged from the glass slide and placed on a petri dish filled with warm DM+ medium. Thereafter, the twitching and walking assays were conducted.

A tetanic pulse (just like in Chap 2) was applied at 1Hz frequency and the twitch length (active displacement of the cantilever was observed), while the biobot sits on its "back" – the curved convex side of the skeleton, thereby minimizing friction for the twitch. When the biobot sits on its legs, it could exhibit net translation because of the asymmetric structure of the skeleton (**Fig.** 58, 59A). However, if the muscle is too weak, translation is not observed. C2C12 based muscle are inherently weak, and so this walking model serves as a great model to study improvements in walking.

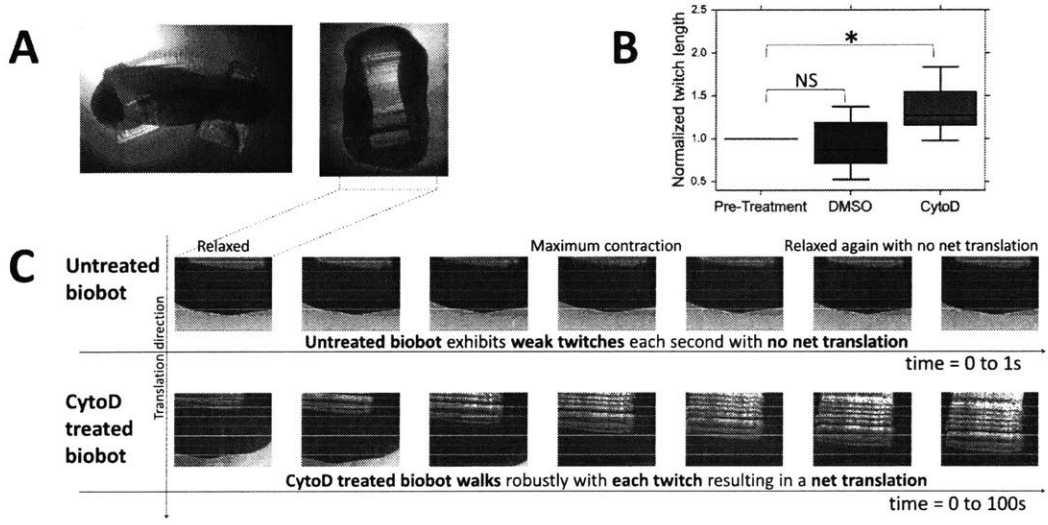

Fig. 59: CytoD treatment increases the twitch length of a weak biobot and this improvement also results in translation of the biobot (which was so weak prior to treatment that it didn't exhibit net translation upon optogenetic stimulation). The yellow lines are fixed and were overlaid on the timelapse for easier visualization of the translation.

5.3.2 Results

As shown in **Fig.** 59B, CytoD treatment (3μM) for 1 hour led to a statistically significant improvement yet modest (~40%) improvement in twitch length (defined as the change in net-separation between the tips of the two legs) of biobots sitting on their "back". We say modest because the active force improvements we observed in Chapter 2 are ~150%.

However, even this modest improvement was sufficient to cause a dramatic improvement in walking of biobots sitting on their legs. These biobots were stimulated continuously with once

a second with a 30Hz 5ms ON blue light pulse like before. As shown in **Fig.** 59C, prior to f-actin disruption, the biobot was so weak that it would simply twitch weakly, without exhibiting any net translation. However 1 hour after CytoD treatment, it starts translating across the field of view.

5.4 Future studies

5.4.1 Recovery of function in muscle disease models

There is a range of skeletal muscle disorders such as muscular dystrophy (MD) and muscle wasting that could be modeled using our system described in Chapter 2. It would be interesting to test if f-actin disruption could be a potential new therapeutic option for any of these disorders.

MD refers to a group of muscle disorders that increasingly result in weaker muscle and muscle breakdown over time. The most common MD is Duchenne Muscle Dystrophy which is of genetic origin. It is also a common side effect of hyperlipidemia drugs (statins). Currently there are no cures for MD and treatments including physical therapy and corrective surgery have poor outcomes. Studying MD with our system would be a very feasible follow-on study as there are many ways to model MD, using chemically (statins, tropomyosin inhibitors etc.) and genetically inducible methods (targeting the dystrophin gene). Likewise, there are well established models of muscle wasting, for instance glucocorticoid induced that could be used to develop a Sarcopenia model.

5.4.2 Drug delivery system

For this study to be a useful model for muscle disorders, we need to develop methods to disrupt f-actin in only skeletal muscle, as systemic f-actin disruption could lead to fatal toxicities (eg. Cardiotoxicity). The following 3 options could potentially be fruitful starting points for targeted delivery of f-actin disrupting therapies to skeletal muscle. 1) The use of actin disrupting agents encapsulated within muscle targeted nanoparticles, 2) adeno-associated viruses that skeletal muscles uptake preferentially as well as 3) viral gene therapies that deliver f-actin disrupting genes (gelsolin, cofilin etc.) with skeletal muscle specific promoters. This is an area worth investigating further.

5.4.3 Targeted f-actin disruption

CytoD, Latrunculin etc. are toxic chemicals. In order for f-actin disruption to become an effective therapeutic, we must find safer methods of f-actin disruption.

Actin binding proteins such as Profilin and Cofilin (described in Section 3.6), are alternate targets that could be used for f-actin disruption. Inhibiting Profilin may slow the rate of addition of G-actin monomers to the barbed end of dynamic f-actin filaments. Overexpressing Coflin may severe f-actin filaments. We may also screen for actin binding protein isoforms that may be skeletal muscle specific in order to prevent the off skeletal muscle toxicity. Alternatively, we could fin novel targets by using Si-RNA and/or CRISPR libraries to find novel targets that may allow translation of the f-actin disruption phenomenon described in this thesis in to a therapeutic.

Appendix 1: Primer sequences for RT-PCR used in Sec. 2.4.2 and 4.2

Mouse primer sequence for real-time RT-PCR.

Target Gene	*Forward primer sequence (5'-3')*	*Reverse primer sequence (5'-3')*
Actg1	AATCGCCGCACTCGTCATT	CCCTACGATGGAAGGGAACAC
18S rRNA	GTAACCCGTTGAACCCCATT	CCATCCAATCGGTAGTAGCG
Actb	GGCTGTATTCCCCTCCATCG	CCAGTTGGTAACAATGCCATGT
AKT1	CTGCTCCTAGTCCACCACCT	AGAGACCTCCATTATCGCTACC
ATP2A1	TGTTTGTCCTATTTCGGGGTG	AATCCGCACAAGCAGGTCTTC
ATP2A2	TGGAACAACCCGGTAAAGAGT	CACCAGGGGCATAATGAGCAG
Caspase3	TGGTGATGAAGGGGTCATTTATG	TTCGGCTTTCCAGTCAGACTC
Citrate synthase	GGACAATTTTCCAACCAATCTGC	TCGGTTCATTCCCTCTGCATA
Cytochrome c	CCAAATCTCCACGGTCTGTTC	ATCAGGGTATCCTCTCCCCAG
FABP-3	ACCTGGAAGCTAGTGGACAG	TGATGGTAGTAGGCTTGGTCAT
FoxO1	CCCAGGCCGGAGTTTAACC	GTTGCTCATAAAGTCGGTGCT
GAPDH	AGGTCGGTGTGAACGGATTTG	TGTAGACCATGTAGTTGAGGTCA
Glut1	CCTCCCTGACATGGAAATGGT	TGCGCTGCTGACCTTAACAG
GSK-3B	TGGCAGCAAGGTAACCACAG	CGGTTCTTAAATCGCTTGTCCTG
HIF1-a	ACCTTCATCGGAAACTCCAAAG	CTGTTAGGCTGGGAAAAGTTAGG
MHC1	GCGAATCGAGGCTCAGAACAA	GTAGTTCCGCCTTCGGTCTTG
MHC2b	AGGACCAACTGAGTGAAGTGA	GGGAAAACTCGCCTGACTCTG
mTORc1	TTTGTCTACGACTGTTCCAATGC	GCTACCTCTAGTTCCTGCTCC
MYL1	AGTGCTGACCAGATTGCCG	TCATGGGCAGAAACTGTTCAAA
MYL3	TGGGGAAGCCAAAACAGGAAG	AGCCATCAGTTTCTCTACCTCA
p70S6K	AGACACAGCGTGCTTTTACTT	GTGTGCGTGACTGTTCCATCA
VEGF-C	GAGGTCAAGGCTTTTGAAGGC	CTGTCCTGGTATTGAGGGTGG

Appendix 2: Code for cantilever edge detection

```
# Import packages

# Import packages

#importing some useful packages
import matplotlib.pyplot as plt
import matplotlib.image as mpimg
import numpy as np
import cv2
import math
import os
import sys
import glob
import time
import shutil
import ggplot
import pandas as pd
from tqdm import tqdm
import imageio

%matplotlib inline

# SUPPORTING FUNCTIONS

def region_of_interest(img, vertices):
    """
    Applies an image mask.

    Only keeps the region of the image defined by the polygon
    formed from `vertices`. The rest of the image is set to black.
    """
    #defining a blank mask to start with
    mask = np.zeros_like(img)

    #defining a 3 channel or 1 channel color to fill the mask with depending on the input image
    if len(img.shape) > 2:
        channel_count = img.shape[2]  # i.e. 3 or 4 depending on your image
        ignore_mask_color = (255,) * channel_count
    else:
        ignore_mask_color = 255

    #filling pixels inside the polygon defined by "vertices" with the fill color
    cv2.fillPoly(mask, vertices, ignore_mask_color)

    #returning the image only where mask pixels are nonzero
    masked_image = cv2.bitwise_and(img, mask)
    return masked_image
# MAIN FUNCTION FOR CANTILEVER DIPLACEMENT TRACKING
# INPUT: Name of cantilever videos folder
```

```
# OUTPUT: Max displacement vector for all videos
# TUNABLES: image roi, auto-thresholding selection locations

def cantilever_disp(img_dir, display = False, thresh = 0.8):

    ###################################################
    # Read in folder videos and extract filenames with avis
    ###################################################
    if os.path.exists(img_dir+"results"):
        shutil.rmtree(img_dir+"results")

    os.makedirs(img_dir+"results")  # to store some results

    cantilever_max_disps = []  # store each video's max displacemen here
    print ("starting to process videos in " + img_dir)

    for file_index,filepath in enumerate(sorted(glob.glob(img_dir+ "*.avi"))):
        print (filepath)
        timestr = time.strftime("%Y%m%d-%H%M%S")  #to name image results

        ####################################################
        # Read in video and convert to an image array
        ####################################################
        reader = imageio.get_reader(filepath)

        frames = []  # this stores the video as an array of images
        # video has non-duplicate frames in locations 0, 3, 7, 11, 15, 19
        frame = reader.get_next_data()
        frames.append(frame)  # store frame 0

        for i, frame in enumerate(reader):
            if i%4 ==2:
                frames.append(frame)


        ####################################################
        # FOR EACH IMAGE, EXTRACT THE BOUNDARIES
        ####################################################
        cantilever_edges = []  # array of slope-intercept values of all lines

        n_frames = len(frames)
        print("total frames = %d"%(n_frames))

        for i in range(n_frames-1):

#           for i in range(90,110):
            img = frames[i]

            #plt.imshow(img)
            #print(img.shape)
            img_grey = cv2.cvtColor(img, cv2.COLOR_RGB2GRAY)
            #img_norm = cv2.equalizeHist(img_grey)
```

```
# Estimate threshold for each video frame

if i == 0:
  img_width = img_grey.shape[1]

  img_grey_left = np.median(img_grey[:, :30].flatten().astype(float))
  img_grey_right = np.median(img_grey[:, (img_width-40):].flatten().astype(float))
#img_grey_left = img_grey.flatten().astype(float).min()
#img_grey_right = img_grey.flatten().astype(float).max()

  threshold = thresh*img_grey_left + (1-thresh)*img_grey_right

#img_norm = np.maximum(((img_grey.astype(float) - 1.1*img_grey_left)        \
#          /(0.3*img_grey_right-0.4*img_grey_left)*255), 0).astype(np.uint8)

img_norm  = cv2.GaussianBlur(img_grey, (15, 15), 0)

      # use an edge preserving filter here since our measurement depends on the edge
for j in range(5):
  img_norm = cv2.medianBlur(img_norm, 7)       # Median filtering

#print ("threshold in frame %d is %f"%(i,threshold))
img_norm = (img_norm < threshold).astype(np.uint8)  # Thresholded

edges = cv2.Canny(img_norm, 0, 1)         # Edge detection
#edges = cv2.Canny(img_norm, 20, 60)

# define ROI that covers cantilever edge, cut out the boundaries
vertices = np.array([[[5,10],[(img_width-20),10], \
              [(img_width-20),290],[5,290]]], dtype=np.int32)

edges_in_roi = region_of_interest(edges, vertices)


# APPLY HOUGH TRANSFORM
rho = 2 # distance resolution in pixels of the Hough grid
theta = np.pi/180 # angular resolution in radians of the Hough grid
threshold_hough = 10   # minimum number of votes (intersections in Hough grid cell)
min_line_length = 20  #minimum number of pixels making up a line
max_line_gap = 25   # maximum gap in pixels between connectable line segments
lines = cv2.HoughLinesP(edges_in_roi, rho, theta, threshold_hough, np.array([]), \
            minLineLength=min_line_length, maxLineGap=max_line_gap)

# Adaptively fit Hough Transform to the videos if a longer line can't be found
if lines is None:
  while (lines is None):
    min_line_length -= 5
    if min_line_length == 0:
      print ("Adaptive Hough func failed in frame %d"%(i+1))
      plt.figure(figsize = (20,5))
      plt.subplot(1,5,1)
```

```
            plt.imshow(img)
            plt.subplot(1,5,2)
            plt.imshow(img_norm, cmap='gray')
            plt.subplot(1,5,3)
            plt.imshow(edges, cmap = 'gray')
            plt.subplot(1,5,4)
            plt.imshow(edges, cmap = 'gray')
            plt.subplot(1,5,5)
            plt.imshow(edges, cmap = 'gray')

            return cantilever_max_disps
        else:
            lines = cv2.HoughLinesP(edges_in_roi, rho, theta, threshold, np.array([]), \
                    minLineLength=min_line_length, maxLineGap=max_line_gap)


    # plot lines on original image
    line_img = np.zeros((img.shape[0], img.shape[1], 3), dtype=np.uint8)
    line_img1 = np.zeros((img.shape[0], img.shape[1], 3), dtype=np.uint8)

    x_line = []
    y_line = []
    weights_line = []

    for line in lines:
        for (x1,y1,x2,y2) in line:
            cv2.line(line_img1, (x1,y1), (x2,y2), [0, 255, 0], 1)  # plot all hough lines
            weight = np.absolute(x1-x2)+np.absolute(y1-y2)  #longer lines get a bigger weight
            x_line.append(x1)
            y_line.append(y1)
            weights_line.append(weight)
            x_line.append(x2)
            y_line.append(y2)
            weights_line.append(weight)

    weights_norm = weights_line/np.sum(weights_line)

    # interchanged x and y; because most lines are close to vertical
    # this will give x = my + c
    line1, res, _, _, _ = np.polyfit(y_line, x_line, deg=1, w=weights_norm, full = True)

#       print(type(res))
#       print(res)
#       print(res.shape)

    if res>2:  # The 2 is tunable
        print ("detected large cantilever displacement at frame %d"%(i+1) + " with res " + str(res)
)
        x_line_temp = []
        y_line_temp = []
        weights_line_temp = []
```

```
            x_mean = np.mean(x_line)
            for count1,x_val in enumerate(x_line):
              if x_val < x_mean:
                continue
              else:
                x_line_temp.append(x_line[count1])
                y_line_temp.append(y_line[count1])
                weights_line_temp.append(weights_line[count1])

            weights_norm = weights_line_temp/np.sum(weights_line_temp)
            line1, res, _, _, _ = np.polyfit(y_line_temp, x_line_temp, deg=1, w=weights_norm, full = True)

            if res < 1:
              print ("correctly captured with res " + str(res))
            else:
              print ("could not capture with res " + str(res))



          if display==True or i==0:
            # plot just the final fitted line on original image
            cv2.line(line_img, (int(img.shape[0]*line1[0]+line1[1]),img.shape[0]), \
                 (int(line1[1]),0), [255, 0, 0], thickness=2)
            plt.figure(figsize = (20,5))
            plt.subplot(1,5,1)
            plt.imshow(img)
            plt.subplot(1,5,2)
            plt.imshow(img_norm, cmap='gray')
            plt.subplot(1,5,3)
            plt.imshow(edges, cmap = 'gray')
            plt.subplot(1,5,4)
            plt.imshow(cv2.addWeighted(line_img1, 0.8, img, 1, 0))
            plt.subplot(1,5,5)
            plt.imshow(cv2.addWeighted(line_img, 0.8, img, 1, 0))
            plt.suptitle("frame %d "%(i+1)+ filepath[-21:] + " %f"%(line1[1]) + "  residual " + str(res/l
en(x_line)))
            if i==0:
              plt.savefig(img_dir+"results/"+"edge" + "%d"%(file_index+1) + ".jpg", \
                    bbox_inches='tight', pad_inches = 0, dpi=400)


          cantilever_edges.append(line1)
          #print ("processed frame %d"%(i+1))

        print ("Processed %d frames"%(n_frames-1))

        ##################################################
        # Aggregate image edges and compute displacements
        ##################################################
        cantilever_edges = np.array(cantilever_edges)
        #cantilever_edges.shape
```

```
    x_intercepts = cantilever_edges[:,1]
    mslope = cantilever_edges[:,0].mean()  # mean_cantilever_slope

    # note: here mslope = tan(theta) is dx/dy
    # also 1px = 0.644um
    x_disp = [(x - x_intercepts[0])/(1+math.pow(mslope,2))*0.644  for x in x_intercepts]

    np.savetxt(img_dir+"results/"+'disp' + "%d"%(file_index+1) + '.csv', x_disp, delimiter=',')

    # find max displacement in first half, second half and average
    xmax1 = np.amax(x_disp[0:int(len(x_disp)/2)])
    xmax2 = np.amax(x_disp[int(len(x_disp)/2):])
    xmax = 0.5*(xmax1+xmax2)

    # Plot displacement as a function of time
    plt.figure()
    plt.plot(x_disp)  # note the two twitches
    plt.title("Max disp = %.2f um"%(xmax))
    plt.ylabel("Cantilever displacement (in microns)")
    plt.savefig(img_dir+"results/"+"cant_disp_" + "%d"%(file_index+1) + ".jpg", \
            bbox_inches='tight', pad_inches = 0, dpi=400)

    cantilever_max_disps.append(xmax)

  return cantilever_max_disps
```

References

1 Neal, D., Sakar, M. S., Ong, L.-L. S. & Harry Asada, H. Formation of elongated fascicle-inspired 3D tissues consisting of high-density, aligned cells using sacrificial outer molding. *Lab on a Chip* **14**, 1907-1916, doi:10.1039/C4LC00023D (2014).

2 Troosters, T. *et al.* Resistance Training Prevents Deterioration in Quadriceps Muscle Function During Acute Exacerbations of Chronic Obstructive Pulmonary Disease. *American Journal of Respiratory and Critical Care Medicine* **181**, 1072-1077, doi:10.1164/rccm.200908-1203OC (2010).

3 Resistance training induces qualitative changes in muscle morphology, muscle architecture, and muscle function in elderly postoperative patients. *Journal of Applied Physiology* **105**, 180-186, doi:10.1152/japplphysiol.01354.2007 (2008).

4 Effect of resistance training on single muscle fiber contractile function in older men. *Journal of Applied Physiology* **89**, 143-152, doi:10.1152/jappl.2000.89.1.143 (2000).

5 Ouellette, M. M. *et al.* High-Intensity Resistance Training Improves Muscle Strength, Self-Reported Function, and Disability in Long-Term Stroke Survivors. *Stroke* **35**, 1404-1409, doi:10.1161/01.str.0000127785.73065.34 (2004).

6 Dela, F. & Kjaer, M. Resistance training, insulin sensitivity and muscle function in the elderly. *Essays In Biochemistry* **42**, 75-88, doi:10.1042/bse0420075 (2006).

7 Fiatarone, M. A. *et al.* High-intensity strength training in nonagenarians: Effects on skeletal muscle. *JAMA* **263**, 3029-3034, doi:10.1001/jama.1990.03440220053029 (1990).

8 Strength conditioning in older men: skeletal muscle hypertrophy and improved function. *Journal of Applied Physiology* **64**, 1038-1044, doi:10.1152/jappl.1988.64.3.1038 (1988).

9 Evans, W. J. Exercise training guidelines for the elderly. *Med Sci Sports Exerc* **31**, 12-17, doi:10.1097/00005768-199901000-00004 (1999).

10 Cauza, E. *et al.* The Relative Benefits of Endurance and Strength Training on the Metabolic Factors and Muscle Function of People With Type 2 Diabetes Mellitus. *Archives of Physical Medicine and Rehabilitation* **86**, 1527-1533, doi:https://doi.org/10.1016/j.apmr.2005.01.007 (2005).

11 Vincent, H. K. & Vincent, K. R. The Effect of Training Status on the Serum Creatine Kinase Response, Soreness and Muscle Function Following Resistance Exercise. *Int J Sports Med* **28**, 431-437, doi:10.1055/s-2007-972660 (1997).

12 Kalapotharakos, V. I. *et al.* The Effects of High- and Moderate-Resistance Training on Muscle Function in the Elderly. *Journal of Aging and Physical Activity* **12**, 131-143, doi:10.1123/japa.12.2.131 (2004).

13 Resistance training improves single muscle fiber contractile function in older women. *American Journal of Physiology-Cell Physiology* **281**, C398-C406, doi:10.1152/ajpcell.2001.281.2.C398 (2001).

14 Reeves, N. D., Narici, M. V. & Maganaris, C. N. In vivo human muscle structure and function: adaptations to resistance training in old age. *Experimental Physiology* **89**, 675-689, doi:10.1113/expphysiol.2004.027797 (2004).

15 Andersen, L. L. *et al.* The effect of resistance training combined with timed ingestion of protein on muscle fiber size and muscle strength. *Metabolism* **54**, 151-156, doi:https://doi.org/10.1016/j.metabol.2004.07.012 (2005).

16 Sandra, M. *et al.* Effects of aerobic or aerobic and resistance training on cardiorespiratory and skeletal muscle function in heart failure: a randomized controlled pilot trial. *Clinical Rehabilitation* **23**, 207-216, doi:10.1177/0269215508095362 (2009).

17 Willoughby, D. S. Effects of heavy resistance training on myostatin mRNA and protein expression. *Med Sci Sports Exerc* **36**, 574-582, doi:10.1249/01.mss.0000121952.71533.ea (2004).

18 Kongsgaard, M., Backer, V., Jørgensen, K., Kjær, M. & Beyer, N. Heavy resistance training increases muscle size, strength and physical function in elderly male COPD-patients—a pilot study. *Respiratory Medicine* **98**, 1000-1007, doi:https://doi.org/10.1016/j.rmed.2004.03.003 (2004).

19 Dibble, L. E. *et al.* High-intensity resistance training amplifies muscle hypertrophy and functional gains in persons with Parkinson's disease. *Movement Disorders* **21**, 1444-1452, doi:10.1002/mds.20997 (2006).

20 Skelton, D. A., Young, A., Greig, C. A. & Malbut, K. E. Effects of Resistance Training on Strength, Power, and Selected Functional Abilities of Women Aged 75 and Older. *Journal of the American Geriatrics Society* **43**, 1081-1087, doi:10.1111/j.1532-5415.1995.tb07004.x (1995).

21 Macaluso, A. & De Vito, G. Muscle strength, power and adaptations to resistance training in older people. *European Journal of Applied Physiology* **91**, 450-472, doi:10.1007/s00421-003-0991-3 (2004).

22 Effect of leucine metabolite β-hydroxy-β-methylbutyrate on muscle metabolism during resistance-exercise training. *Journal of Applied Physiology* **81**, 2095-2104, doi:10.1152/jappl.1996.81.5.2095 (1996).

23 Schoenfeld, B. J. The Mechanisms of Muscle Hypertrophy and Their Application to Resistance Training. *The Journal of Strength & Conditioning Research* **24**, 2857-2872, doi:10.1519/JSC.0b013e3181e840f3 (2010).

24 Fielding, R. A. *et al.* High-Velocity Resistance Training Increases Skeletal Muscle Peak Power in Older Women. *Journal of the American Geriatrics Society* **50**, 655-662, doi:10.1046/j.1532-5415.2002.50159.x (2002).

25 Resistance training reduces the acute exercise-induced increase in muscle protein turnover. *American Journal of Physiology-Endocrinology and Metabolism* **276**, E118-E124, doi:10.1152/ajpendo.1999.276.1.E118 (1999).

26 Human skeletal sarcoplasmic reticulum Ca2+ uptake and muscle function with aging and strength training. *Journal of Applied Physiology* **86**, 1858-1865, doi:10.1152/jappl.1999.86.6.1858 (1999).

27 Increased rate of force development and neural drive of human skeletal muscle following resistance training. *Journal of Applied Physiology* **93**, 1318-1326, doi:10.1152/japplphysiol.00283.2002 (2002).

28 Rommel, C. *et al.* Mediation of IGF-1-induced skeletal myotube hypertrophy by PI(3)K/Akt/mTOR and PI(3)K/Akt/GSK3 pathways. *Nature Cell Biology* **3**, 1009, doi:10.1038/ncb1101-1009 (2001).

29 Bodine, S. C. *et al.* Akt/mTOR pathway is a crucial regulator of skeletal muscle hypertrophy and can prevent muscle atrophy in vivo. *Nature Cell Biology* **3**, 1014, doi:10.1038/ncb1101-1014 (2001).

30 Signaling in Muscle Atrophy and Hypertrophy. *Physiology* **23**, 160-170, doi:10.1152/physiol.00041.2007 (2008).

31 Sandri, M. *et al.* Signalling pathways regulating muscle mass in ageing skeletal muscle. The role of the IGF1-Akt-mTOR-FoxO pathway. *Biogerontology* **14**, 303-323, doi:10.1007/s10522-013-9432-9 (2013).

32 Glass, D. J. in *Phosphoinositide 3-kinase in Health and Disease: Volume 1* (eds Christian Rommel, Bart Vanhaesebroeck, & Peter K. Vogt) 267-278 (Springer Berlin Heidelberg, 2011).

33 Song, Y.-H. *et al.* Insulin-Like Growth Factor I-Mediated Skeletal Muscle Hypertrophy Is Characterized by Increased mTOR-p70S6K Signaling without Increased Akt Phosphorylation. *Journal of Investigative Medicine* **53**, 135-142, doi:10.2310/6650.2005.00309 (2005).

34 Spangenburg, E. E., Le Roith, D., Ward, C. W. & Bodine, S. C. A functional insulin-like growth factor receptor is not necessary for load-induced skeletal muscle hypertrophy. *The Journal of Physiology* **586**, 283-291, doi:10.1113/jphysiol.2007.141507 (2008).

35 Sarbassov, D. D., Guertin, D. A., Ali, S. M. & Sabatini, D. M. Phosphorylation and Regulation of Akt/PKB by the Rictor-mTOR Complex. *Science* **307**, 1098-1101, doi:10.1126/science.1106148 (2005).

36 Bolster, D. R., Jefferson, L. S. & Kimball, S. R. Regulation of protein synthesis associated with skeletal muscle hypertrophy by insulin-, amino acid- and exercise-induced signalling. *Proceedings of the Nutrition Society* **63**, 351-356, doi:10.1079/PNS2004355 (2004).

37 Schiaffino, S. & Mammucari, C. Regulation of skeletal muscle growth by the IGF1-Akt/PKB pathway: insights from genetic models. *Skeletal Muscle* **1**, 4, doi:10.1186/2044-5040-1-4 (2011).

38 Sarbassov, D. D., Ali, S. M. & Sabatini, D. M. Growing roles for the mTOR pathway. *Current Opinion in Cell Biology* **17**, 596-603, doi:https://doi.org/10.1016/j.ceb.2005.09.009 (2005).

39 von Maltzahn, J., Bentzinger, C. F. & Rudnicki, M. A. Wnt7a–Fzd7 signalling directly activates the Akt/mTOR anabolic growth pathway in skeletal muscle. *Nature Cell Biology* **14**, 186, doi:10.1038/ncb2404

https://www.nature.com/articles/ncb2404#supplementary-information (2011).

40 Ohanna, M. *et al.* Atrophy of S6K1−/− skeletal muscle cells reveals distinct mTOR effectors for cell cycle and size control. *Nature Cell Biology* **7**, 286, doi:10.1038/ncb1231

https://www.nature.com/articles/ncb1231#supplementary-information (2005).

41 Sandri, M. *et al.* Foxo Transcription Factors Induce the Atrophy-Related Ubiquitin Ligase Atrogin-1 and Cause Skeletal Muscle Atrophy. *Cell* **117**, 399-412, doi:https://doi.org/10.1016/S0092-8674(04)00400-3 (2004).

42 Lai, K.-M. V. *et al.* Conditional Activation of Akt in Adult Skeletal Muscle Induces Rapid Hypertrophy. *Molecular and Cellular Biology* **24**, 9295-9304, doi:10.1128/mcb.24.21.9295-9304.2004 (2004).

43 Latres, E. *et al.* Insulin-like Growth Factor-1 (IGF-1) Inversely Regulates Atrophy-induced Genes via the Phosphatidylinositol 3-Kinase/Akt/Mammalian Target of Rapamycin (PI3K/Akt/mTOR) Pathway. *Journal of Biological Chemistry* **280**, 2737-2744, doi:10.1074/jbc.M407517200 (2005).

44 Stitt, T. N. *et al.* The IGF-1/PI3K/Akt Pathway Prevents Expression of Muscle Atrophy-Induced Ubiquitin Ligases by Inhibiting FOXO Transcription Factors. *Molecular Cell* **14**, 395-403, doi:https://doi.org/10.1016/S1097-2765(04)00211-4 (2004).

45 Léger, B. *et al.* Akt signalling through GSK-3β, mTOR and Foxo1 is involved in human skeletal muscle hypertrophy and atrophy. *The Journal of Physiology* **576**, 923-933, doi:10.1113/jphysiol.2006.116715 (2006).

46 Glass, D. J. Signalling pathways that mediate skeletal muscle hypertrophy and atrophy. *Nature Cell Biology* **5**, 87, doi:10.1038/ncb0203-87 (2003).

47 Glass, D. J. Skeletal muscle hypertrophy and atrophy signaling pathways. *The International Journal of Biochemistry & Cell Biology* **37**, 1974-1984, doi:https://doi.org/10.1016/j.biocel.2005.04.018 (2005).

48 Heineke, J. *et al.* Genetic Deletion of Myostatin From the Heart Prevents Skeletal Muscle Atrophy in Heart Failure. *Circulation* **121**, 419-425, doi:10.1161/circulationaha.109.882068 (2010).

49 Smith, R. C. & Lin, B. K. Myostatin inhibitors as therapies for muscle wasting associated with cancer and other disorders. *Current Opinion in Supportive and Palliative Care* **7**, 352-360, doi:10.1097/SPC.0000000000000013 (2013).

50 Hulmi, J. J. *et al.* Acute and long-term effects of resistance exercise with or without protein ingestion on muscle hypertrophy and gene expression. *Amino Acids* **37**, 297-308, doi:10.1007/s00726-008-0150-6 (2009).

51 Qiao, C. *et al.* Myostatin Propeptide Gene Delivery by Adeno-Associated Virus Serotype 8 Vectors Enhances Muscle Growth and Ameliorates Dystrophic Phenotypes in mdx Mice. *Human Gene Therapy* **19**, 241-254, doi:10.1089/hum.2007.159 (2008).

52 Myostatin inhibits cell proliferation and protein synthesis in C2C12 muscle cells. *American Journal of Physiology-Endocrinology and Metabolism* **280**, E221-E228, doi:10.1152/ajpendo.2001.280.2.E221 (2001).

53 Holzbaur, E. L. F. *et al.* Myostatin inhibition slows muscle atrophy in rodent models of amyotrophic lateral sclerosis. *Neurobiology of Disease* **23**, 697-707, doi:https://doi.org/10.1016/j.nbd.2006.05.009 (2006).

54 Walsh, F. S. & Celeste, A. J. Myostatin: a modulator of skeletal-muscle stem cells. *Biochemical Society Transactions* **33**, 1513-1517, doi:10.1042/bst0331513 (2005).

55 Skeletal muscle myostatin mRNA expression is fiber-type specific and increases during hindlimb unloading. *American Journal of Physiology-Regulatory, Integrative and Comparative Physiology* **277**, R601-R606, doi:10.1152/ajpregu.1999.277.2.R601 (1999).

56 Thomas, M. *et al.* Myostatin, a Negative Regulator of Muscle Growth, Functions by Inhibiting Myoblast Proliferation. *Journal of Biological Chemistry* **275**, 40235-40243, doi:10.1074/jbc.M004356200 (2000).

57 Benny Klimek, M. E. *et al.* Acute inhibition of myostatin-family proteins preserves skeletal muscle in mouse models of cancer cachexia. *Biochemical and Biophysical Research Communications* **391**, 1548-1554, doi:https://doi.org/10.1016/j.bbrc.2009.12.123 (2010).

58 Murphy, K. T. *et al.* Antibody-directed myostatin inhibition in 21-mo-old mice reveals novel roles for myostatin signaling in skeletal muscle structure and function. *The FASEB Journal* **24**, 4433-4442, doi:10.1096/fj.10-159608 (2010).

59 Sakuma, K., Watanabe, K., Sano, M., Uramoto, I. & Totsuka, T. Differential adaptation of growth and differentiation factor 8/myostatin, fibroblast growth factor 6 and leukemia inhibitory factor in overloaded, regenerating and denervated rat muscles. *Biochimica et Biophysica Acta (BBA) - Molecular Cell Research* **1497**, 77-88, doi:https://doi.org/10.1016/S0167-4889(00)00044-6 (2000).

60 Nakatani, M. *et al.* Transgenic expression of a myostatin inhibitor derived from follistatin increases skeletal muscle mass and ameliorates dystrophic pathology in mdx mice. *The FASEB Journal* **22**, 477-487, doi:10.1096/fj.07-8673com (2008).

61 Ohsawa, Y. *et al.* Muscular atrophy of caveolin-3–deficient mice is rescued by myostatin inhibition. *Journal of Clinical Investigation* **116**, 2924-2934, doi:10.1172/JCI28520 (2006).

62 Myostatin reduces Akt/TORC1/p70S6K signaling, inhibiting myoblast differentiation and myotube size. *American Journal of Physiology-Cell Physiology* **296**, C1258-C1270, doi:10.1152/ajpcell.00105.2009 (2009).

63 Lee, S.-J. & McPherron, A. C. Regulation of myostatin activity and muscle growth. *Proceedings of the National Academy of Sciences* **98**, 9306-9311, doi:10.1073/pnas.151270098 (2001).

64 Wang, Q. & McPherron, A. C. Myostatin inhibition induces muscle fibre hypertrophy prior to satellite cell activation. *The Journal of Physiology* **590**, 2151-2165, doi:10.1113/jphysiol.2011.226001 (2012).

65 Lee, S.-J. *et al.* Role of satellite cells versus myofibers in muscle hypertrophy induced by inhibition of the myostatin/activin signaling pathway. *Proceedings of the National Academy of Sciences* **109**, E2353–E2360, doi:10.1073/pnas.1206410109 (2012).

66 Amthor, H. *et al.* Muscle hypertrophy driven by myostatin blockade does not require stem/precursor-cell activity. *Proceedings of the National Academy of Sciences* **106**, 7479-7484, doi:10.1073/pnas.0811129106 (2009).

67 Zhu, X., Hadhazy, M., Wehling, M., Tidball, J. G. & McNally, E. M. Dominant negative myostatin produces hypertrophy without hyperplasia in muscle. *FEBS Letters* **474**, 71-75, doi:10.1016/S0014-5793(00)01570-2 (2000).

68 Zimmers, T. A. *et al.* Induction of Cachexia in Mice by Systemically Administered Myostatin. *Science* **296**, 1486-1488, doi:10.1126/science.1069525 (2002).
69 Whittemore, L.-A. *et al.* Inhibition of myostatin in adult mice increases skeletal muscle mass and strength. *Biochemical and Biophysical Research Communications* **300**, 965-971, doi:https://doi.org/10.1016/S0006-291X(02)02953-4 (2003).
70 Schuelke , M. *et al.* Myostatin Mutation Associated with Gross Muscle Hypertrophy in a Child. *New England Journal of Medicine* **350**, 2682-2688, doi:10.1056/NEJMoa040933 (2004).
71 Follistatin induces muscle hypertrophy through satellite cell proliferation and inhibition of both myostatin and activin. *American Journal of Physiology-Endocrinology and Metabolism* **297**, E157-E164, doi:10.1152/ajpendo.00193.2009 (2009).
72 Lee, S.-J. Quadrupling Muscle Mass in Mice by Targeting TGF-ß Signaling Pathways. *PLOS ONE* **2**, e789, doi:10.1371/journal.pone.0000789 (2007).
73 Huxley, A. F. Muscle structure and theories of contraction. *Progress in biophysics and biophysical chemistry* **7**, 255-318 (1957).
74 Huxley, A. F. & Simmons, R. M. Proposed Mechanism of Force Generation in Striated Muscle. *Nature* **233**, 533, doi:10.1038/233533a0 (1971).
75 Patel, T. J. & Lieber, R. L. Force transmission in skeletal muscle: from actomyosin to external tendons. *Exercise and sport sciences reviews* **25**, 321-363 (1997).
76 Musarò, A. *et al.* Localized Igf-1 transgene expression sustains hypertrophy and regeneration in senescent skeletal muscle. *Nature Genetics* **27**, 195, doi:10.1038/84839 (2001).
77 Duclos, F. *et al.* Progressive Muscular Dystrophy in α-Sarcoglycan–deficient Mice. *The Journal of Cell Biology* **142**, 1461-1471, doi:10.1083/jcb.142.6.1461 (1998).
78 Ling, K. K. Y., Lin, M.-Y., Zingg, B., Feng, Z. & Ko, C.-P. Synaptic Defects in the Spinal and Neuromuscular Circuitry in a Mouse Model of Spinal Muscular Atrophy. *PLOS ONE* **5**, e15457, doi:10.1371/journal.pone.0015457 (2010).
79 Acehan, D. *et al.* Cardiac and Skeletal Muscle Defects in a Mouse Model of Human Barth Syndrome. *Journal of Biological Chemistry* **286**, 899-908, doi:10.1074/jbc.M110.171439 (2011).
80 Cai, D. *et al.* IKKβ/NF-κB Activation Causes Severe Muscle Wasting in Mice. *Cell* **119**, 285-298, doi:https://doi.org/10.1016/j.cell.2004.09.027 (2004).
81 Lai, Y. *et al.* Dystrophins carrying spectrin-like repeats 16 and 17 anchor nNOS to the sarcolemma and enhance exercise performance in a mouse model of muscular dystrophy. *The Journal of Clinical Investigation* **119**, 624-635, doi:10.1172/JCI36612 (2009).
82 Deconinck, A. E. *et al.* Utrophin-Dystrophin-Deficient Mice as a Model for Duchenne Muscular Dystrophy. *Cell* **90**, 717-727, doi:https://doi.org/10.1016/S0092-8674(00)80532-2 (1997).
83 Carnwath, J. W. & Shotton, D. M. Muscular dystrophy in the mdx mouse: Histopathology of the soleus and extensor digitorum longus muscles. *Journal of the Neurological Sciences* **80**, 39-54, doi:https://doi.org/10.1016/0022-510X(87)90219-X (1987).
84 Raman, R. *et al.* Optogenetic skeletal muscle-powered adaptive biological machines. *Proceedings of the National Academy of Sciences* **113**, 3497-3502, doi:10.1073/pnas.1516139113 (2016).
85 Sierra, E. *et al.* Comparative histology of muscle in free ranging cetaceans: shallow versus deep diving species. *Scientific Reports* **5**, 15909, doi:10.1038/srep15909 (2015).
86 Luna, V. M., Daikoku, E. & Ono, F. "Slow" skeletal muscles across vertebrate species. *Cell & Bioscience* **5**, 62, doi:10.1186/s13578-015-0054-6 (2015).

87 Osaki, T., Sivathanu, V. & Kamm, R. D. Crosstalk between developing vasculature and optogenetically engineered skeletal muscle improves muscle contraction and angiogenesis. *Biomaterials* **156**, 65-76, doi:https://doi.org/10.1016/j.biomaterials.2017.11.041 (2018).

88 Burattini, S. *et al.* C2C12 murine myoblasts as a model of skeletal muscle development: morpho-functional characterization. *European journal of histochemistry : EJH* **48**, 223-233 (2004).

89 Fujita, H., Nedachi, T. & Kanzaki, M. Accelerated de novo sarcomere assembly by electric pulse stimulation in C2C12 myotubes. *Experimental Cell Research* **313**, 1853-1865, doi:https://doi.org/10.1016/j.yexcr.2007.03.002 (2007).

90 Engler, A. J. *et al.* Myotubes differentiate optimally on substrates with tissue-like stiffness: pathological implications for soft or stiff microenvironments. *The Journal of Cell Biology* **166**, 877-887, doi:10.1083/jcb.200405004 (2004).

91 Skwarek-Maruszewska, A., Hotulainen, P., Mattila, P. K. & Lappalainen, P. Contractility-dependent actin dynamics in cardiomyocyte sarcomeres. *Journal of Cell Science* **122**, 2119-2126, doi:10.1242/jcs.046805 (2009).

92 Wang, J., Sanger, J. M. & Sanger, J. W. Differential effects of latrunculin-A on myofibrils in cultures of skeletal muscle cells: Insights into mechanisms of myofibrillogenesis. *Cell Motility and the Cytoskeleton* **62**, 35-47, doi:10.1002/cm.20083 (2005).

93 Fritzsche, M. *et al.* Cytoskeletal actin dynamics shape a ramifying actin network underpinning immunological synapse formation. *Science Advances* **3** (2017).

94 McGrath, J. L., Tardy, Y., Dewey, C. F., Meister, J. J. & Hartwig, J. H. Simultaneous Measurements of Actin Filament Turnover, Filament Fraction, and Monomer Diffusion in Endothelial Cells. *Biophysical Journal* **75**, 2070-2078, doi:https://doi.org/10.1016/S0006-3495(98)77649-0 (1998).

95 Star, E. N., Kwiatkowski, D. J. & Murthy, V. N. Rapid turnover of actin in dendritic spines and its regulation by activity. *Nature Neuroscience* **5**, 239, doi:10.1038/nn811

https://www.nature.com/articles/nn811#supplementary-information (2002).

96 Winder, S. J. & Ayscough, K. R. Actin-binding proteins. *Journal of Cell Science* **118**, 651 (2005).

97 Rizvi, S. A. *et al.* Identification and Characterization of a Small Molecule Inhibitor of Formin-Mediated Actin Assembly. *Chemistry & Biology* **16**, 1158-1168, doi:https://doi.org/10.1016/j.chembiol.2009.10.006 (2009).

98 Currier, M. A. *et al.* Identification of Cancer-Targeted Tropomyosin Inhibitors and Their Synergy With Microtubule Drugs. *Molecular Cancer Therapeutics*, doi:10.1158/1535-7163.mct-16-0873 (2017).

99 Stehn, J. R. *et al.* A Novel Class of Anticancer Compounds Targets the Actin Cytoskeleton in Tumor Cells. *Cancer Research* **73**, 5169-5182, doi:10.1158/0008-5472.can-12-4501 (2013).

100 Kee, A. J. *et al.* An actin filament population defined by the tropomyosin Tpm3.1 regulates glucose uptake. *Traffic (Copenhagen, Denmark)* **16**, 691-711, doi:10.1111/tra.12282 (2015).

101 Ramachandran, I., Terry, M. & Ferrari, M. B. Skeletal muscle myosin cross-bridge cycling is necessary for myofibrillogenesis. *Cell Motility and the Cytoskeleton* **55**, 61-72, doi:10.1002/cm.10113 (2003).

102 Pujol, T., du Roure, O., Fermigier, M. & Heuvingh, J. Impact of branching on the elasticity of actin networks. *Proceedings of the National Academy of Sciences* **109**, 10364-10369, doi:10.1073/pnas.1121238109 (2012).

103 Bae, Y. H. *et al.* A FAK-Cas-Rac-Lamellipodin Signaling Module Transduces Extracellular Matrix Stiffness into Mechanosensitive Cell Cycling. *Science signaling* **7**, ra57-ra57, doi:10.1126/scisignal.2004838 (2014).

104 Wang, J., Fan, Y., Dube, D. K., Sanger, J. M. & Sanger, J. W. Jasplakinolide reduces actin and tropomyosin dynamics during myofibrillogenesis. *Cytoskeleton* **71**, 513-529, doi:10.1002/cm.21189 (2014).

105 Rueckschloss, U. & Isenberg, G. Cytochalasin D reduces Ca(2+) currents via cofilin-activated depolymerization of F-actin in guinea-pig cardiomyocytes. *The Journal of Physiology* **537**, 363-370, doi:10.1111/j.1469-7793.2001.00363.x (2001).

106 Raman, R., Cvetkovic, C. & Bashir, R. A modular approach to the design, fabrication, and characterization of muscle-powered biological machines. *Nature Protocols* **12**, 519, doi:10.1038/nprot.2016.185

https://www.nature.com/articles/nprot.2016.185#supplementary-information (2017).